DROUGHT-INDUCED TREE MORTALITY ASSESSMENT IN MEDITERRANEAN ECOSYSTEMS USING TIME SERIES ANALYSIS

ALMA RAUNAK

APRIL, 2024

SUPERVISORS:

Dr. Ing. Margarita Huesca Martinez
Dr. Panagiotis Nyktas

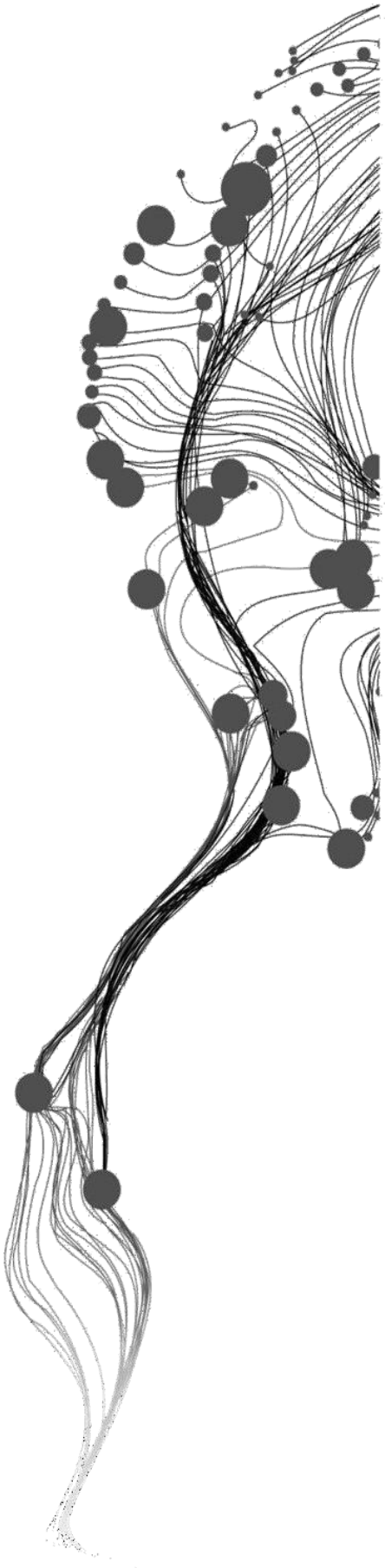

DROUGHT-INDUCED TREE MORTALITY ASSESSMENT IN MEDITERRANEAN ECOSYSTEMS USING TIME SERIES ANALYSIS

ALMA RAUNAK

Enschede, The Netherlands, APRIL, 2024

Thesis submitted to the Faculty of Geo-Information Science and Earth Observation of the University of Twente in partial fulfilment of the requirements for the degree of Master of Science in Geo-information Science and Earth Observation.
Specialization: Natural Resources Management

SUPERVISORS:
Dr. Ing. Margarita Huesca Martinez
Dr. Panagiotis Nyktas

THESIS ASSESSMENT BOARD:
Dr.ir, A. Vrieling (Chair)
Prof. Silvia Merino De Miguel (External Examiner, Universidad Politécnica de Madrid)

ABSTRACT

Remote sensing techniques are crucial in monitoring and assessing forest health, particularly in detecting tree mortality events. This study investigates the effectiveness of spectral indices and Spectral Unmixing (SU) derived from satellite data in identifying tree mortality in Mediterranean forest ecosystems. The study demonstrates the utility of Unmanned Aerial Systems (UAS) imagery as ground truth data, showcasing its high correlation with direct field observations (R^2 = 0.95, RMSE = 2.97), thus offering a way to complement and/or simplify traditional field campaigns. UAS also verifies the reliability of SU (R^2 = 0.75, RMSE = 12.4) in estimating vegetation percentage within mixed pixels despite challenges such as variability in vegetation composition and spatial resolution limitations. Time series analysis reveals the minimal influence of a recent single drought event (which happened in 2015-2016) on vegetation indices derived from satellite time series imagery. Tree mortality found in the area is explained by disturbances that occurred in the late 1990s and mid-2000s, highlighting the need for having 2 or more droughts consequently for high tree mortality. Change detection using the LandTrendr algorithm (including using a novel technique of detecting changes in SU's outputs with LandTrendr) confirms significant vegetation loss, with SU highlighting more pixels with changes than traditional vegetation indices. Despite SU having the lowest overall accuracy, evaluation of the presence of tree mortality accuracy demonstrates SU's superiority (97.96% accuracy) over vegetation indices (i.e., 93.88% NDVI, 93.75% NDWI) while acknowledging challenges in detecting the absence of tree mortality (i.e., 50% SU, 78.57% NDVI, 73.33% NDWI), presumably due to the overestimation of SU comparing to UAS data. Additionally, the research highlights the potential of NDVI in capturing changes in canopy dynamics as well as highlighting areas of drought-resilient tree species and NDWI in identifying areas of high drought susceptibility. The regression analysis between vegetation indices and tree mortality percentage, and between SU and tree mortality percentage, reveals low R^2 values for NDVI, NDWI, and SU (0.37, 0.18, and 0.35 respectively), and high RMSE values of 56.9, 84.9, and 26.6 respectively, including significantly lower correlations using NDWI. However, removing plots with tree mortality percentages higher than 80% helps to improve it, resulting in R^2 of NDVI, NDWI, and SU to be 0.42, 0.35 and 0.51; RMSE: 58.2, 80.9, and 20.8 respectively. The study also discusses the importance of spatial and temporal resolutions in remote sensing data to accurately assess tree mortality and the potential of ensemble approaches with higher spatial resolution imagery to improve detection accuracy. Moreover, the findings underscore the significance of early detection of forest decline and the resilience of vegetation to environmental stressors, providing valuable insights for forest management and conservation efforts. Overall, this research advances our understanding of remote sensing applications in monitoring tree mortality and offers recommendations for future studies to enhance detection methodologies and improve forest management strategies.

Keywords: Unmanned Aerial Systems (UAS), Spectral Unmixing, NDVI, NDWI, tree mortality, vegetation indices, change detection, drought monitoring, remote sensing, LandTrendr algorithm, Landsat, Mediterranean ecosystem.

ACKNOWLEDGMENTS

First and foremost, I would like to express my deepest gratitude to my brilliant supervisors, Dr Marga and Dr Panagiotis, for their invaluable participation in discussions, guidance, support, and encouragement throughout this research endeavour. Dr Marga's comments on the content of this research, quick response to any question, and fixing the body of text brought this research to where you can find it now. Thanks to Dr Panagiotis for arranging so many things during the fieldwork, such deep knowledge of the study area, and, of course, flying drones. This data is the cornerstone of this work. Thank you so much for everything! Without you, this thesis would not have been possible.

I am also immensely thankful to Thesis Assessment Board's Chair, Dr. Anton Vrieling, for his constructive feedback and scholarly input during the development of this thesis.

Thanks to Manolis Kontoudakis and Nikiforos Nikiforakis for providing us with a differential (Leica) GNSS to use during fieldwork.

Thanks to ITC for choosing me two years ago and granting me the scholarship.

I am very proud of myself while I am typing these words for bringing this research to this last point. But also, I want to thank myself for deciding to pursue a master's degree and to do it abroad. This decision is one of the best decisions I have made and one of the best things that has happened to me.

I met so many brilliant and kind and lovely people along my way here at ITC! I cannot believe my luck. Thank you, my dearest Jasin, for everything. Thanks to my beautiful friends Sachi, Chakshu, Aparna, Salsa, Minh, Wibisana, Adina and many more. You are making me happy, and I love you.

Thanks to my family, my mommy and daddy, my brothers, my aunt, my azhe for everything. I cannot even list it because it doesn't matter how many things I will write down, it would not cover everything you have done for me. All of you live in me. Azhe, I hope I make you smile up there.

While this thesis is carrying my name, this whole journey would not have been possible or would have been less enjoyable without all the people around me, all the people I did or did not mention here.

Барлығына рахмет және спасибо, әсіресе маған. Люблю.

TABLE OF CONTENTS

LIST OF FIGURES

APPENDIX

LIST OF TABLES

LIST OF ABBREVIATIONS

EVI	Enhanced Vegetation Index
FAO	Food and Agriculture Organization
GEE	Google Earth Engine
NBR	Normalized Burn Ratio
NDII	Normalized Difference Infrared Index
NDVI	Normalized Difference Vegetation Index
NDWI	Normalized Difference Water Index
NIR	Near-Infrared
R	Correlation Coefficient
RGB	Red-Green-Blue
RS	Remote Sensing
RMSE	Root Mean Squared Error
SU	Spectral Unmixing
SWIR	Short-Wave Infrared
TM	Tree Mortality
UAS	Unmanned Aerial Systems
VI	Vegetation Index
VIs	Vegetation Indices

1. INTRODUCTION

1.1. The problem of drought and the role of (Mediterranean) forest

The adverse effects of drought impede nature's ability to provide a diverse range of environmental, social, and economic benefits (Li et al., 2023). Drought is characterized by an extended duration of high temperature and/or low precipitation, resulting in a persistent water deficit in a specific region over a specified period (Haied et al., 2023). Due to climate change, we expect more frequent and intense drought events in the near future. The possible consequences of drought are increasing fire risk, biodiversity loss, habitat destruction, etc. Drought is the slowest but one of the world's most dangerous and widespread hazards (Mo et al., 2023). Therefore, its impact could be followed and investigated in long-term periods.

Forests play a crucial role in preventing biodiversity crisis and the further development of global change. Conservation of forests, especially mature and old-growth communities, is essential to preserve its ecosystem services (Woodall et al., 2023). Therefore, there is a particular interest in the impact of droughts on forest ecosystems. There are different criteria to evaluate the effect of changing climate on forests. Such as its direct impact on trees via physiological processes (for example, water content) or considering other factors such as insect attacks (Hartmann et al., 2022). All of this generally results in forest degradation and, ultimately, tree mortality.

Droughts have been causing widespread tree mortality in Mediterranean ecosystems and semi-arid regions (Schröter et al., 2005). Mediterranean climate regions cover almost 5 % of the Earth but contain about one-fifth of the global plant biodiversity, as well as have extremely high rates of endemic and rare species (Cowling et al., 1996). This area represents the biome on the border between subtropical dry forest and semi-arid ecosystems, in other words it locates on the border between temperate and arid zones (Barbeta et al., 2015). Mediterranean species of flora and fauna are adapted to prolonged dry seasons but nowadays the drought events are becoming more intense and frequent that the ecosystem cannot support them anymore. So, this region is overly sensitive to climate change, especially to expected increasing temperatures and reduced precipitation in the future (Schröter et al., 2005). Thus, it is indispensable to study this type of ecosystem to preserve global biodiversity, protect Mediterranean biodiversity hot-spots, and prevent or reduce desertification in other Mediterranean areas in the future.

1.2. Tree mortality as an indicator of drought impact

Tree mortality as an indicator of droughts is one of the most pivotal factors of changes in the carbon cycle (Liu et al., 2023). This is not only due to the reduction of forests' ecosystem services but also due to the destruction of both standing and fallen biomass, including aboveground vegetation and belowground roots of dead and dying trees, which has an impact on the process of carbon sequestration and the exchange of elements within the ecosystem (Anderegg et al., 2012). Besides, there is an increase of forest fire risk due to increased fuel to burn. This is especially important in Mediterranean ecosystems due to the habitat destruction that forest fires might cause.

Tree mortality is the last stage of the effect of drought on a forest and an indicator of drought impact. The process of tree death due to drought can be divided into several stages (Gaylord et al., 2015). However, it is crucial to emphasize that the specific timeline and progression of these phases can differ significantly based on factors such as tree species, soil conditions, the severity of the drought, and environmental factors. The initial stage involves the tree experiencing drought stress. This occurs when the soil moisture levels drop significantly, leading to reduced water uptake by the tree's roots. As a response to water scarcity, the tree may begin to close its stomata (small openings on leaves) to conserve water, leading to reduced photosynthesis. As the drought stress continues, the tree may exhibit visible signs of wilting, where leaves droop or curl to minimize water loss through transpiration. The next step is a so-called hydraulic failure when air bubbles

produced in the xylem block the flow of water and nutrients from roots up to leaves. As the drought persists, the tree's growth is severely impacted. It gives way to reduced photosynthesis, limited nutrient uptake, and, furthermore, weakened defence mechanisms, making them more susceptible to attacks by pests and pathogens. These organisms take advantage of the tree's compromised defenses, causing further damage to the tree. The tree's canopy may start to thin as more leaves are shed, and the remaining leaves may become discolored and show signs of damage. Also, drought can damage the tree's root system, particularly in shallow-rooted species. As the soil dries and shrinks, roots may become desiccated or die, further reducing the tree's ability to access water and nutrients. The combination of the above factors eventually leads to the tree's death. The exact cause of death may vary but is typically related to a critical inability to transport water and nutrients throughout the tree (Gaylord et al., 2015).

In summary, droughts can retard the growth of plants, which leads to a reduction of primary growth in general and such consequences as a decline in fruit production, the smaller size of leaves and their number, and changes in phenological cycles and reproductive phases (Silva et al., 2013). Moreover, it makes trees more prone to wildfires. Also, it increases autotrophic respiration, which leads to a decline in the tree's natural ability to absorb carbon dioxide and release oxygen (Brando et al., 2019). Overall, the influence of droughts on tree communities reduces the profit of their ecosystem services and contributes further to anthropogenic climate change (Ewane et al., 2023).

Thus, precise estimation and mapping of tree mortality may help to understand and assess the total drought-induced impact on the forest, identify areas of priority intervention, and help develop restoration plans. Consequently, this information will help forest managers in the decision-making process to prevent or reduce the impact of drought in other Mediterranean areas, thus reducing the risk of desertification. Remote Sensing (RS) seems to be the most appropriate approach for this type of analysis because it can cover larger and/or inaccessible areas, reduce the cost of fieldwork, and cover data from the past.

1.3. Tree mortality detection using Remote Sensing

There are diverse types of RS data to be used. Multispectral data is the most widely used to monitor tree mortality due to their high temporal resolution. Multispectral data typically involves the utilization of vegetation indices (VIs), which emphasize various object properties. Among them, the most widely used is the Normalized Difference Vegetation Index (NDVI) (Rouse et al., 1974). NDVI has been commonly recognized in RS as the 'greenness' index and was used to detect land cover changes in different ecosystems, including semi-arid ecosystems (Almalki et al., 2022; Chaulagain et al., 2023; Worqlul et al., 2023; X. Zhang et al., 2022).

Another well-used VI is the Normalized Difference Water Index (NDWI) (Gao, 1996). The NDWI is capable of detecting alterations in the moisture levels of vegetation, making it a valuable tool for assessing and tracking the moisture status of vegetation canopies across large areas (Chou et al., 2022; Marusig et al., 2020; Taherizadeh et al., 2023).

NDVI has been utilized to detect tree mortality and the impact of droughts on forests. For example, Garrity et al. (2013) examined tree mortality of a mixed species forest in the southwestern U.S. using bi-temporal (before and after tree mortality) differencing of NDVI, with an accuracy of 97.9 %. Another study used change metrics (calculated using differences in VI's summer and winter values) derived from three years of MODIS data in the *Pinus* plantation of southern New South Wales, Australia. It proved that NDVI outperforms other indices such as Enhanced Vegetation Index (EVI) and Normalized Difference Infrared Index (NDII) in estimating tree mortality (R^2=0.37 using NDVI against 0.04 and 0.15 using EVI and NDII respectively) (Verbesselt et al., 2009).

NDWI has been widely used as a proxy for vegetation stress during droughts (Huete & Didan, 2004; Marusig et al., 2020; Sturm et al., 2022; Xulu et al., 2019). For instance, Anderson et al. (2010)examined the impact of the 2005 drought in Amazonia through VIs and climatological variables correlations. They revealed that NDWI shows a significant

inverse correlation ($P < 0.09$) with tree mortality. Sturm et al. (2022) used NDWI to examine pre-drought conditions, resistance during a drought, and post-drought recovery of temperate forests in Central Europe. Results showed a decline in index values (i.e., the decline in water content) during the drought, highlighting low-resistance areas. So, NDWI's response to a drought event is prompt.

Mediterranean forests are characterized by an open canopy, resulting in a considerable influence of soil and understory vegetation on the reflected signal from the top of the canopy using mid-spatial resolution data. To help with that, there is an auspicious approach, Spectral Unmixing or Spectral Mixture Analysis (SU or SMA), which is widely used in hyperspectral RS but can also be implemented with multispectral data. It is capable of breaking down a blended pixel's spectral signal into a set of fractional abundances (Elmore et al., 2000). So, the final output provides information on the element cover at the sub-pixel level. Thus, SU may help isolate the vegetation fraction at the sub-pixel level, eliminating or minimizing the impact of soil signal.

SU techniques have been applied to investigate various aspects of tree mortality and forest diseases using multispectral (Landsat and MODIS) and hyperspectral (AVIRIS and Hyperion) data. For instance, He et al. (2019) examined disease-caused tree mortality in the areas of oak forests in the Western United States using SU to extract sub-pixel disease presence using yearly Landsat data. Brewer et al. (2017) explored change in land cover after a severe drought event in pinyon-juniper woodland of New Mexico, U.S., using the SU approach and showed its ability to map physical changes in vegetation. So, for example, a 24.6 % decline in *Pinus edulis* woodlands and a 23.8 % increase in dead *Pinus edulis* were detected. Somers et al. (2010) explored different unmixing methods for defoliation detection using Landsat and Hyperion images in the eucalyptus plantations in Southern Australia. He et al. (2020) explored green vegetation dynamics in semi-arid regions using SU with Landsat images for the 1999-2014 period and emphasized its performance in heterogeneous areas. One of the first and foremost papers comparing the results of NDVI and SU was the research done by Elmore et al. (2000) that quantified vegetation change in semi-arid environments using a Landsat time series of five years (1991-1996). Their results showed that SMA outperforms NDVI. It accurately determined the sense of change (whether it was positive or negative) of live vegetation cover.

Due to tree mortality, a structural change in the time series or a break in the pattern is expected. LandTrendr is a well-known tool for detecting land cover change over time (Z. Zhu, 2017). It makes use of so-called temporal segmentation, where the tool breaks down a time series of vegetation index into segments, each representing a distinct period of land cover change. It identifies abrupt and gradual changes to determine the boundaries of these segments and then fits the best model based on simple fitting statistics. This provides information on the magnitude and direction of change during that specific time frame (Kennedy et al., 2010). For example, Tao et al. (2023)applied the LandTrendr algorithm to identify disruptions (extreme climate events and insect outbreaks) in both planted and natural woodlands in a temperate zone of Northern China between 1985 and 2020, utilizing Landsat and Sentinel-2 satellite data. Cohen et al. (2017) compared seven forest change detection algorithms over the contiguous United States and reported that LandTrendr is more sensitive to subtle changes.

1.4. UAS data as reference data

The results obtained from the multispectral data analysis require reference data for validation. Direct in-situ observations are often the most accurate reference data for validation (Chen et al., 2023). However, very high spatial resolution data, such as imagery derived through Unmanned Aerial Systems (UAS), may increase the number of observations to complement field measurements (Alvarez-Vanhard et al., 2021). For instance, Schiefer et al. (2023) used UAS red-green-blue (RGB) imagery as ground reference data to recognize not fallen dead tree crowns automatically. Kattenborn et al. (2019) used UAS data to map invasive tree species as an alternative to field observations. Also, the study mentioned above about the spectral separability of land cover classes in

New Mexico used a four-band camera mounted on a light-wing aircraft to obtain high spatial resolution (5 cm) aerial imagery for accuracy assessment (Brewer et al., 2017).

1.5. Problem Statement

Mediterranean ecosystems are critically important due to their rich biodiversity, which is pivotal in sustaining complex ecological relationships. This type of ecosystem faces imminent threats from global warming, increased incidence of forest fires, and heightened tree mortality resulting from prolonged drought. A few research papers investigating tree mortality proved the high performance of NDVI in detecting it. However, NDVI is usually utilized as an index for live vegetation. Therefore, the particular interest is to investigate not only live vegetation but also dead tree communities and pay attention to very open (Mediterranean) ecosystems where soil significantly influences the pixel signal. NDWI has been used for drought detection and post-drought recovery in arid or temperate forest areas. Meanwhile, tree mortality detection using this index and the Mediterranean areas has yet to be explored. Additionally, time series analysis of indices for tree mortality estimation has yet to be extensively investigated. The particular interest is in comparing the performance of different vegetation indices. Here, one biomass-related index (NDVI) will be used along with a water-related index (NDWI). As stated above, NDWI's faster (than other VIs) response to disturbances will be compared to response of NDVI. SU is an option to detect subtle changes in areas of high landscape heterogeneity by disaggregating the pixel into components, even with mid-spatial resolution imagery. It has been used for tree mortality detection as an outcome of forest disease, quantifying drought-induced tree mortality areas, and exploring green vegetation dynamics in semi-arid climates. Thus, SU was not used to estimate tree mortality in Mediterranean ecosystems but mainly to detect land cover changes in other types of ecosystems. As a result of this research, the comparison of NDVI, NDWI, and SU in detecting and estimating tree mortality in the Mediterranean ecosystem will be explored. This, as well as the utilization of LandTrendr for the detection of vegetation cover changes derived from SU as a way to detect and estimate tree mortality, have not been examined before.

1.6. Objectives and research questions

1.6.1. General research objective

This study aims to identify droughts' impact on forest communities by assessing drought-induced tree mortality in Mediterranean ecosystems. High and ultra-high-resolution multispectral and RGB imagery will be used to determine the most accurate technique to evaluate tree mortality.

This study will evaluate how NDVI and NDWI perform in assessing tree mortality and if removing the influence of soil in open forests using SU techniques may improve the accuracy of tree mortality detection and estimation.

1.6.2. Specific research objectives, questions, and hypotheses

Objective 1: To compare performances of NDVI and NDWI in detecting and quantifying tree mortality using time series analysis.

> RQ1: Is there a significant difference in the performance of the two indices in detecting tree mortality?
>
> H_1: There is a significant difference between the two VIs.
>
> RQ2: Is there any relationship between the magnitude of the drop and the percentage of tree mortality?
>
> H_1: Higher drops are associated with higher tree mortality percentage.
>
> RQ3: Is there any time lag between the two VIs in detecting tree mortality?
>
> H_1: NDWI's responses to drought-induced tree mortality are faster than those of NDVI's.

Objective 2: To evaluate the performance of SU in improving tree mortality detection and estimation.

RQ4: What is the performance rate of SU in comparison with VIs?

H_1: SU performs better in detecting and quantifying tree mortality than VIs.

2. STUDY AREA AND DATASETS

2.1. Study area

The above research hypotheses will be investigated in Lefka Ori National Park in Crete, Greece. Specifically, the south slopes of the Lefka Ori (White Mountains) massif in the southwest of Crete Island (Figure 1). This region is a vivid example of forest communities in Mediterranean ecosystems of semi-arid regions, and it might be considered the limit of having a forest in the Mediterranean ecosystem. This area's most common tree species (*Pinus Brutia*) is one of the most drought-resilient tree species (Christopoulou et al., 2022). Consequently, it dominates the driest forest zone throughout Lefka Ori.

Tree mortality typically happens some years after a drought. So, those tree communities experience various mortality rates in the following years after the drought starts. In the case of ubiquitous tree mortality there is a massive threat of losing forest communities here and thus turning into a desert. The area is part of Samaria National Park, the UNESCO MAB reserve, and the Natura 2000 site. The reserve management is highly concerned about desertification, i.e., the shift from open forest to shrubland.

The mountain range covers an area of approximately 1100 km^2. The southern section of the massif, which descends sharply into the Libyan Sea, exhibits a steep and rugged terrain in contrast to the gentler landscape of the vast northern foothills (Vogiatzakis et al., 2003).

The climate of Crete is categorized as warm and semi-arid. The annual precipitation at the lower elevations of the White Mountains is 450 to 600 millimetres. Nevertheless, higher elevations are the wettest place on the island, where average annual precipitation up to 2000 mm, primarily (80 % of the yearly rainfall) is concentrated during the months spanning November to April (Grove & Rackham, 1993; Varouchakis et al., 2018).

Lefka Ori has the highest local and regional endemism rate among the Greek mountains, hosting 22 threatened species (Strid, 1995). Calcareous woodland is prevalent throughout the Lefka Ori massif. Pines (*Pinus brutia Ten.)* occur on drier substrates, particularly on the southern slopes, where they coexist with cypresses *(Cupressus sempervirens L.)* and oaks (*Quercus coccifera L*.), growing at elevations up to 1200 m above sea level (a.s.l.) (Turland et al., 1993). The upper boundary for forest growth on the southern slopes of Lefka Ori is situated at altitudes ranging from 1600 to 1650 m a.s.l.

Grazing by sheep and goats is the most significant human influence in the Lefka Ori region. The animals are herded to the high mountain areas in spring and summer, specifically from March to October. Also, at lower altitudes, apiaries are common.

Three sites within the study area were chosen. All sites are different in terms of elevation, topography, landforms, flora, and accessibility. Site 1 is located on a higher elevation between 750-1000 m and has the steepest terrain. Also, this site is notable due to its heterogeneous tree species composition. Here, cypresses occur as often as pines and rarer oaks. On the other two sites, almost all trees are *Pinus Brutia*. Site 2 is located in mid valley region at elevation between 650-700 m and has less steep incline. Site 3 is located at an elevation between 460-650 m and is the only site which faces north (Figure 1).

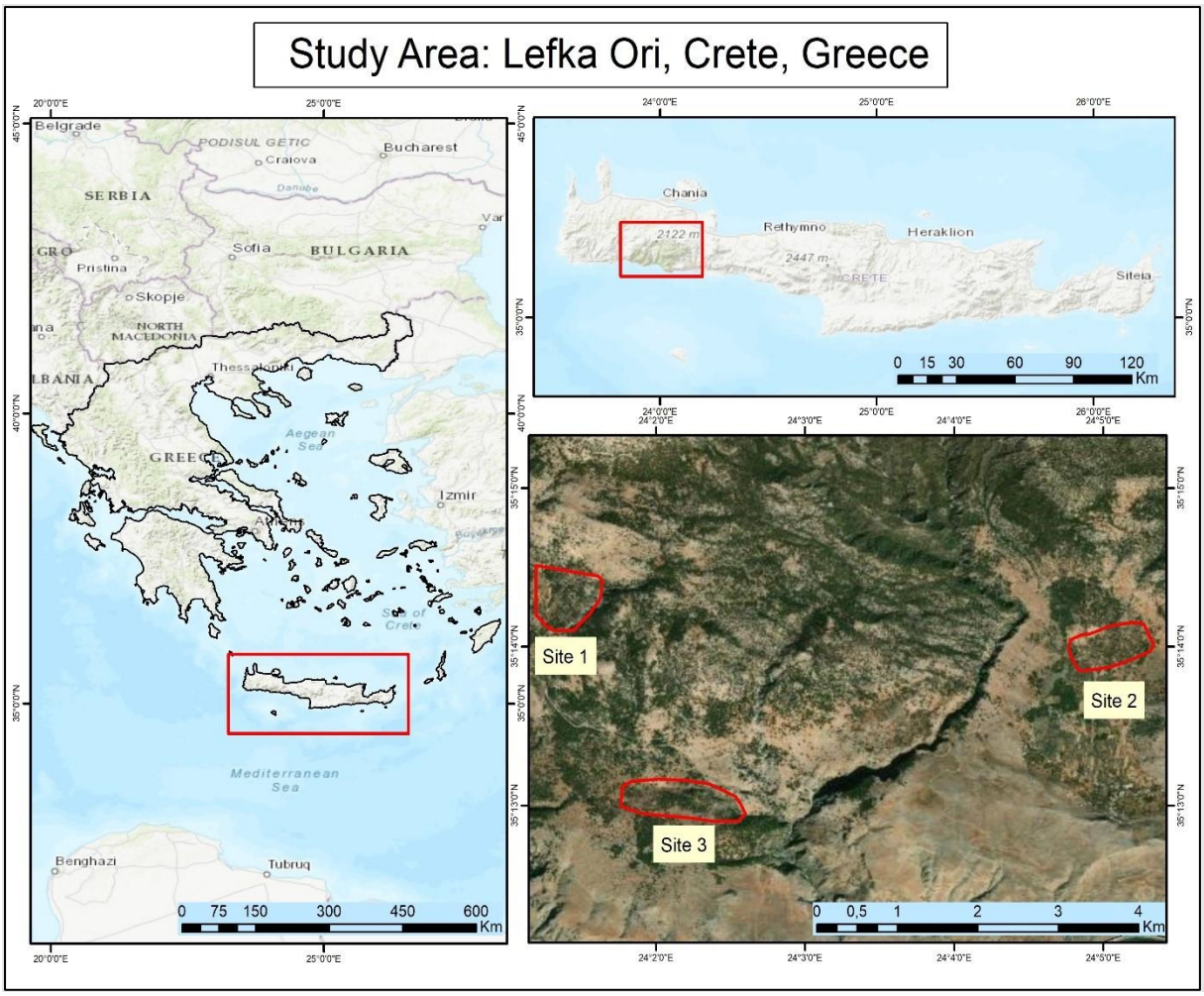

Figure 1. Location of the study area

2.2. Remote Sensing Data

2.2.1. Multispectral satellite data

This research made use of several sources of multispectral data, such as Landsat 5 TM, Landsat 7 ETM+, Landsat 8 OLI and Sentinel-2. These sources were chosen because of their convenient accessibility and spatial and temporal resolution suitable for the goals of the present study. The Landsat satellite missions have been delivering images with a spatial resolution of 30 m since April 1972 and continue to do so (P. Li et al., 2013). These satellites operate on a 16-day repeat cycle. Sentinel-2 has a spatial resolution of 10 (i.e., red and near-infrared (NIR) bands) and 20 (i.e., shortwave infrared (SWIR) bands) m and a revisiting time of 5–10 days (Soriano-González et al., 2022). Landsat and Sentinel-2 imagery were used to estimate NDVI, NDWI and SU during the study period to detect vegetation greenness and water content response to disturbances.

All the images were accessed using Google Earth Engine (GEE) cloud computing platform with names as follows:

- Landsat 5 TM: LANDSAT/LT05/C01/T1_SR
- Landsat 7 ETM+: LANDSAT/LE07/C01/T1_SR
- Landsat 8 OLI: LANDSAT/LC08/C01/T1_SR
- Sentinel-2 Top-of-atmosphere reflectance: COPERNICUS/S2_HARMONIZED
- Sentinel-2 Surface reflectance: COPERNICUS/S2_SR_HARMONIZED

2.2.2. Unmanned Aerial System (UAS)

UAS data was collected using 'DJI Mavic 3M'. Its high spatial resolution RGB camera is able to capture very ultra high-resolution images (20MP), which is highly beneficial for the objectives of this study. Additionally, this drone is equipped with a Real-Time Kinematic Global Navigation Satellite System (RTK GNSS) that provides a few centimetres level precision positioning. At the same time, surveying and allows it to produce georeferenced images right after taking them. Furthermore, 'DJI Mavic 3M' has a terrain follow feature that uses sensors at the bottom. That allowed us to fly a drone in the area of uneven terrain without additional efforts of using digital elevation models.

UAS settings during the flights were: flying height is 100 m above ground level, speed is 6.7 m/sec, the front overlap is 85 %, and side overlap is 75 %. A total of 1192, 952, and 1010 images for sites 1, 2 and 3, respectively, were collected. The spatial resolution of the created orthomosaics is 3.26, 3.14, and 3.13 cm for sites 1, 2, and 3, respectively.

2.3. Field observations

The fieldwork was conducted in late August – early September 2023 and lasted for nine days. Data from 33 plots spread across all three sites were collected (Figure 2). Each plot is a 30x30m square. The centres of plots correspond to the centres of Sentinel-2 pixels.

The information collected for each plot was:

- the location of the centre of a plot and four edge points using RTK GNSS,
- for each tree
    - species name,
    - diameter at breast height (DBH),
    - defoliation and discolouration status (where '5' means dead tree),
- pictures of the plot.

Defoliation status and discolouration status were described following the 'Manual for visual assessment of forest crown condition' by the Food and Agriculture Association of the United Nations (FAO, 2014).

Site 1 has 12 plots (plots IDs are from 22 to 33), site 2 has nine plots (plots IDs are from 1 to 8), site 3 has 13 plots (plots IDs are from 9 to 21). More observations are taken from sites 1 and 3 to account for their variable topography. The maximum number of trees observed within one plot is 53, and the minimum is 3. Site 2 has the highest variety of number of trees per plot from 11 trees in plot 3 to 53 tress in plot 2. On the contrary, the number of trees per plot on site 3 varies from 3 to 28 (Figure 3). Tree density is higher on sites 1 and 2 because they tend to have more trees per plot than on site 3 (Figure 4). The percentage of tree mortality on site 3 is higher than on other sites. So, dead trees there cover between 30 percent and up to 79 % of all trees on the plot. Additionally, pines homogenously cover site 2, while site 1 has a vast number of cypresses spread across the whole area (Figure 5). Also, a small number of oaks were found on some plots.

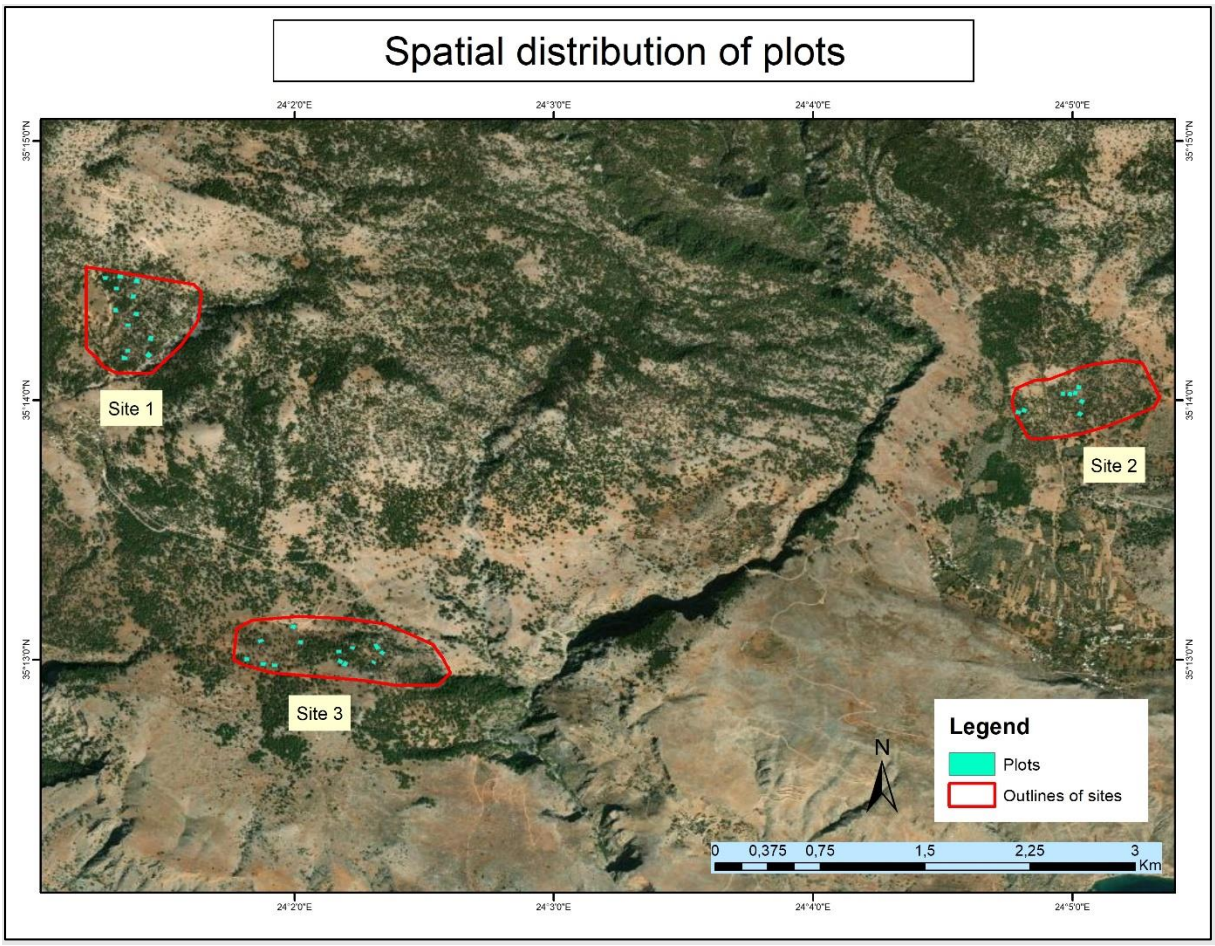

Figure 2. Location of the plots within the study area

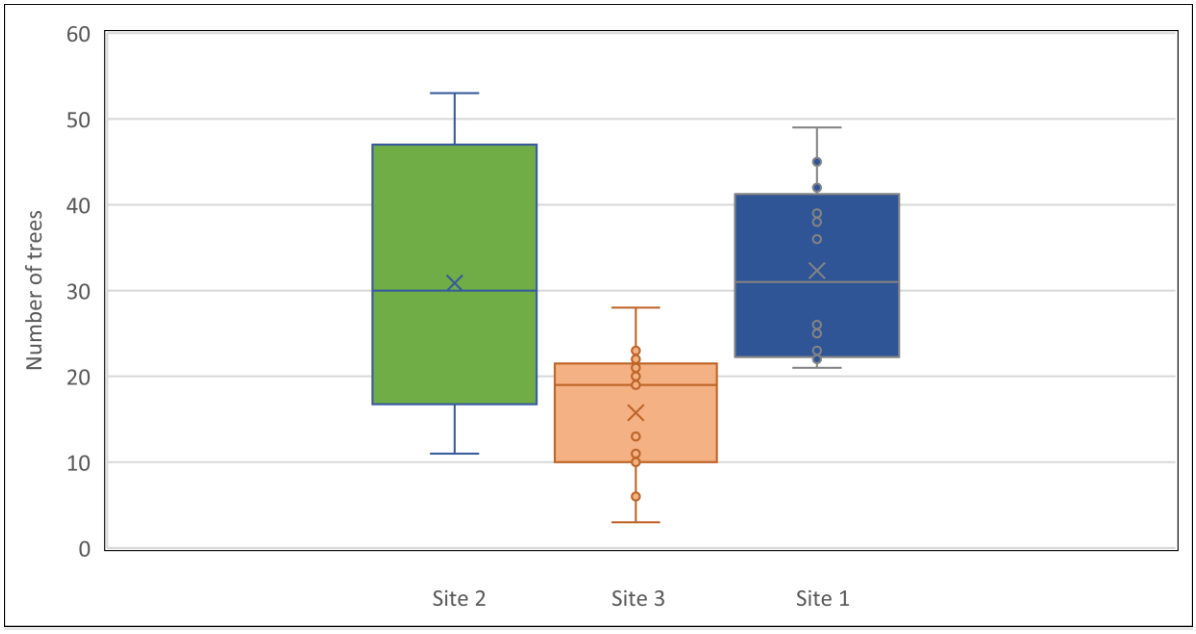

Figure 3. Box plots illustrate how many trees all the plots have within each site

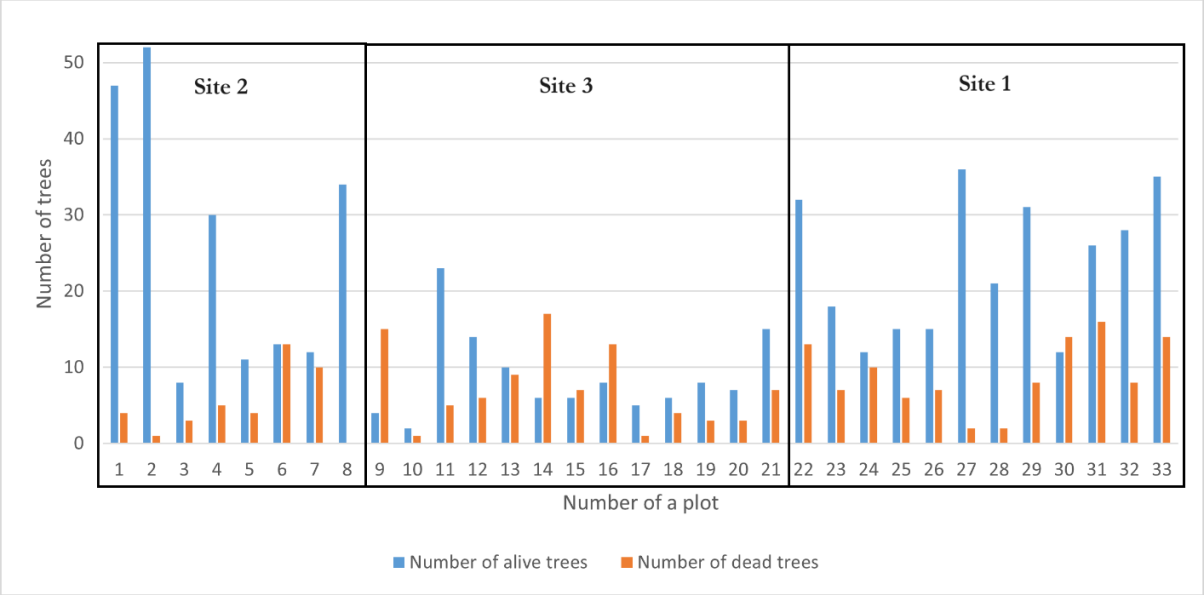

Figure 4. Distribution of alive and dead trees across plots

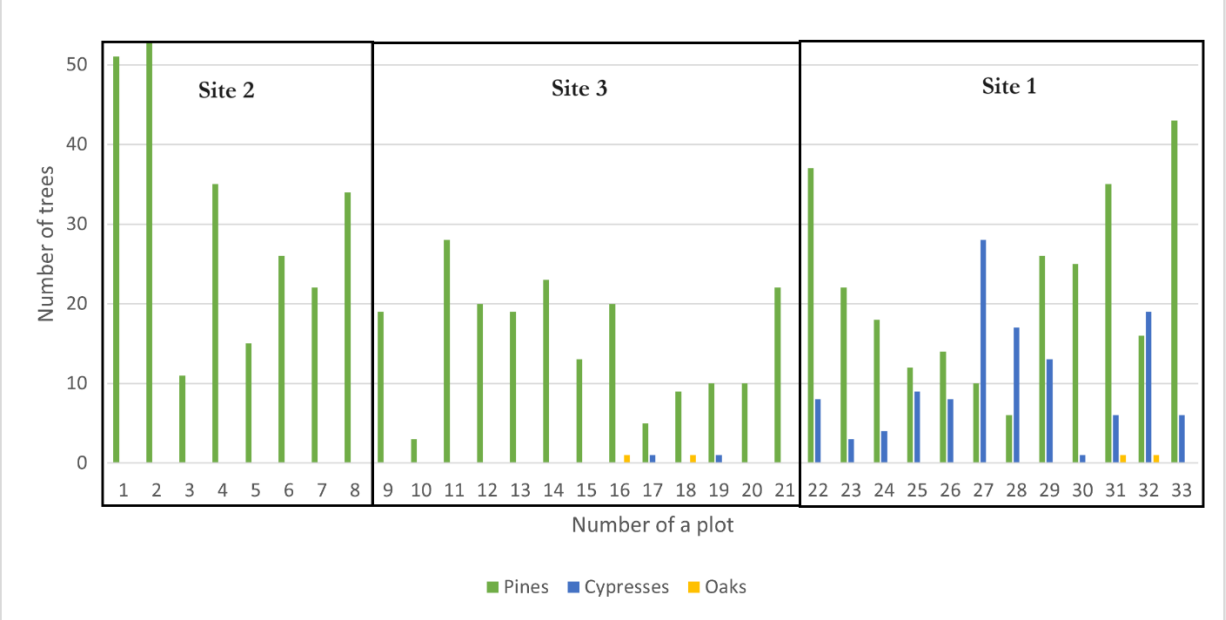

Figure 5. Distribution of tree species across plot

3. RESEARCH METHODS

This section outlines the steps required to carry out this research. The methodology was divided into three main phases to align with the research goals. A flowchart of the overall methodology can be seen in Figure 6.

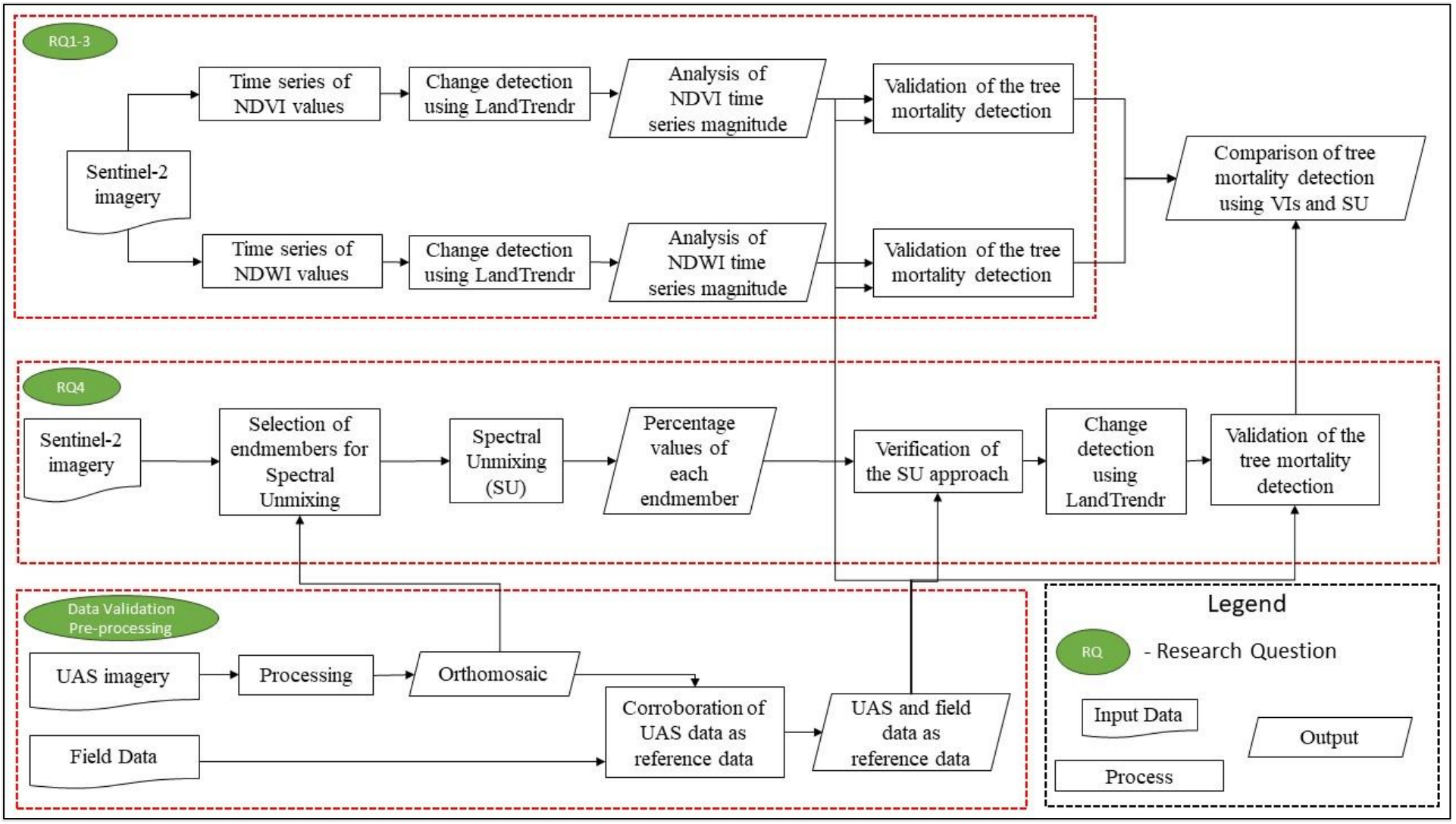

Figure 6. The flowchart of the overall methodology used for this research

3.1. Ortho-rectification and mosaicking of UAS imagery

UAS drones take pictures of the surface sequentially, following a flight plan. The outcome data of the flight is some number of images and not one image covering a big area as if it were satellite imagery. This happens due to the drone's relatively much smaller flying height and consequently much more limited field of view. That is why there is a need to create a mosaic. Mosaicking is stitching multiple UAS images together in one whole image of the study area. It is done with the help of the geolocation that every image has, and side and front overlap images have between each other.

The acquired aerial images can exhibit geometric distortions, such as stretching, squeezing, and twisting in certain areas, due to factors like sensor instability and atmospheric conditions (Zhang et al., 2023) that can affect UAV aerial photography operations. Consequently, it is essential to perform geometric ortho-rectification before creating a mosaic of the aerial images. This process corrects these distortions and aligns the imagery with their actual positions.

The UAS images collected were processed using the Pix4Dmapper software, designed specifically for photogrammetry and geospatial applications utilizing UAS imagery. It performs ortho-rectification and mosaicking automatically and results in a useful orthomosaic.

3.2. Calculation of NDVI & NDWI

The calculation of NDVI and NDWI, as well as creating their times series, were executed using Sentinel-2, Landsat 5, 7 and 8 imagery using GEE.

NDVI was calculated according to the formula given by Rouse et al. (1974):

$$\text{NDVI} = \frac{(NIR\ band) - (red\ band)}{(NIR\ band) + (red\ band)}$$

Where NIR band corresponds to the bands 8, 4, and 5 of Sentinel-2, Landsat 5/7 and Landsat 8 respectively and red band corresponds to bands 4, 3 and 4 of Sentinel-2, Landsat 5/7 and Landsat 8 respectively.

NDVI values are dimensionless and range from -1 to 1, where negative values correspond to water bodies, values from 0 to 0.25 for the soil without vegetation, and values from 0.25 to 0.4 show soil with sparse vegetation. Values more than 0.4 correspond to vegetated surfaces. Values closer to 1 represent dense canopies and strong vegetation vigour (Filgueiras et al., 2019).

NDWI was calculated according to the formula given by Gao, 1996:

$$\text{NDWI} = \frac{R\ (842) - R\ (1610)}{R\ (842) + R\ (1610)}$$

Where R (842) imply reflectance in the wavelength of 842 nm (corresponds to NIR bands 8, 4, and 5 of Sentinel-2, Landsat 5/7 and Landsat 8, respectively) and R (1610) imply reflectance in the wavelength of 1610 nm (corresponds to SWIR bands 11, 5 and 6 of Sentinel-2, Landsat 5/7 and Landsat 8 respectively).

NDWI values are dimensionless and range from -1 to 1. High NDWI values indicate high vegetation water content and high vegetation fraction cover. Conversely, lower NDWI values signify low vegetation water content and low vegetation fraction cover. During periods of water scarcity or stress, NDWI is expected to decline.

3.3. Change detection using the LandTrendr algorithm

The change detection approach LandTrendr applied to the Landsat time series was used to detect significant changes in the time series at the pixel level. LandTrendr typically provides information about when and where changes occurred, as well as about the

magnitude of the change. It has the ability to identify sudden and gradual shifts and patterns within the annual time series. LandTrendr has been adapted for use on the GEE platform, simplifying data management and ensuring prompt algorithm processing. This leverages cloud-based processing to efficiently monitor forest disturbances, making the process less time-intensive and more effective.

LandTrendr is a pixel-based algorithm used to analyse how the values of a pixel change over time in a sequence of connected straight segments. Breakpoints or vertices define these segments and represent the annual behaviour of the pixel in a time series (Kennedy et al., 2018). The algorithm follows a two-step process for temporal segmentation. Firstly, it identifies candidate vertices through iterative anomaly detection to locate breakpoints that distinguish periods of significant change and stability in the spectral trajectory over time. Once the vertices are identified, the algorithm connects straight segments and fits them to the observed spectral values using linear regression, ensuring the segment is anchored between two vertices. The best-fitting segment is iteratively calculated to determine the most suitable representation of the time series using linear regression from vertex to vertex, establishing the best-fitting straight-line trajectory across the vertices (Cohen et al., 2018). In each iteration, a goodness-of-fit statistic is estimated to adjust the vertices and segments to the spectral values, resulting in spectral segmentation. The outcome for each pixel is a fitted trajectory with a set of vertices and segments that reveal information about distinct phases in the data over time (Kennedy et al., 2010). The temporal segmentation process yields a set of metrics, including the duration of change, the year when the change occurs, and the magnitude of disturbance.

This research made use of the LandTrendr JavaScript module in GEE developed by Kennedy et al. (2018) for detecting changes in VIs time series. LandTrendr JavaScript module uses USGS Landsat Surface Reflectance Tier 1 datasets. Clouds, cloud shadows, snow and water were masked out, which is done automatically using the findings of Zhu et al. (2015). The algorithm has to have one spectral value per pixel for each year. Annual composite images are created utilizing a medoid approach. For each pixel in a given image, the medoid represents the band value that is numerically closest to the median of corresponding pixels across all considered images within a specified annual data range. Annual medoid compositing incorporates Landsat 5 TM and Landsat 7 ETM+ data without modification. However, for Landsat 8 OLI images bands 2, 3, 4, 5, 6, and 7 are subset and adjusted to match the spectral characteristics of ETM+ bands 1, 2, 3, 4, 5, and 7, respectively. This step is necessary due to newly introduced bands in the Landsat 8 OLI sensor, which do not exist in previous Landsat sensors. This adjustment is achieved using slopes and intercepts derived from reduced significant axis regressions, as detailed in Roy et al. (2016).

To compare changes in VI's and SU's time series, the same change detection algorithm needs to be used. To do so, a novel approach was made based on the existing LandTrendr script in GEE. That script was complemented by creating time series of SU's outputs containing a percentage of vegetation per pixel, and after that, it detects changes using the original LandTrendr technique.

LandTrendr uses different criteria to control the temporal segmentation process. The values used to run this tool were fine-tuned during the iterative procedure of (1) finding the best fit (using Root Mean Square Error (RMSE)) between the spectral trajectory and the temporal segmentation and (2) experimenting with different values to observe how they impact the segmentation results visually. These criteria are:

- 'maxSegments' determines the maximum number of temporal segments that the algorithm will attempt to identify for each pixel in the time series. This can be useful for capturing different phases of vegetation growth, disturbance, or recovery. Each segment represents a distinct temporal trend or change in the vegetation signal. If data has frequent and complex changes in vegetation dynamics, setting a higher value (e.g., ten or higher) might be appropriate. Here, this value was set to 6.
- 'spikeThreshold' determines how sensitive the algorithm is to rapid changes or spikes in the time series. A higher value (e.g., 0.8 – 1) makes the algorithm less

sensitive to sudden changes. This setting is helpful if filtering out short-term fluctuations and focusing on larger, more sustained changes in vegetation are needed. Here, this value was set to 0.9.

- 'vertexCountOvershoot' influences the level of detail in the detected segments. A higher value allows the algorithm to use a more detailed representation of the temporal trends in the data to capture fine-scale changes or rapid fluctuations. Setting a value '3' (which was used here) means that the initial number of vertices used in the segmentation process can be exceeded by up to three times during the optimization process.
- 'preventOneYearRecovery' was set to 'true'. It prevents the algorithm from detecting recovery within a single year as a separate segment. This can be useful to avoid detecting short-term fluctuations as significant changes.
- 'recoveryThreshold' determines the threshold for detecting recovery in the time series. It represents the proportion of the range between the minimum and maximum values of the time series that the recovery segment must cover. Setting a value to '0.25' (which was used here) means that the recovery segment must cover at least 25% of the range between the minimum and maximum values to be considered significant.
- 'pvalThreshold' sets the significance level for the statistical test used to determine whether a segment is significant. A lower value makes the algorithm more stringent when considering a segment as a substantial change. A used value of 0.05 implies that the algorithm requires relatively statistical solid evidence to consider a segment as a significant change.
- 'bestModelProportion' determines the proportion of the best model to use when constructing the final segmentation. The used value of 0.75 implies that it gives more weight to the model which the algorithm considers the most representative and makes the segmentation more robust to outliers or noisy data by reducing the influence of less optimal models.
- 'minObservationsNeeded' specifies the minimum number of observations required for a pixel to be included in the analysis. Pixels with fewer observations than 6 (which was used here) will not be processed by the LandTrendr algorithm. Requiring a minimum of 6 observations ensures that only pixels with a relatively substantial amount of data are considered in the analysis. This can enhance the reliability of the results by excluding pixels with sparse or incomplete time series.

A specific timeframe (June 1st to August 31st) for selecting images was chosen to depict dry summer conditions caused by a lack of summer rainfall and to reduce within-year fluctuations in the captured conditions.

3.4. Spectral Unmixing Approach

The typical approach for addressing the mixed pixel issue is SU. This process contains the decomposition of the spectrum of a pixel into two main components: a collection of endmembers and a set of fractions (abundances) that correspond to these endmembers. These abundance values essentially represent the fractional coverage, indicating the proportion of each endmember present within the target pixel (Celik, 2023).

SU is usually carried out in two consecutive steps: (1) endmember extraction and (2) abundance estimation. Endmember extraction means deriving endmembers using pure pixels from imagery or reference data. Here endmembers were derived from Landsat multispectral satellite imagery. The endmembers selected are live vegetation (photosynthetically active vegetation) and non-photosynthetically active vegetation with bare soil. The areas for endmember selection were chosen using UAS data collected during the field campaign. Furthermore, fractional abundances were calculated using spectra of the given endmembers. SU was performed using GEE.

3.5. Validation

Corroboration of UAS data as reference data was done by comparing field observations from all 33 plots with UAS data. It was assessed whether UAS can provide information comparable to direct field observations and if it can be used as ground truth data. This allows more observations to be selected for the validation.

Tree mortality detection using three different approaches (NDVI, NDWI, SU) were verified using field observations and UAS data to increase the number of field observations. Thirty-three field plots and 30 randomly selected plots from UAS were used, making up 63 plots in total. The validation set for all approaches was the same. The validation was done using a confusion matrix.

Regression analysis was used to evaluate the relationship between two groups: (1) the magnitude of the decrease of VIs or vegetation percentage from SU and the percentage of tree mortality; (2) the magnitude of the decrease and number of dead trees. Values of the magnitude of the drop were taken from LandTrendr results for pixels corresponding to plots from the validation dataset (i.e., 63 plots). These values were compared with the number of dead trees and the percentage of tree mortality (ratio between number of dead trees and total number of trees per plot) derived from UAS data and fieldwork.

SU results were verified at the subpixel level using high-resolution UAS imagery. The validation dataset of 63 plots was used for this verification (after estimating tree mortality percentage within them using UAS data) and compared to SU results to reveal the correctness of endmembers abundances representation throughout pixels.

4. RESULTS

The results acquired using the methods described above are presented in this section. It includes corroboration of UAS imagery as ground truth data and verification of SU approach performance; examines temporal profiles of VIs; performs change detection in the times series of VIs and SU as well as its validation. Finally, it investigates the correlation between the magnitude of the drop in time series and the percentage of tree mortality.

4.1. Corroboration of UAS imagery

The regression model between field observations and UAS data was created to confirm using UAS data as ground truth data. The high R^2 value of 0.95 and low RMSE values of 2.97 suggest a strong relationship between the field observations and the UAS estimation of the number of trees per plot (Figure 7). In more than 80% of the cases (i.e., 27 out of 33), field observations for a total number of trees almost coincide with what is observed using UAS imagery. The difference between these two values is at most 1-3 trees. In 4 cases out of 33 (i.e., 12%), the difference is 4-6 trees; in another two cases (i.e., 6%), the difference is 7-8 trees. Confusion may arise when there is a high density of trees within a plot, and they grow very close to each other. In this situation, it is hard to differentiate between canopies from the top (i.e., using UAS imagery) and state how many trees are actually there (Figure 8). In these cases, usually, the number of trees in the field data exceeds a value taken from a visual assessment of UAS imagery. Another point is about counting dead trees (Figure 9). In some cases, trunks of dead trees lay down on each other or very close to each other, making it difficult to separate them visually from above. It gets even more complicated when stems of dead trees are thin and lay next to each other. Also, in some cases, dead trunks are not clearly visible because of the wide canopies of surrounding trees. It was observed in the field that sometimes people collect dry tree trunks next to each other and drag them from nearby areas to a place they were found. Consequently, it may lead to a clearer interpretation of validation results of tree mortality estimation using time series analysis.

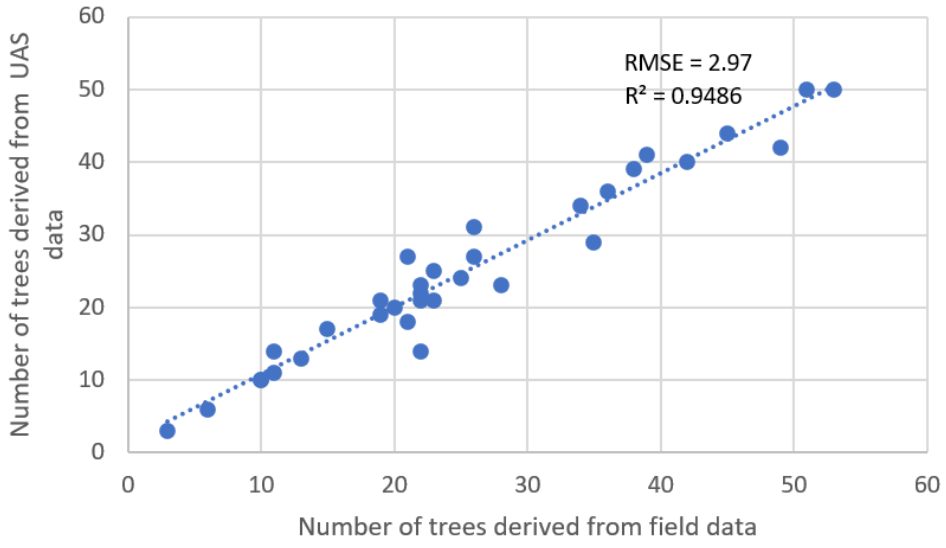

Figure 7. Linear regression chart between field and UAS estimation of number of trees per plot

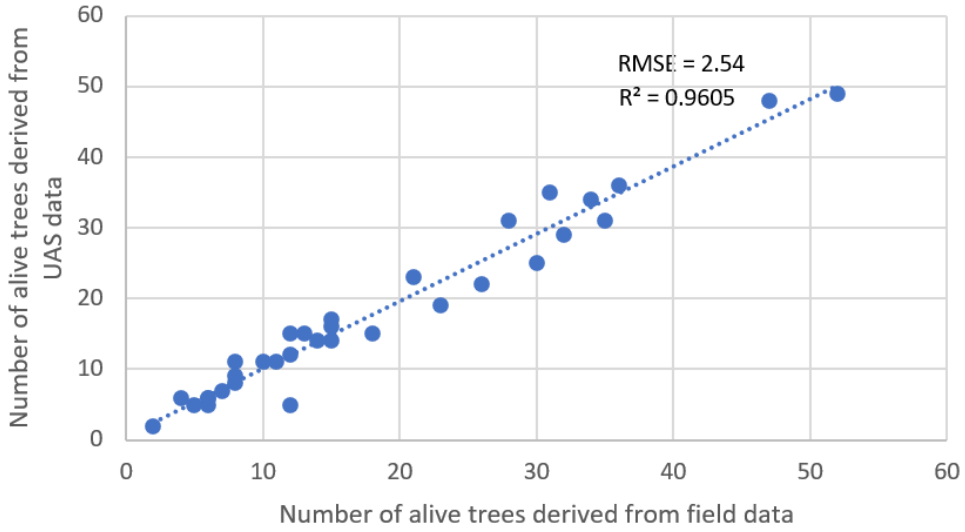

Figure 8. Linear regression chart between field and UAS estimation of number of alive trees per plot

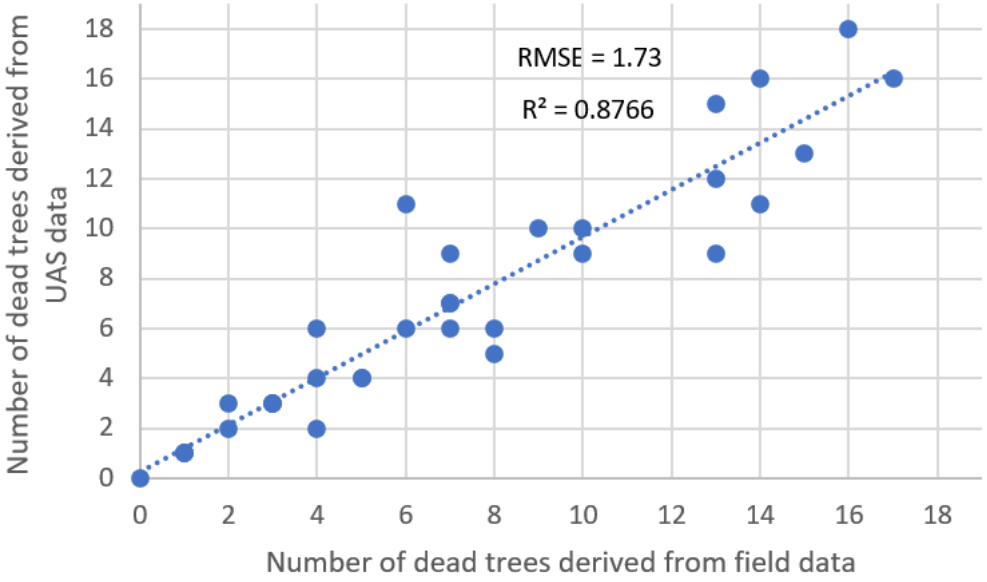

Figure 9. Linear regression chart between field and UAS estimation of number of dead trees per plot

For example, in plot 7, there were 22 trees (12 alive and ten dead) observed during the field campaign (Figure 10a), this is in agreement with what was found in the UAS visual interpretation, thus it is a good example of a coincidence between field observations and UAS imagery. On the other hand, plot 28, with 23 trees (21 alive and two dead) (Figure 10b), shows a good agreement with dead trees, but it is challenging to count 21 alive trees in this image.

a b

Figure 10. Plots 7 (a) and 28 (b) on top of UAS imagery. Red digits show dead trees and yellow digits show alive trees)

4.2. Temporal profiles of NDVI & NDWI

Plots representing different scenarios in terms of tree mortality percentage were selected to explore time series of chosen VIs (two of them are displayed in this section). Firstly, Sentinel-2 imagery was used, namely Level-1C (Top-of-Atmosphere Reflectance, available since 2015-06-23) and Level-2A (Surface Reflectance, available since 2017-03-28). No changes in the magnitude or trends of time series were detected using this type of sensor. The time series patterns remain nearly identical for plots with low and high tree mortality rates (Figures 11 and 12). Small drops were identified in the year of disturbance (November 2015 – March 2016), but during the following years, values stayed at the same high level as before the disturbance. Next, Landsat 8 OLI/TIRS Collection imagery (available since April 2013) was used for building a time series for comparison with already created time series. Time series illustrating plot with high tree mortality does not show any drops in the year of disturbance or later but in the plot with low tree mortality it is seen (Figures 13 and 14). However, the time series subsequently gets back to its regular pattern. Also, it was observed that there are lower values of VIs using Landsat than those of the same pixel using Sentinel-2 probably due to differences in the spatial resolution.

Due to the presence of dead trees on the plots and the absence of changes or drops in the time series, the mortality is expected to happen before the time span that was considered before (2015-2023). Thus, it was decided to inspect datasets available for earlier dates. Landsat 5 TM, Landsat 7 ETM+ and Landsat 8 OLI were used. Figure 15 represents a time series of NDVI values made from image collection from 1985 to 2022 for a plot with a high tree mortality rate. It shows a significant drop from 2000 to 2012 (Figure 16). This, therefore, supports the opinion of considering earlier dates and selecting a wider time frame for further analysis to be able to track the roots of the current situation of widespread tree mortality throughout Lefka Ori. Based on the analysis of the time series, severe tree mortality started around the late 1990s to the late 2000s. Mentioned earlier, datasets of three Landsat missions will be used further, covering the 1995-2022 time span.

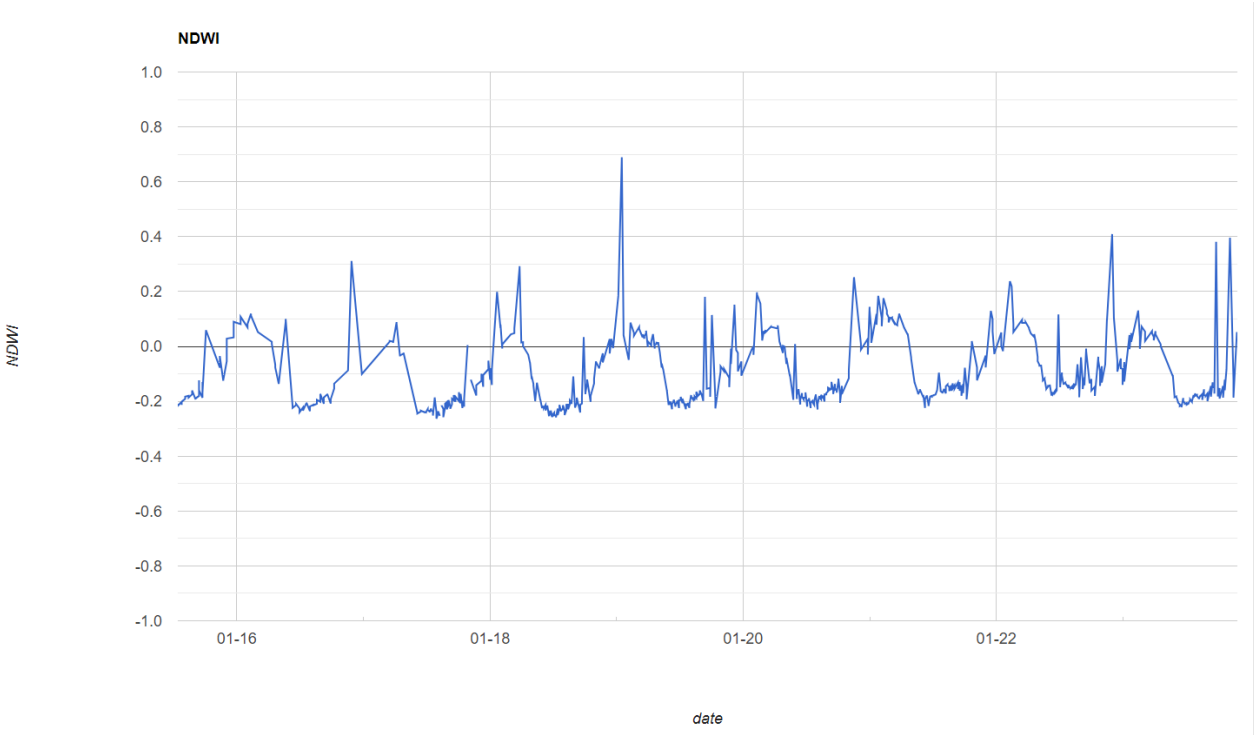

Figure 11. Time series of NDWI values for a plot with high tree mortality rate using Sentinel-2 Level-1C orthorectified top-of-atmosphere reflectance imagery

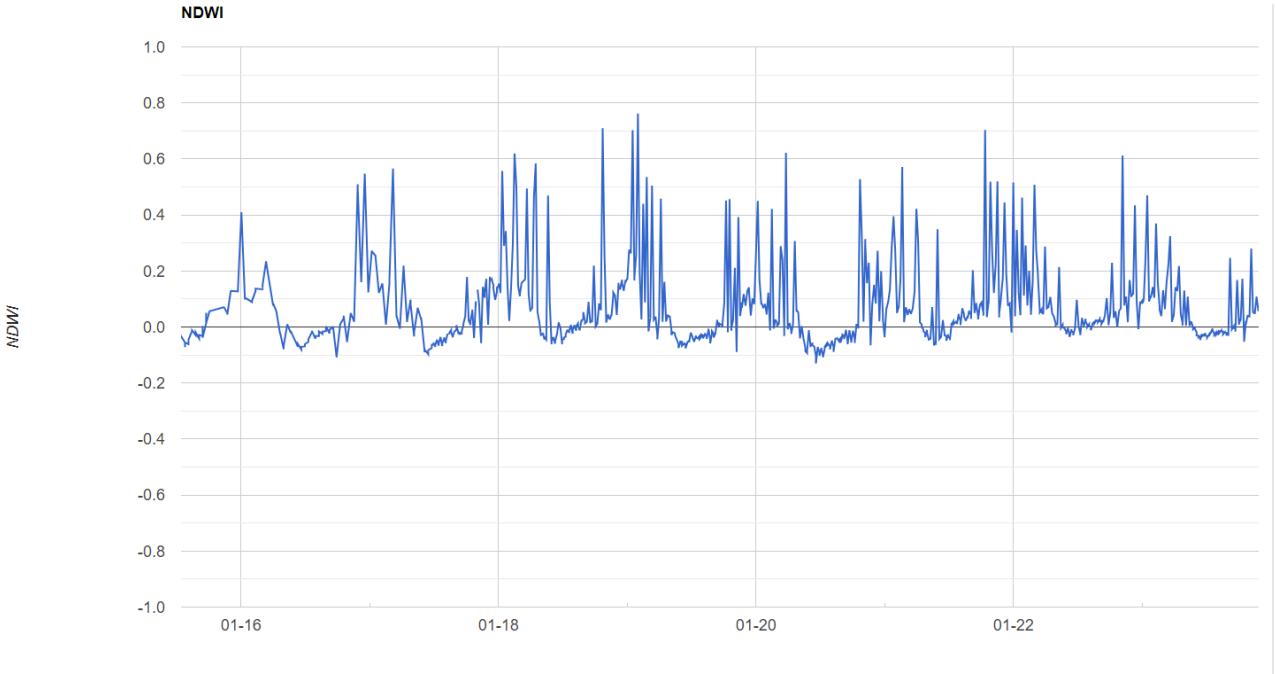

Figure 12. Time series of NDWI values for a plot with dense vegetation and low tree mortality rate using Sentinel-2 2 Level-1C orthorectified top-of-atmosphere reflectance imagery

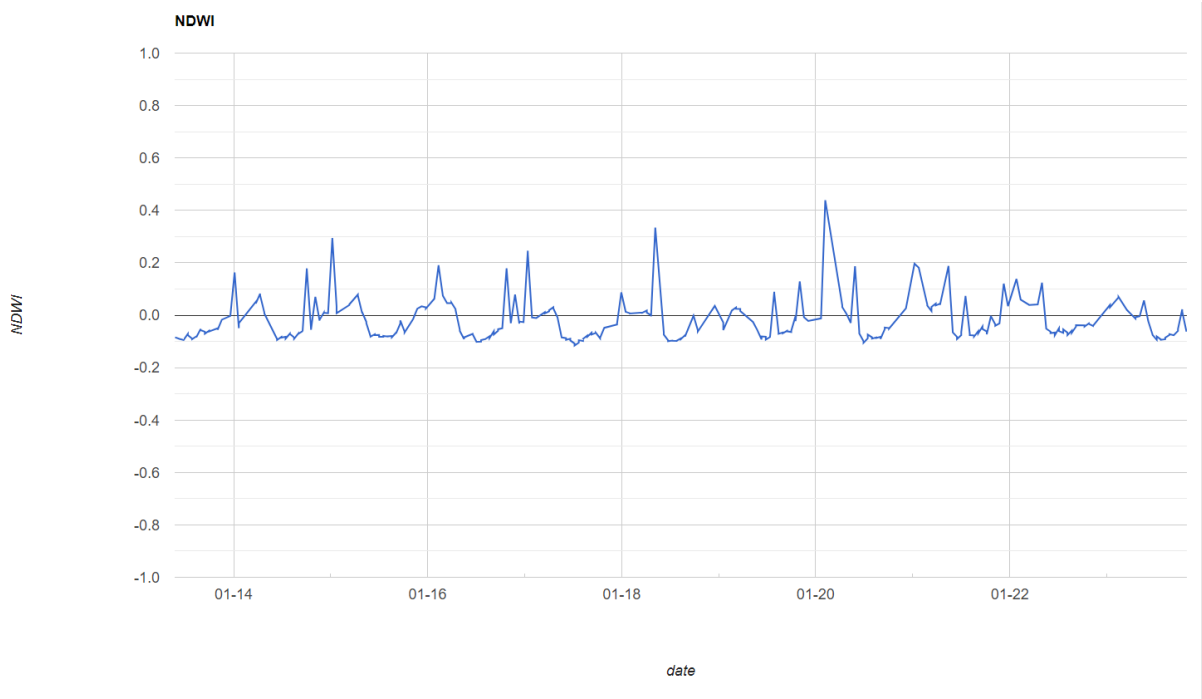

Figure 13. Time series of NDWI values for a plot with high tree mortality rate using Landsat 8 OLI atmospherically corrected surface reflectance

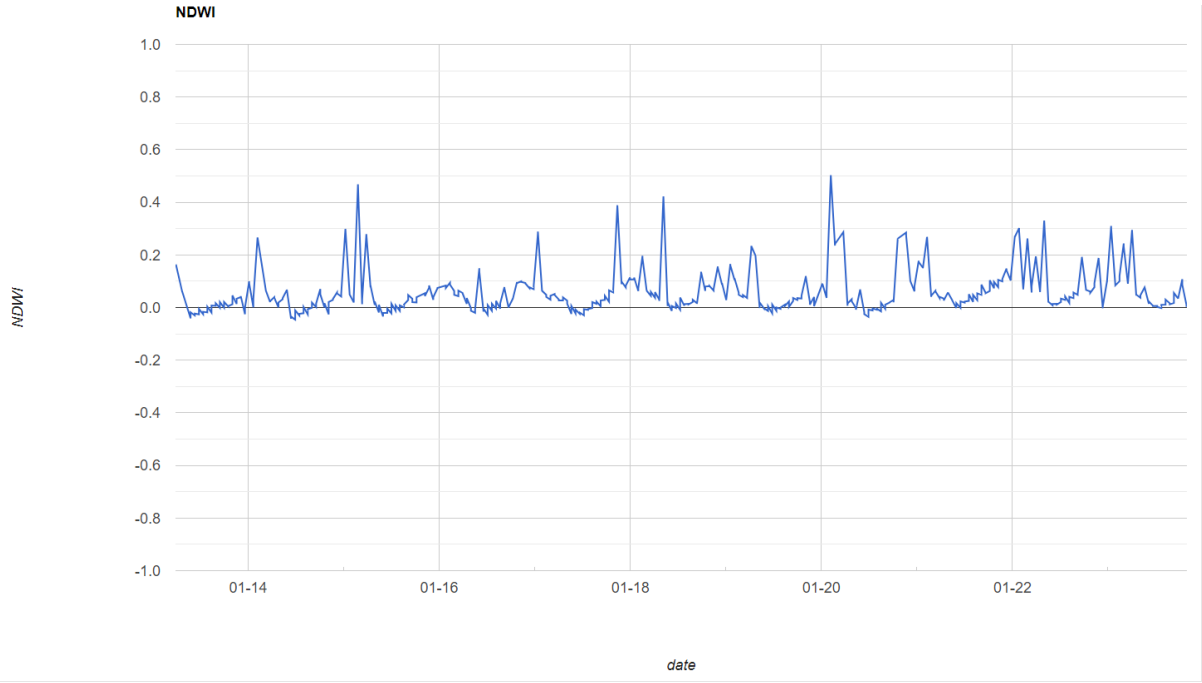

Figure 14. Time series of NDWI values for a plot with dense vegetation and low tree mortality rate using Landsat 8 OLI atmospherically corrected surface reflectance

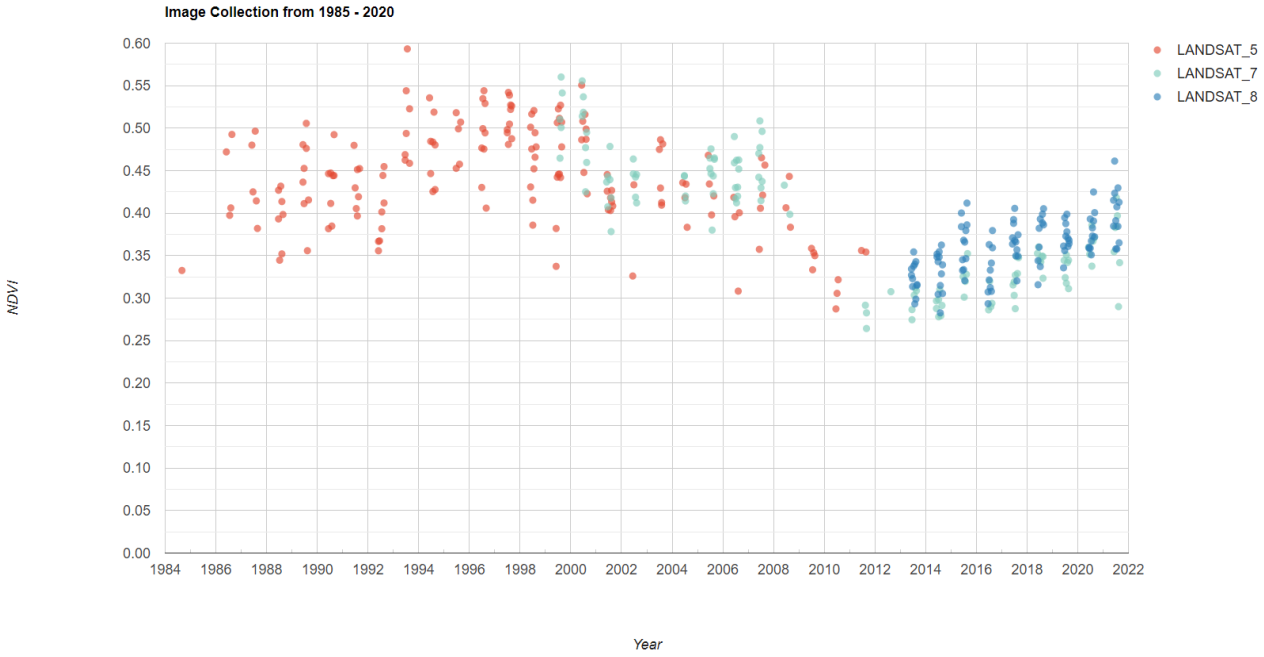

Figure 15. Image collection with calculated NDVI values for 1985 to 2022 for a plot with high tree mortality rate using datasets of Landsat 5 TM, Landsat 7 ETM+ and Landsat 8 OLI

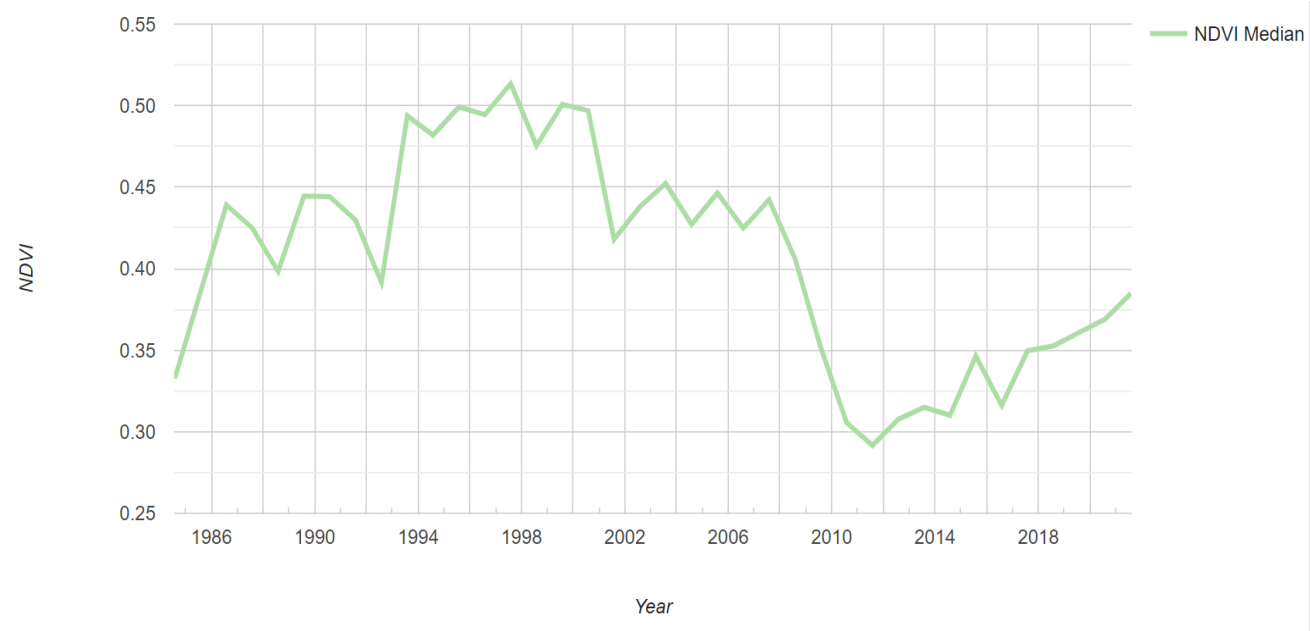

Figure 16. Annual median composite of NDVI values for 1985-2022 for a plot with a high tree mortality rate

4.3. Change detection of VIs time series using LandTrendr

Landtrendr enables the identification of land cover disturbances through temporal segmentation. By assessing the magnitude of change at the pixel level using spectral signatures, the algorithm determines the year of the change by considering the vertex of the change vector's magnitude. Figures 17 and 19 illustrate the year of detection using a

representation of NDVI×1000 and NDWI×1000 values. As you can see, most of the changes started at the beginning of the time frame chosen, 1995. Only a few patches in the south of site 3 had undergone changes in 2009-2022. Also, in these figures, the magnitude of change is shown. The majority of the pixels experienced a decrease in their values for around 100-300 points, which corresponds to a decrease in NDVI and NDWI values by 0.1-0.3. However, in general terms the magnitude of change is higher using NDWI rather than NDVI. Their temporal segmentation is seen in Figures 18 and 20. For the exclusion of non-significant changes and bare soil, pixels whose magnitude of change is more than 100 and pre-change spectral value is more than 300 (for NDVI, because values starting with 0.3 illustrate presence of vegetation) or 0 (for NDWI, because areas having values higher than 0 illustrate (some) presence of water in them and together with absence of water bodies in the area of interest highlight all the possible patches of vegetation) are only included in the Figures 17 and 19.

As seen in Figures 17 and 19, most of the changes happened between 1995-2008. To illustrate this and make the time period of significant changes more vivid, only the mentioned time period was mapped, and each year was assigned a different colour (Figure 21). Here, notable periods are 1996-1999 and 2001-2005, when major changes happened. More significant part of changes has taken place in 1996 what both VIs illustrate equally. However, greater number of patches of different colour throughout the site were detected earlier with NDWI rather than with NDVI (1996 vs 1998, 1996 vs 2000, 2002 vs 2004, etc).

To confirm the year of 1996 as the year of greatest vegetation loss and to confirm that beginning of the time period the year before (i.e., 1995) do not influence such significance of 1996, period of 1990-2008 was mapped (Figure 22). Here, it can be seen that the majority of pixels are not coloured by 1996 as it was before but shifted to later years, 1998 and 1999. If the year of change is not 1996 when the starting year of analysis moved to 5 years earlier could be explained by the influence of the beginning of the time period. Thus, we cannot rely on changes that occur at the beginning of the time series being necessary to consider some years before to confirm this change.

NDWI detected changes in 41% and NDVI detected changes in 35% of the area (NDWI detected changes in 0.23 km^2 in the area equal to 0.55 km^2, NDVI - 0.19 km^2). The calculation was made using changes that happened in 1990-2008 (Figure 22).

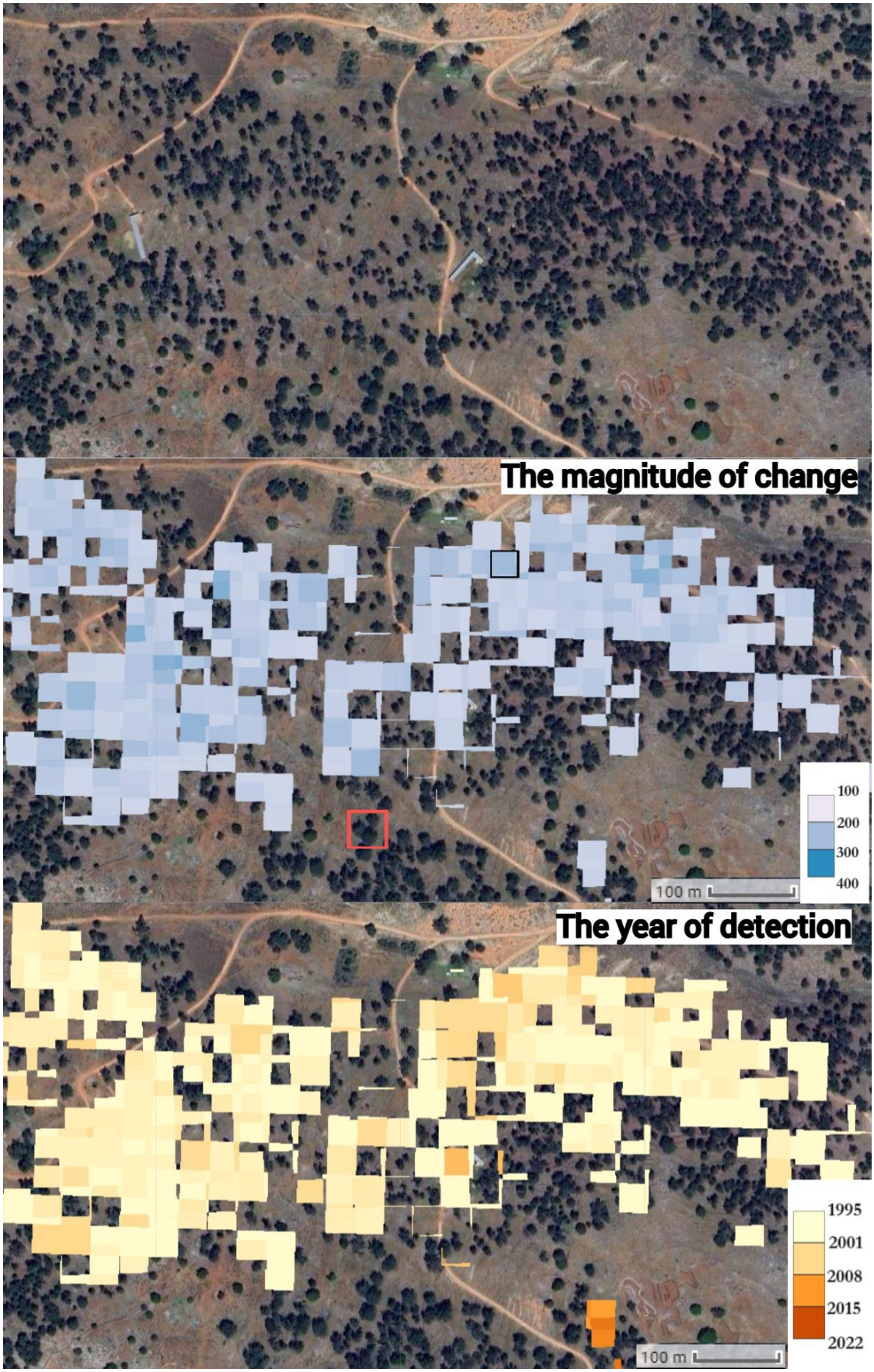

Figure 17. NDVI×1000 the magnitude of change and the year of detection for site 3 using Landtrendr

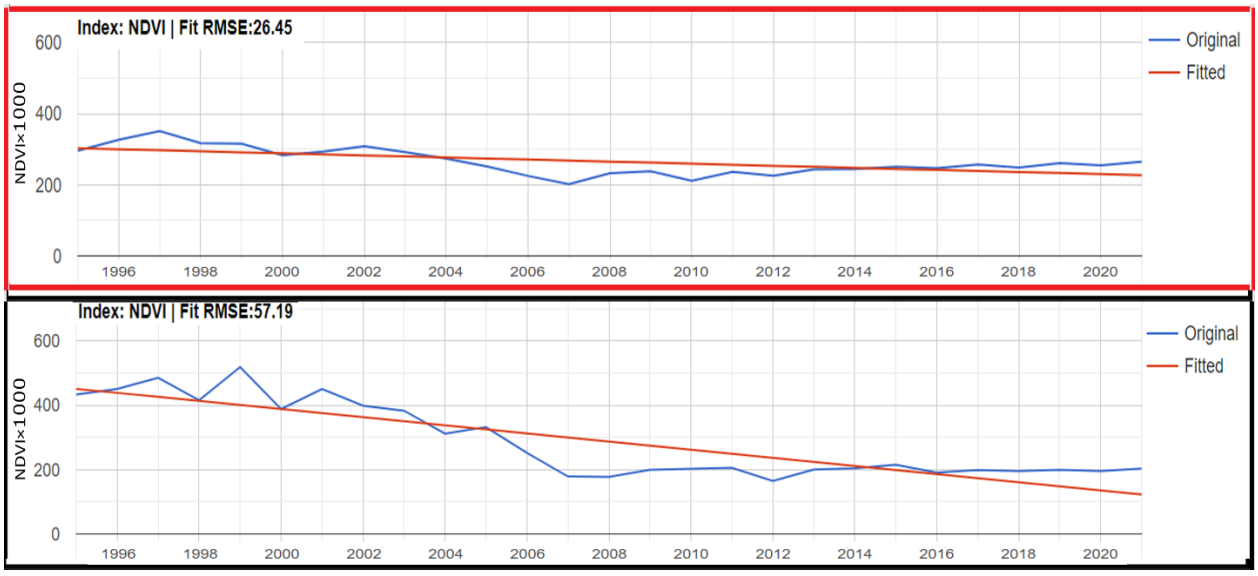

Figure 18. Temporal segmentation scheme for NDVI×1000 corresponding to the pixels in red and black squares on Figure 17 (the magnitude of change)

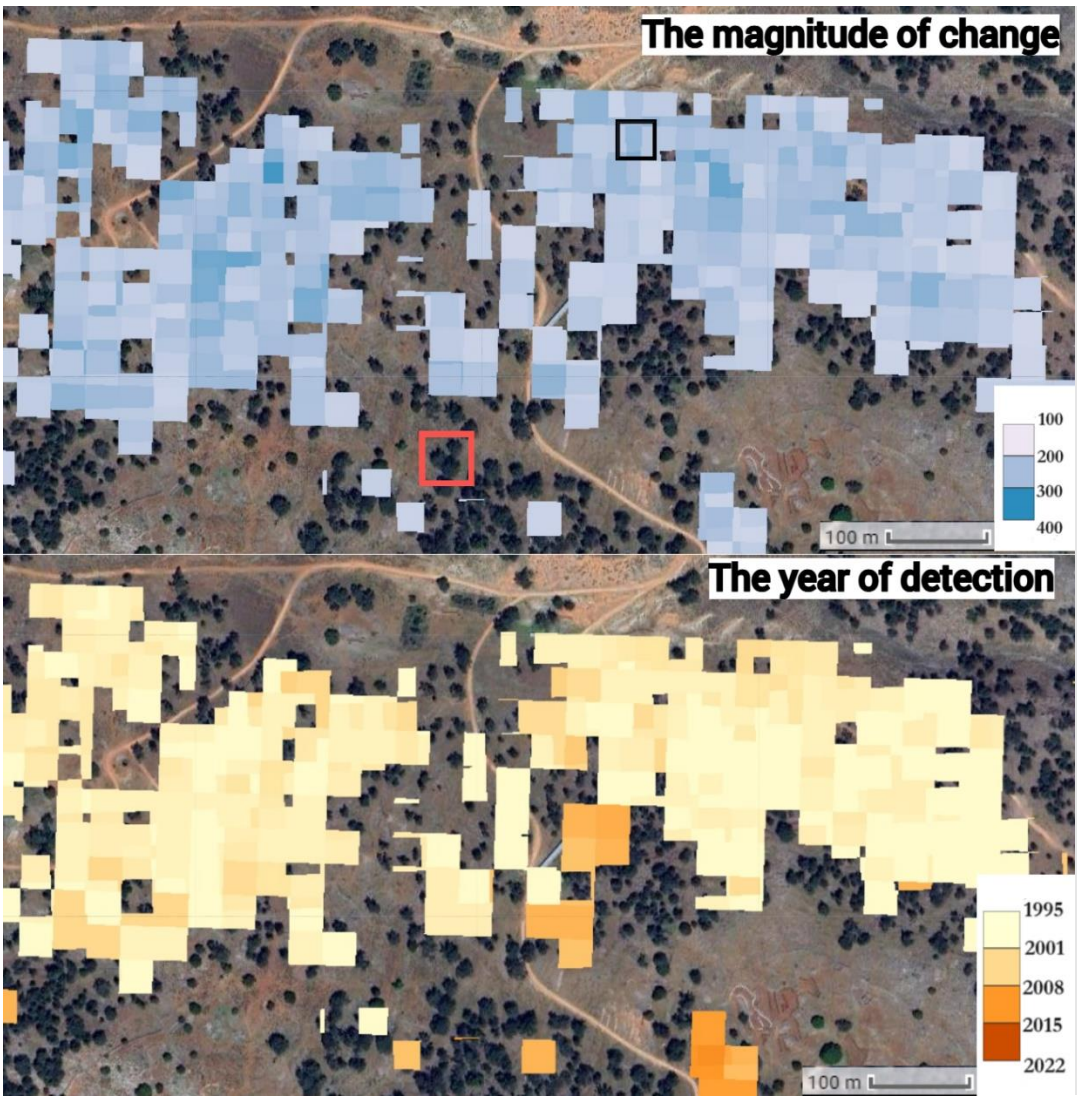

Figure 19. NDWI×1000 the magnitude of change and the year of detection for site 3 using Landtrendr

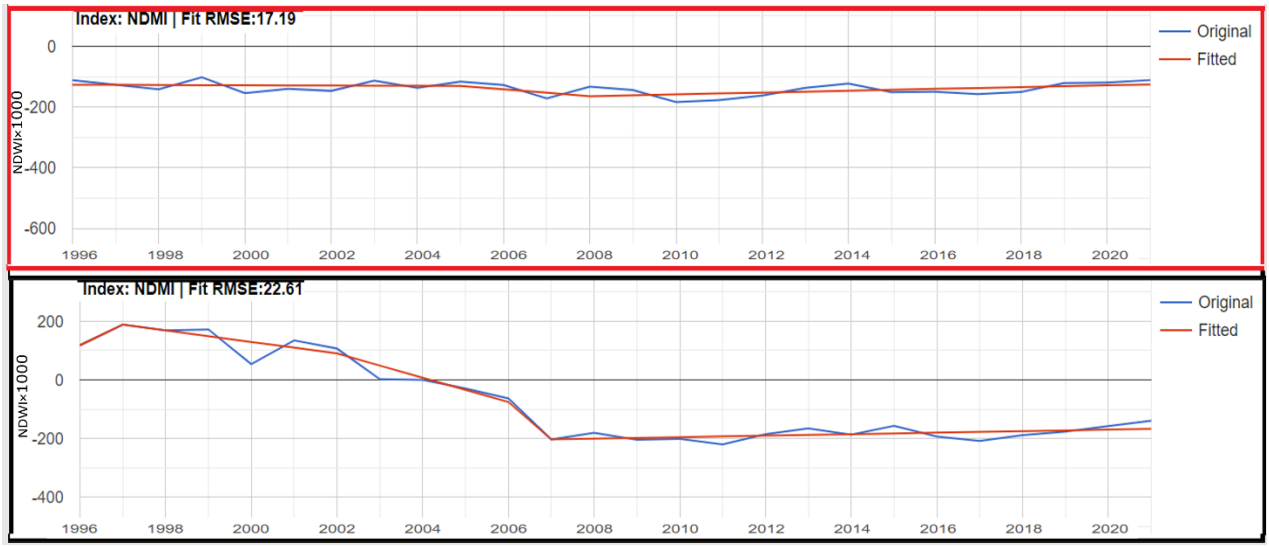

Figure 20. Temporal segmentation scheme for NDWI×1000 corresponding to the pixels in red and black squares on Figure 19 (the magnitude of change)

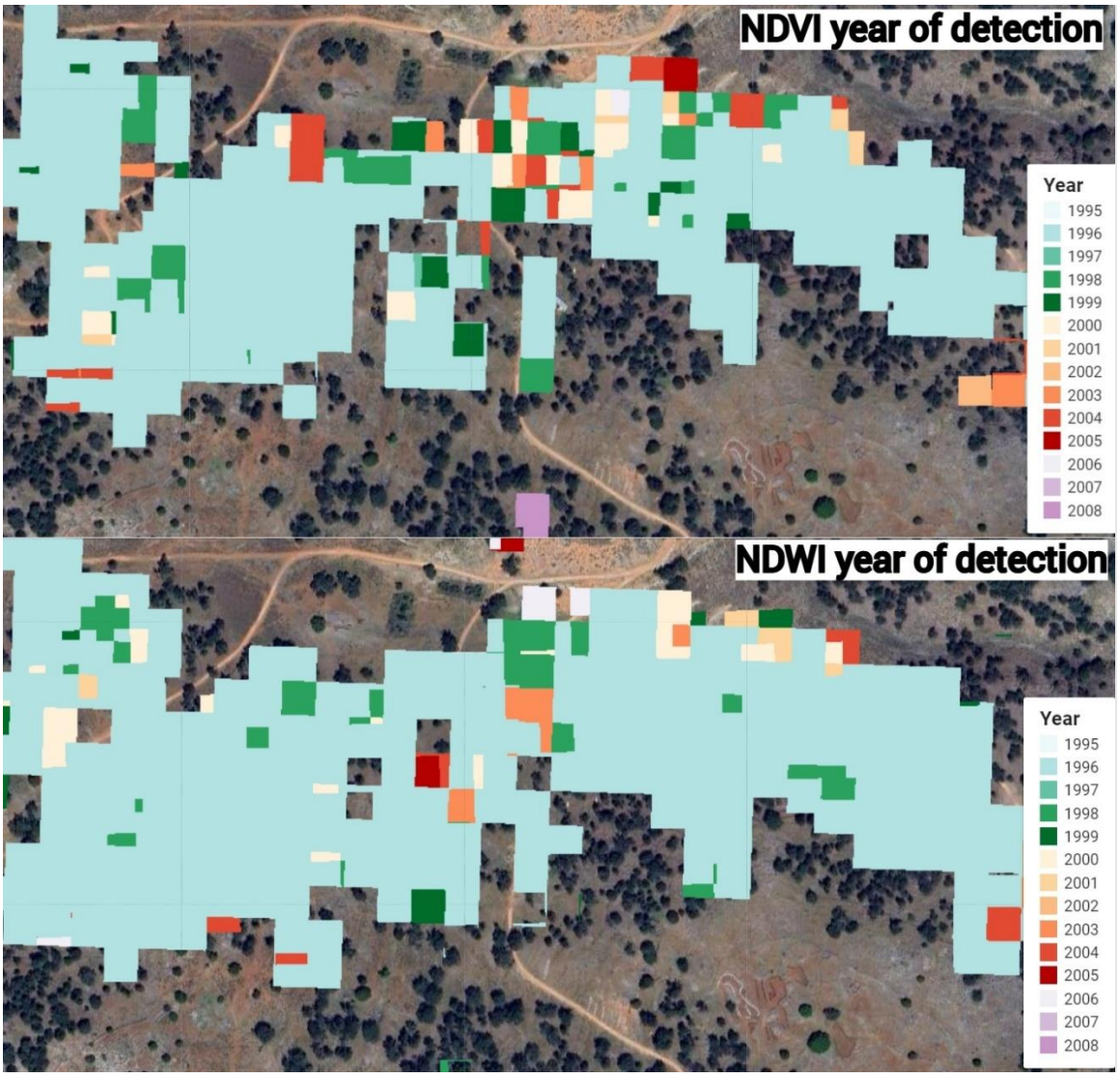

Figure 21. Changes happened in 1995-2008 for stie 3 using Landtrendr, without defined pre-change spectral value and with magnitude of change more than 100

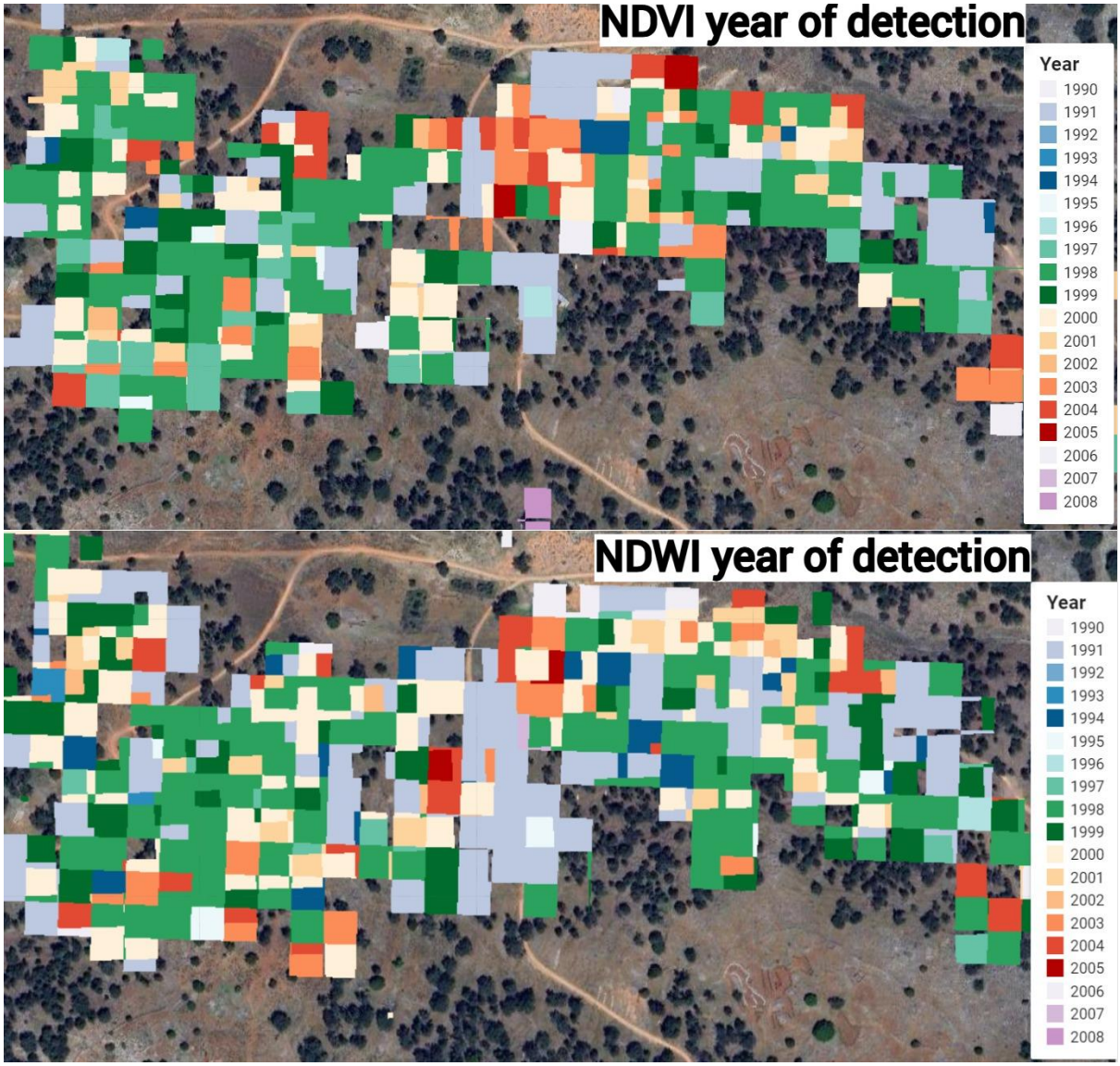

Figure 22. Changes happened in 1990-2008 for stie 3 using Landtrendr, without defined pre-change spectral value and with magnitude of change more than 100

4.4. Validation of tree mortality detection using VIs

Accuracy assessment of tree mortality detection using VIs and reference data was performed using confusion matrixes. The validation dataset consists of 63 observations, 49 of them are plots with observed tree mortality, and 14 are without. NDVI correctly showed a drop in the pixel when a tree mortality was detected in the corresponding plot for 46 observations (Table 1). NDVI correctly showed no drop in the pixel's value when there is no tree mortality detected in the plot for 11 plots. Thus, producer accuracy and user accuracy for plots with tree mortality is 93.88% and for plots without tree mortality is 78.57%. Overall accuracy is 90.48%. NDWI correctly showed a drop in the pixel when there is tree mortality detected in the corresponding plot for 45 observations (Table 2). NDWI correctly showed no drop in the pixel's value when there is no tree mortality detected in the plot for 11 plots. Thus, producer accuracy for plots with tree mortality is 93.75% and for plots without tree mortality is 73.33%. User accuracy for pixels with a drop is 91.84%, and for pixels without a drop is 78.57%. Overall accuracy is 88.89%. Consequently, the detection of tree mortality using NDVI is slightly better than using NDWI and both indices performed with the same accuracy for pixels without tree mortality.

Table 1. Performance measurement of NDVI values using a confusion matrix

Class		Validation Dataset		Total	User Accuracy
		plots with tree mortality	plots without tree mortality		
Using Vegetation Index (NDVI)	pixels with a drop	46	3	49	93,88%
	pixels without a drop	3	11	14	78,57%
Total		49	14	63	-
Producer Accuracy		93,88%	78,57%	-	OA: 90,48%

Table 2. Performance measurement of NDWI values using a confusion matrix

Class		Validation Dataset		Total	User Accuracy
		pixels with tree mortality	pixels without tree mortality		
Using Vegetation Index (NDWI)	pixels with a drop	45	4	49	91,84%
	pixels without a drop	3	11	14	78,57%
Total		48	15	63	-
Producer Accuracy		93,75%	73,33%	-	OA: 88,89%

4.5. Relationship between the VIs' magnitude of the change and tree mortality

Regression functions were used to estimate tree mortality using values of drops of VI's LandTrendr magnitude. Regression analysis was performed in two ways, using a percentage of tree mortality per plot and a number of dead trees per plot. Both of these sets of values were plotted against the VI's magnitude of the drop. Figure 23 illustrates the percentage of tree mortality and NDVI's magnitude of the drop. These values do not show a good correlation, especially among plots with high tree mortality. Only 37% of the variation is explained by this regression, and the RMSE value is also high (i.e., 56.9). When plots with tree mortality percentage higher than 80% are removed (i.e., 3 plots), 42% of variation is explained. The same plots but using NDWI values explain only 18% of the variation; RMSE value is even higher (i.e., 84.9) (Figure 24). NDWI, in general, shows higher values in magnitude of the drop than NDVI for the same plots. Regression between

the magnitude of the drop using NDVI/NDWI values and a number of dead trees show a poor correlation (Figures 25 and 26). Only 24% of the variation is explained by these regressions (RMSE = 81.3 and 106.8 using NDVI and NDWI, respectively). When plots with tree mortality percentage higher than 80% are removed (i.e., 3 plots), 35% of variation is explained. It was proved that NDVI drops are associated with tree mortality, but higher drop magnitude is not associated with higher tree mortality. A hypothesis about this association is only correct in the case of low tree mortality percentage or absence of tree mortality. So, algorithm performs well when there are only a few dead trees within the plot. In these cases, those pixels associate with no magnitude drop or very low drop.

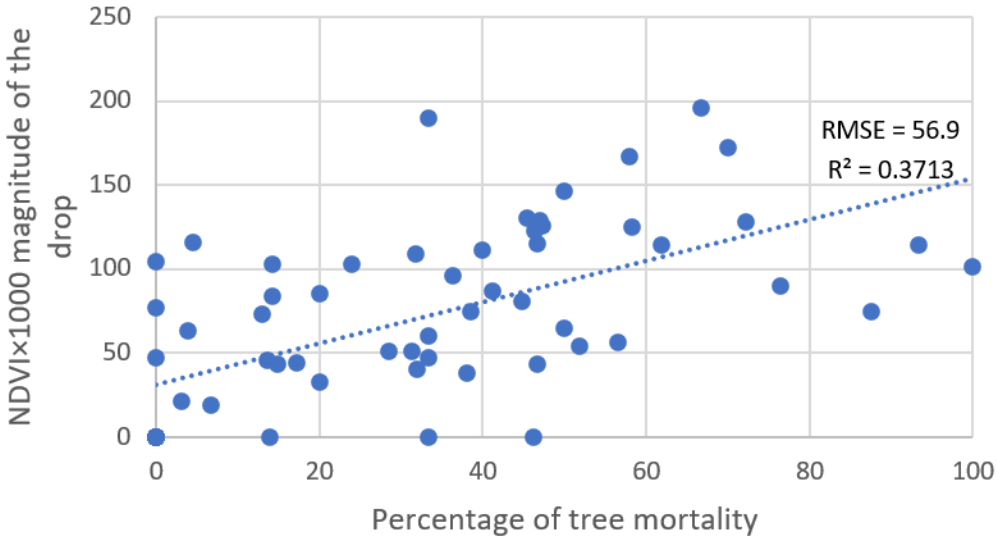

Figure 23. Linear regression between magnitude of the drop (using NDVI values) and estimation of percentage of tree mortality

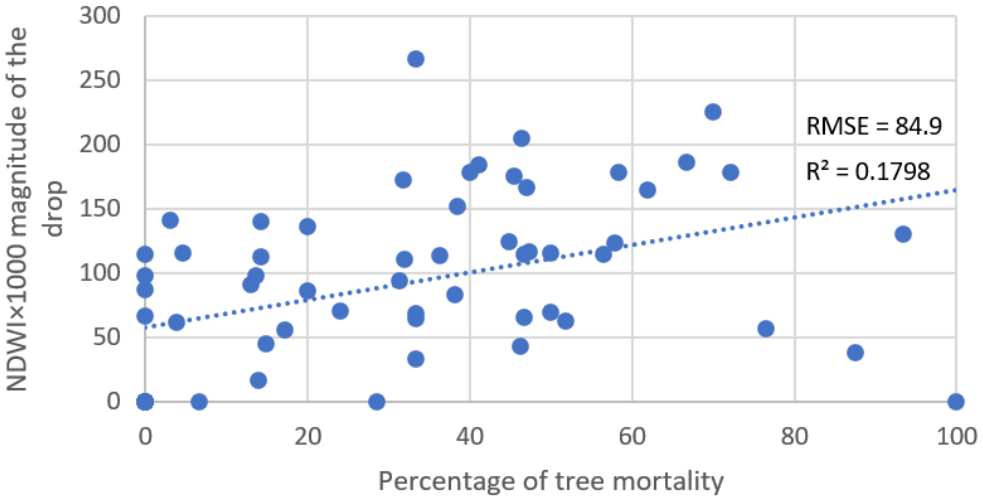

Figure 24. Linear regression between magnitude of the drop (using NDWI values) and estimation of percentage of tree mortality

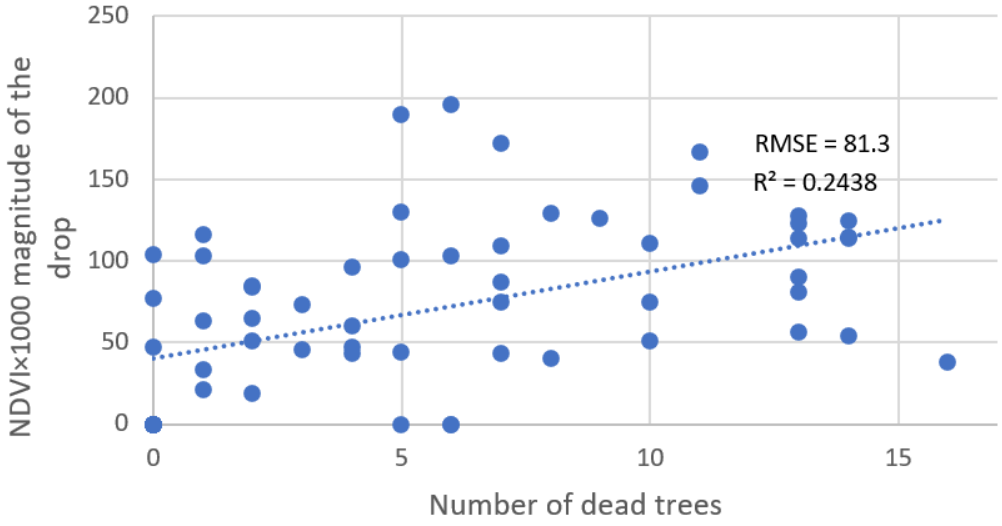

Figure 25. Linear regression between magnitude of the drop (using NDVI values) and number of dead trees

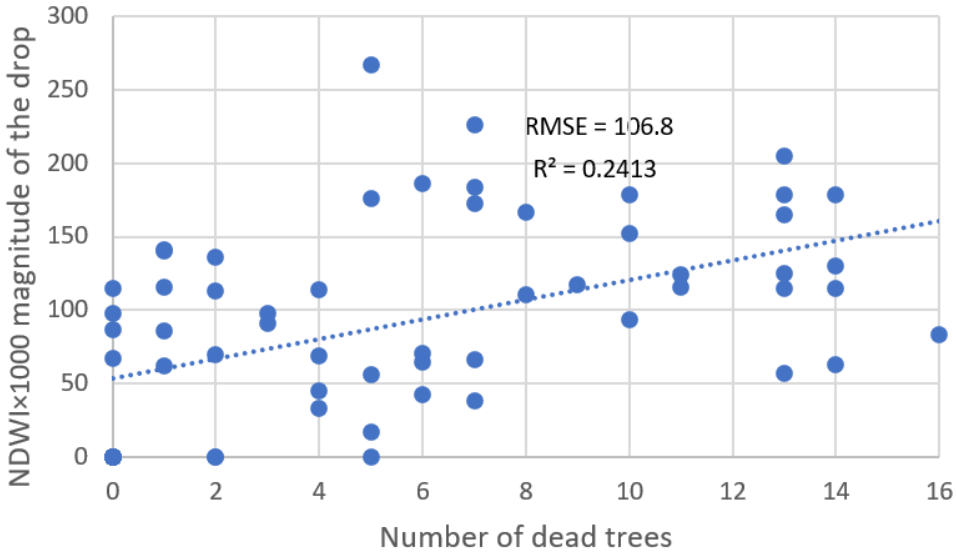

Figure 26. Linear regression between magnitude of the drop (using NDWI values) and number of dead trees

4.6. Verification of SU approach

SU algorithm was run for the area of interest using two selected endmembers, bare soil and live vegetation. It resulted in having two outputs containing one layer for each defined endmember with information about percentage of each endmember in each pixel. For further analysis, output for live vegetation was taken and compared to the calculated area of live vegetation per pixel of the validation dataset using UAS data. Regression analysis was used to illustrate the findings of verification of the SU approach (Figure 27). Seventy-five percent of the variation is explained by this regression (and RMSE = 12.4). SU values are overall higher than those estimated using UAS data. This trend occurs within all the plots via increasing the difference between the variables and the largest difference observed at around 20% of vegetation per pixel. The difference in estimated live

vegetation percentage is approximately 20-30%. Also, it is noticeable that values are much more similar when there is dense vegetation within plots. Consequently, SU is more reliable for pixels with denser vegetation and tends to overestimate for pixels with sparse vegetation.

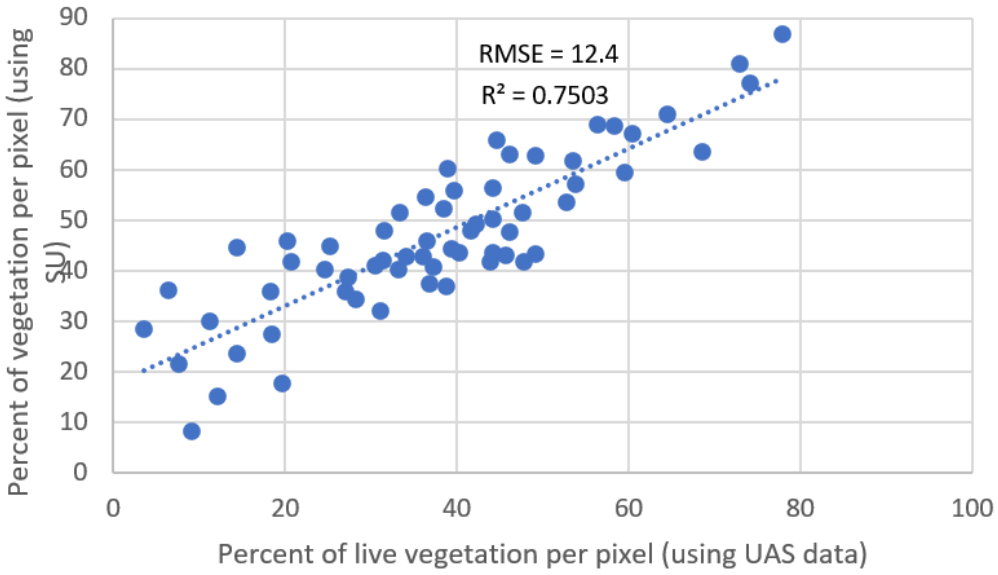

Figure 27. Linear regression between percentage of vegetation within the pixel using SU and derived from UAS data

4.7. Change detection of SU results using LandTrendr

The LandTrendr algorithm was run to assess and detect changes in the percentage of vegetation per pixel using outputs of SU. The magnitude of change and the year of detection are seen in Figure 28 (only pixels where the magnitude is more than ten are shown for comparison with the same picture for changes in the VIs time series). Within pixels where changes have occurred, the magnitude of change is predominantly from 10 to 20% and years of detection are mostly between 1995 and 2008. It is observed more recent changes occurred in the south part of the area. To illustrate this time period of significant changes (1995-2008) and make it more vivid, only these years were mapped, and each year was assigned a different colour (Figure 29). The picture is patchy, but notable years are 1996, 2001-2003 and 2008, when major changes happened. Significant part of changes has taken place in 1996. To confirm the year of 1996 as the year of great vegetation loss and to confirm that beginning of the time period the year before (i.e., 1995) do not influence such significance of 1996, period of 1990-2008 was mapped (Figure 30). It can be seen that almost all the pixels previously taken by 1996 are now covered by 1991. Other pixels mostly remained with the same years as before. This can corroborate the same fact found before with VIs, the start of the time series influences the year of detection.

SU detected changes in 47% of the area (0.26 km^2 in the area equal to 0.55 km^2). The calculation was made using changes that happened in 1990-2008 (Figure 30).

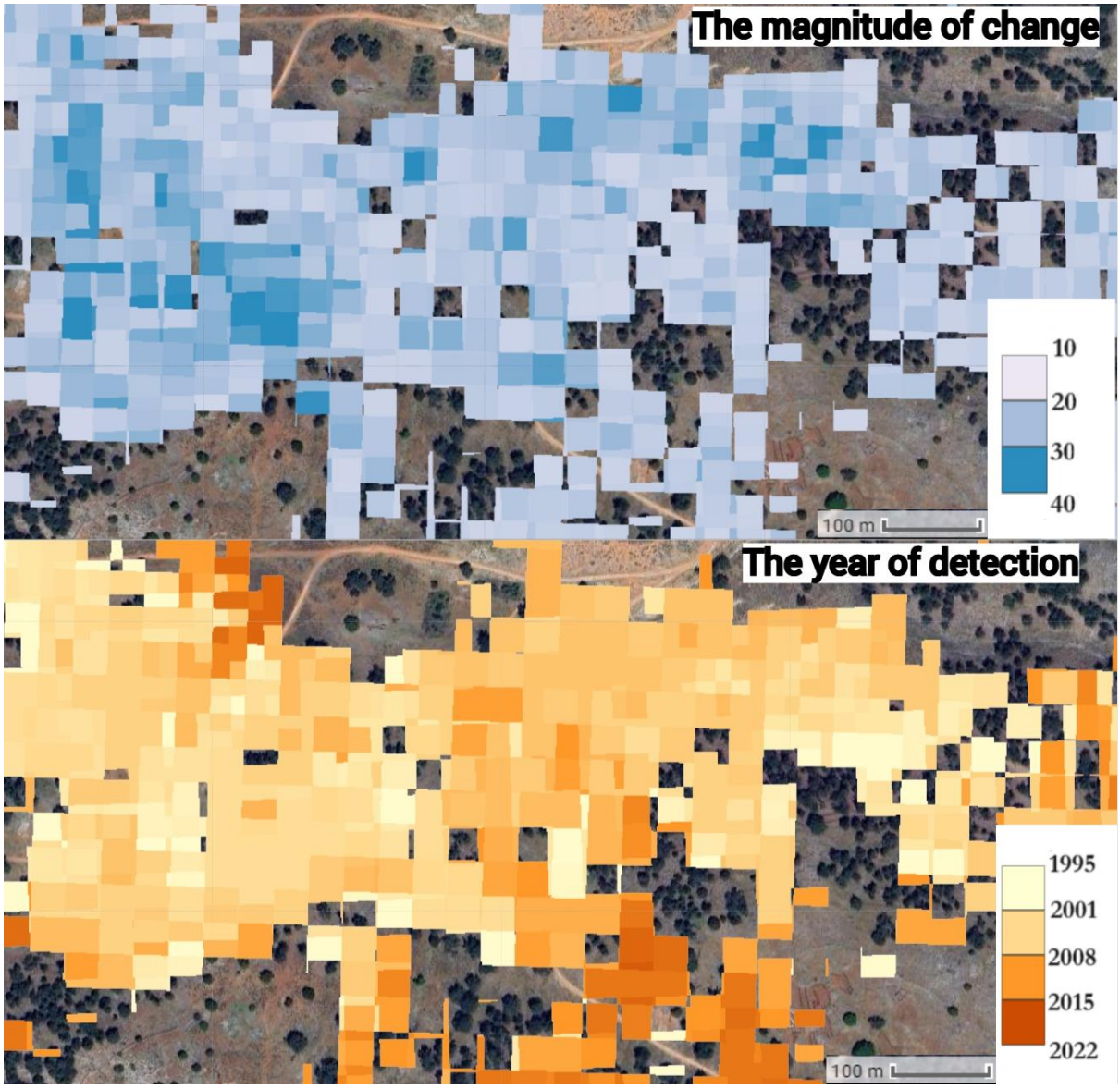

Figure 28. The magnitude of change and the year of detection of percentage of vegetation within the pixel using SU approach for site 3 using (with pixels where the magnitude is more than 10 only)

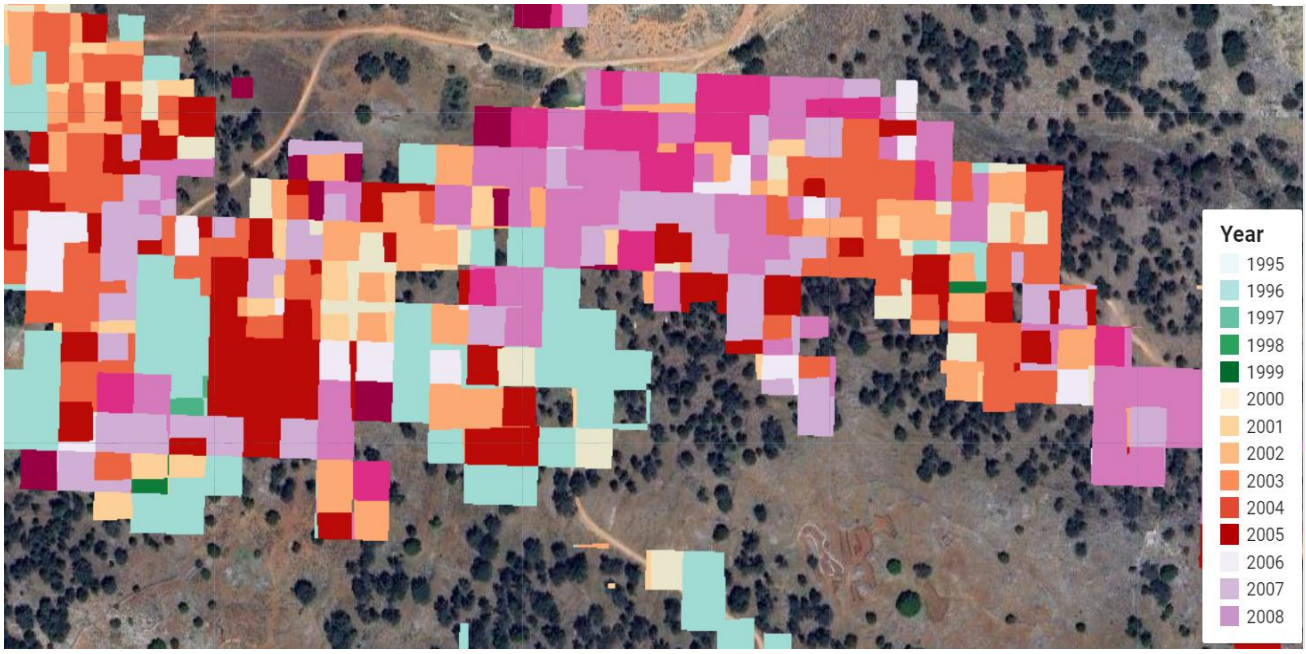

Figure 29. Changes happened in 1995-2008 for stie 3 using Landtrendr (with pixels where magnitude is more than 10 only)

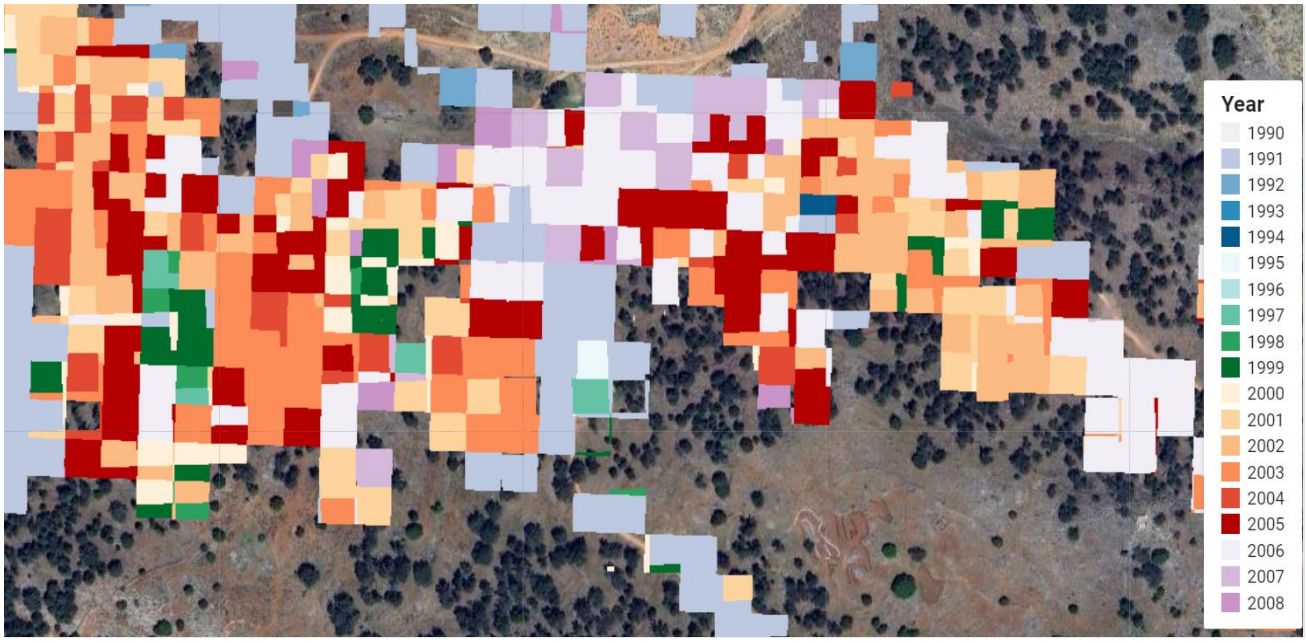

Figure 30. Changes happened in 1990-2008 for stie 3 using Landtrendr (with pixels where magnitude is more than 10 only)

4.8. Validation of tree mortality detection using SU

Accuracy assessment of tree mortality detection using SU and reference data was performed using a confusion matrix (Table 3). It was done in the same way and using the same validation dataset as for the accuracy assessment of tree mortality detection using VIs. SU correctly showed a drop in the pixel when tree mortality was detected in the corresponding plot for 48 observations. It correctly showed no drop in the pixel when there was no tree mortality detected in the plot for seven observations. Thus, producer accuracy for plots with tree mortality is 97.96% and for plots without tree mortality is 50%. User accuracy for pixels with a drop is 87.27%, and for pixels without a drop is 87.50%. Overall accuracy is 87.30%.

Table 3. Performance measurement of SU values using a confusion matrix

Class		Validation Dataset		Total	User Accuracy
		plots with tree mortality	plots without tree mortality		
Using Spectral Unmixing	pixels with a drop	48	7	55	87.27%
	pixels without a drop	1	7	8	87.50%
Total		49	14	63	-
Producer Accuracy		97.96%	50.00%	-	OA: 87,30%

4.9. Relationship between the SU magnitude of the change and tree mortality

Analysis using regression functions was used to relate tree mortality and values of drops of SU's LandTrendr magnitude. Regression analysis was performed in two ways, using a percentage of tree mortality per plot and a number of dead trees per plot. Both of these sets of values were plotted against the SU's magnitude of the drop. Figure 31 illustrates the percentage of tree mortality and SU's magnitude of the drop. These values do not show a good correlation, especially among plots with high tree mortality. Only 35% of the variation is explained by this regression. When plots with tree mortality percentage higher than 80% are removed (i.e., 3 plots), 51% of variation is explained. The regression chart with a magnitude of the drop and the number of dead trees shows a poor correlation (Figure 32). Only 27.6% of the variation is explained by these regressions.

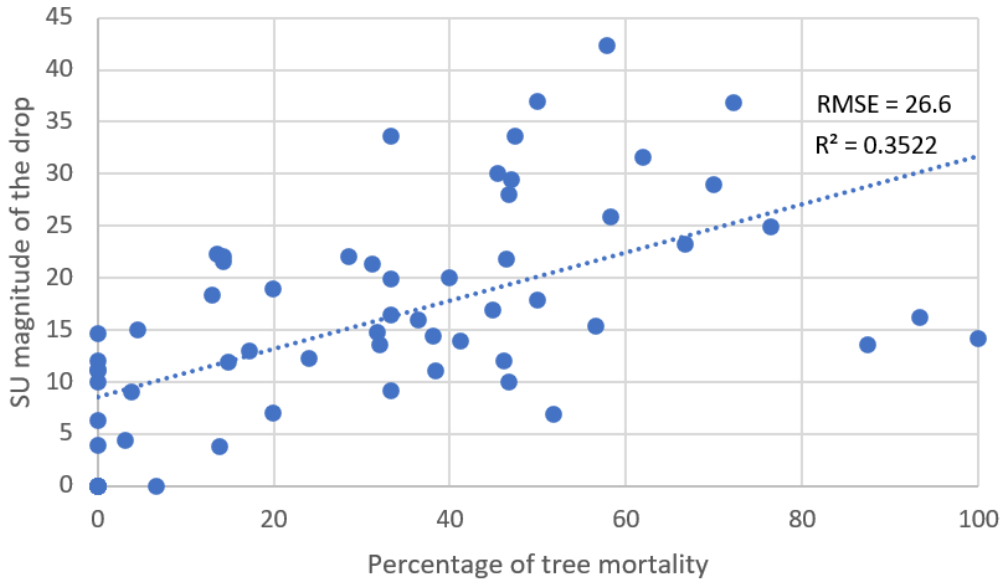

Figure 31. Linear regression between magnitude of the drop (using SU values) and estimation of percentage of tree mortality

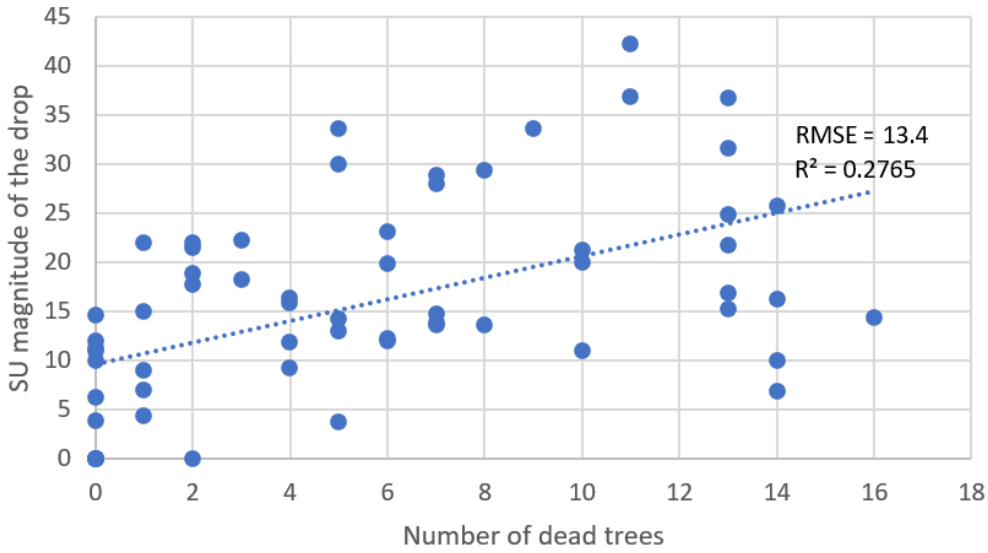

Figure 32. Linear regression between magnitude of the drop (using SU values) and number of dead trees

5. DISCUSSION

The use of UAS imagery as ground truth data has been successfully corroborated with an R^2 value of 0.95 and RMSE of 2.97, which is higher than previous research (Riihimäki et al., 2019). This allowed UAS imagery to be used complementary to direct field observations and increase the number of them without the necessity of prolonging the field campaign. This can complement and reduce field data collection, and it could be an alternative in non-accessible areas for field campaigns due to their challenges, such as high costs, logistical complexities, time-consuming nature, etc. Detecting and quantifying tree mortality, specifically, the cover of dead tree crowns per area faces challenges due to the scarcity and cost of obtaining spatially explicit reference data through field campaigns (Frolking et al., 2009; Schuldt et al., 2020). Earth observation satellite missions like Landsat or Sentinel have limitations in resolving individual trees analysis, hindering the link with ground observations (Pause et al., 2016). UAS offers a solution that provides very high spatial resolution imagery for precise dead tree crown segmentation. The proven very high spatial resolution of UAS RGB imagery allows for accurate segmentation of dead tree crowns (if trees are standing), and the adaptable deployment of UAS has demonstrated efficient detection of tree mortality events over large and inaccessible areas. Future research can leverage these findings, combining them with advancements in pattern recognition and deep learning, such as Convolutional Neural Networks (CNN), to achieve highly accurate crown segmentation of standing dead trees (Alvarez-Vanhard et al., 2021; Kattenborn et al., 2019; Schiefer et al., 2023). Despite the overall high precision of UAS data as reference data, R^2 for regression between field and UAS estimation of a number of only dead trees per plot is comparatively lower (0.88) than regression using a total number of trees. Standing deadwood is well detectable using a bird's eye perspective. Also, the open canopy of the Mediterranean forests helps in distinguishing individual trees. The point of confusion here is primarily due to lying dead tree trunks, often thin or/and very close to each other or on each other. In some cases, local people drag dead trees and collect them at one point as firewood or for construction. All these lead to confusion in observations using both field campaigns and UAS imagery.

Verification of SU outputs using UAS data resulted in an R^2 value of 0.75 and RMSE = 12.4. The analysis was done to prove SU as a reliable approach for estimating vegetation percentage within mixed pixels. In general, verification results support it but also show an overestimation using SU and imperfect agreement, leaving room for discussions of possible reasons. One of them could be variability in vegetation composition in the area. Even though all the data utilized in the research was gathered for summer months when most of the understory vegetation is dried off (it is essential to mention that there is not much understory in the area in the first place) and it was assumed that it would not affect the spectral signature of live vegetation, some of the understory could have affected it an led to confusion. Another reason could be the imperfect match between field plots and satellite imagery's pixels. Fieldwork and field plots were designed to be coincident with Sentinel-2 pixels as at that time Sentinel-2 was considered as the main data source. Later on, after shifting to Landsat and putting its pixels on top of plots it was revealed that not all the trees which are within a plot end up being within a Landsat pixel. Thus, the correction of field plots using UAS data to estimate the right number of live and dead trees within the Landsat pixel could be helpful. Additionally, spatial resolution might affect the performance of SU. Using higher spatial resolution may help improve SU accuracy, as indicated by Zhou et al. (2016).

Creating time series of the chosen VIs showed low influence on changes in temporal profile due to the single (even if severe) recent drought event that occurred in Crete in 2015-2016 (Proutsos et al., 2022). During the early stages of the present study, the period of 2015-2023 and Sentinel-2 data were chosen to investigate drops and changes in

vegetation indices under the influence of this severe drought. Investigation of temporal profiles of pixels representing dissimilar land cover fractions, such as of vigorous vegetation or of high tree mortality, revealed very low or absence of drops/changes. So, pixels with high tree mortality do not change during or after the mentioned disturbance and those with low tree mortality and vigorous vegetation contain small drops but return to a regular pattern soon after. This supports the findings of Dorman et al. (2013) about the 'resulting damage' of a second drought period that intensifies the negative impact of a single drought period and leads to higher mortality risk. The research by Dorman et al. (2013) was carried out in forests of Israel with a climatic gradient ranging from semi-arid continental in the centre to Mediterranean conditions in the north of the country. Here the effect of the severe drought from 1998-2000 was intensified by the moderate drought from 2005-2011. Almost coinciding with these drought periods, periods of increasing tree mortality are seen in the region of interest in this study, too. This could have resulted in the current situation of widespread tree mortality throughout Lefka Ori.

Recent drought event did not affect tree mortality. Using the Landsat sensor helped us to detect drops in time series that could be related to observed tree mortality that happened in the earlier dates. Meteorological data is available from stations within the study area (Palaiochora does not have continuous data) and in the city of Chania (which holds data from the 1950s). Temperature patterns in Palaiochora and Chania meteorological stations are similar (Figure 33), with Palaiochora consistently being 1.5-2 degrees warmer than Chania due to its location and topography. The precipitation in Palaiochora (Figure 34) is continuously lower than in Chania. The precipitation difference varies significantly, starting from 20-50 mm (1987, 2009), rising up to 260 mm (2016) and reaching 350-550 mm (during 1991-1997). The first drought period of the mid-1990s matches with observed significant drops in the VIs time series (Figure 35). Also, the drought of 2015-2016 is noticeable. Given the abovementioned theory of 'resulting damage', widespread tree mortality of the late 1990s could be an outcome of that severe drought period, which intensified previous drought which occurred throughout Greece in mid-1980s to early 1990s (Varlas et al., 2022). The reason for the absence of recent tree mortality, even with the observed drought of 2015-2016, could be that this drought is the first period of low precipitation and/or high temperatures in some time.

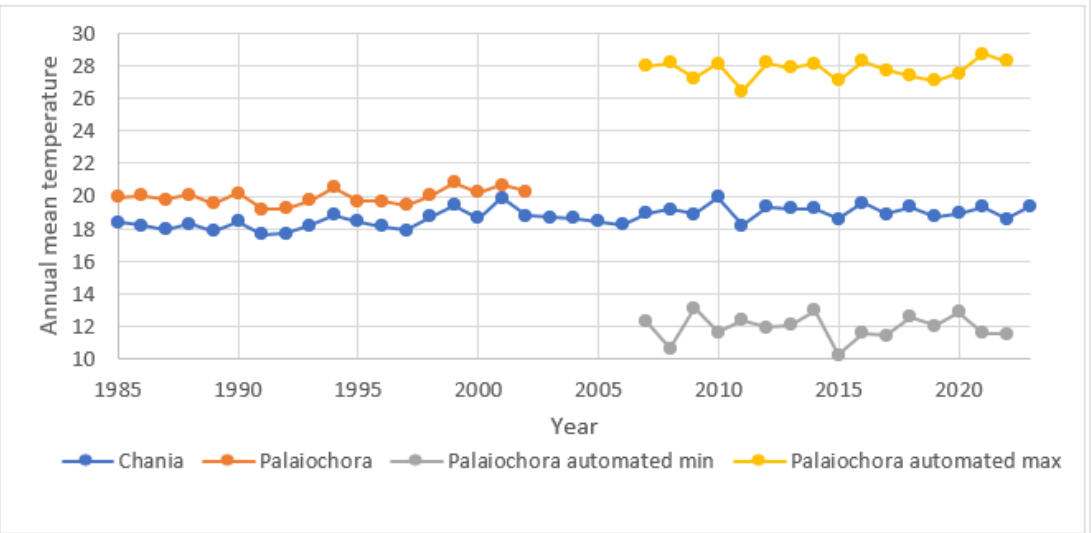

Figure 33. Annual mean temperature for Chania, Palaiochora, annual mean max and annual mean min temperatures for Palaiochora automated station

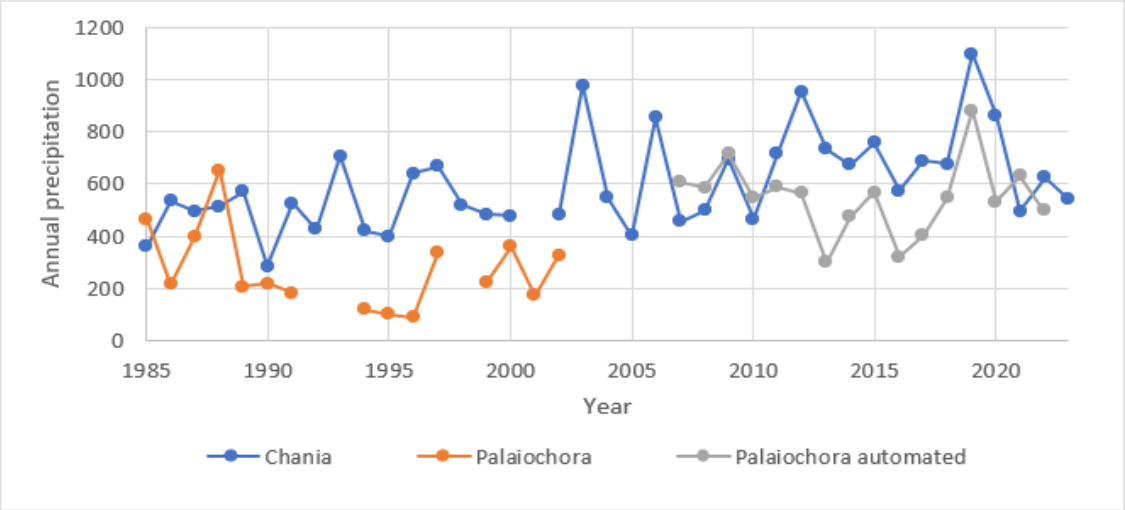

Figure 34. Annual precipitation for Chania, Palaiochora and Palaiochora automated stations

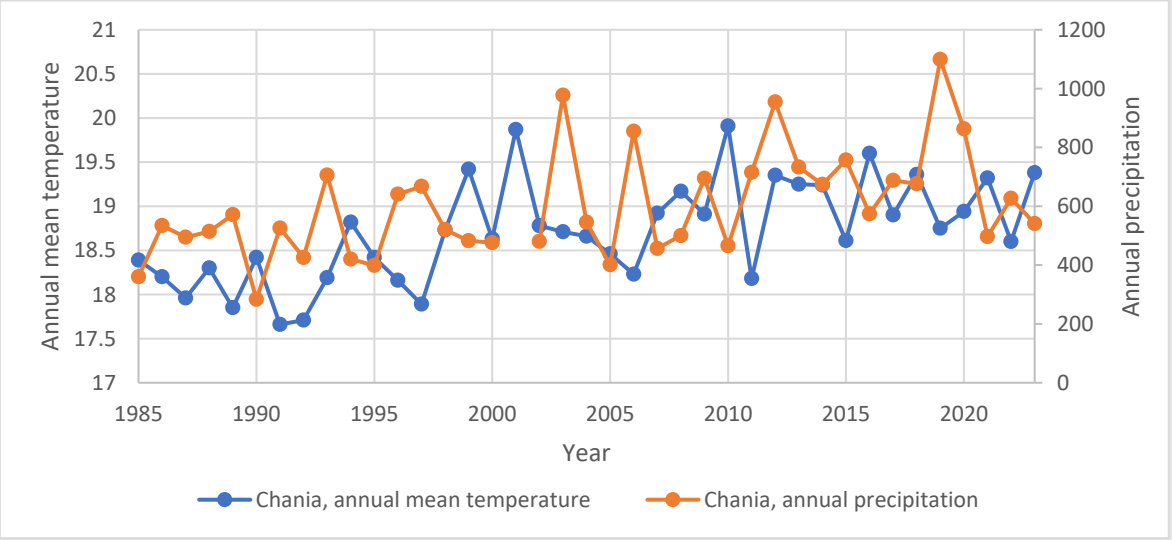

Figure 35. Annual mean temperature and annual precipitation for Chania

Another interesting aspect concerns the analysis and comparison of the temporal profiles of the same VIs with different multispectral data sources (for the same period). The values of VIs obtained from Landsat-8 imagery are lower than those from the corresponding pixel in Sentinel-2 imagery. This is due to the very open ecosystem where it is difficult to find large patches of vegetation and soil, which significantly influences the pixel signal. Landsat pixels cover nine times the area of Sentinel-2 pixels. As a result, within a single Landsat pixel, there could be a mix of vegetation, non-vegetation, and other land cover types. This mixing of land cover types can weaken the vegetation signal captured by Landsat, leading to lower NDVI values in the area compared to Sentinel-2, which has finer spatial resolution and can better capture vegetation details within its pixels.

The LandTrendr algorithm was chosen to perform change detection in the time series of VIs and SU. All three methods used (i.e., NDVI, NDWI and SU) have confirmed nearly the same area as areas that have experienced changes (there is overlap in the affected areas using all methods). It is an area detected by NDVI because this method highlighted the least number of pixels (34% of the area, 0.19 km^2 in the area equal to 0.55 km^2). NDWI highlighted more than NDVI (42% of the area, 0.23 km^2, 21% more than NDVI), and SU

highlighted more than NDWI (47% of the area, 0.26 km^2, 13% more than NDWI and 37% more than NDVI). Also, NDVI's magnitude of change is lower than that of NDWI. And SU's magnitude is higher than NDWI's magnitude. So, changes in NDVI mostly have a magnitude of 0.1-0.2; changes in NDWI are also present in more pixels as it was commented before, and many of them have a change of 0.2-0.3. In the case of SU, even more pixels with significant drops were detected, and the magnitude of the loss varies uniformly among pixels from 10% to 40%. It is essential to mention that 10% of vegetation loss per pixel using SU may not be the same loss as 0.1 of VIs. Several drops were observed near roads and in areas neighbouring buildings which were built during the time period chosen. This may mean that anthropogenic factors contributed to the observed changes. Additionally, the year of detection using all methods confirmed the importance of indicating a starting year in order to detect changes correctly. Thus, when the starting year is set to 1995, LandTrendr tends to mark 1996 as the year of significant changes. The same is true with 1990; 1991 was the year of major changes, but 1996 was no longer notable. So, to detect changes correctly, it is crucial to have a few years before the period of interest.

The visual assessment of the year of detection among VIs and SU proves NDWI to detect changes in most cases earlier or in the same year as NDVI. SU detects changes a few years later than VIs. This is explainable given that VIs detect all changes, including subtle changes in vegetation health, and SU estimates changes in live vegetation fraction (for example, when trees transit from one state (alive) to another (dead)), which takes much more time. Thus, the possibility of NDWI to detect forest disturbances earlier than NDVI was proven in this study and previous research (Sturm et al., 2022; Aljahdali et al., 2021). It might detect areas less resilient to drought, give early warnings in areas of high drought/tree mortality risk, and help foresters in the decision-making process to prevent massive tree loss.

Comparison of magnitude (drop) of VI's and SU's time series and the percentage of tree mortality in corresponding plot was assessed using regression functions. These values do not show good correlations; only 37% of the variation is explained using NDVI values, 35% using SU values, 18% using NDWI values, and RMSE values are 56.9, 26.6, and 84.9 for NDVI, SU and NDWI respectively. When plots with tree mortality percentage higher than 80% are removed (i.e., 3 plots), 51%, 42%, 35% of variation is explained for SU, NDVI and NDWI respectively. Also, it helps to increase the degree of correlation between these variables ($R = 0.71, 0.64, 0.59$ for SU, NDVI and NDWI respectively). So, SU and tree mortality percentage are highly correlated, but we cannot use SU as a predictor of percentage of tree mortality in a very accurate way. Additionally, SU is relatively better in terms of how close the predicted values are to the actual values, and NDVI better indicates how well the independent variables explain the variability of the dependent variable. Spruce et al. (2019) investigated mapping tree mortality using MODIS data and aerial imagery as reference data. Depending on the MODIS product used, linear regression analyses could explain 36% to 54% of the variation. The differences are most noticeable for the extreme tree mortality values (i.e., the lowest and the highest levels of tree mortality percentage), which coincide with the present study's findings.

The performance of two VIs and SU in tree mortality detection has been assessed using confusion matrixes. Accuracies of VIs are nearly identical, with NDVI slightly overperforming NDWI in detecting tree mortality (46 observations are correct out of 49 for NDVI and 45 for NDWI). SU's accuracy is higher than VIs in detecting the presence of tree mortality (48 observations are correct out of 49; accuracy is 97.96% versus 93.88% and 93.75% in NDVI and NDWI respectively). However, it has the lowest accuracy in detecting the absence of tree mortality (7 observations are correct out of 14, and accuracy is 50% in SU versus 78.57% and 73.33% in NDVI and NDWI respectively). Validation of

SU reveals this approach's tendency to overestimate the percentage of tree mortality. The possible reason for this could be an overestimation of SU in the vegetation percentage, (i.e. showing higher values than the actual amount of vegetation in the plot). Liu et al. (2021) also state that the greenness-related index NDVI is performing better in predicting tree mortality than the water-related index NDII, suggesting that fluctuations in greenness predominantly influenced the canopy dynamics observed. As a result, initial drought stress on the canopy may cause a reduction in chlorophyll content (leading to a decrease in NDVI) while maintaining relatively constant water content (stable NDII), indicating forest resilience to climate change.

There are various reasons why not in all cases NDWI show changes earlier than NDVI. The possible reason for that is the SWIR band being affected by atmospheric absorption, which makes the signal more noisy, or the severity of the drought was higher, and water and biomass were reduced within the same year. Liu et al. (2021) state that drought-tolerant species reduce greenness before water, unlike species not drought-tolerant. This explains why, in some cases, NDWI detect changes later than NDVI – those are less drought-tolerant species. Additionally, NDVI uses red and NIR bands, which many remote sensing satellites (SPOT, Proba-V, PlanetScope, etc.) are equipped with. It makes utilization of this index more feasible as most widely used and free satellites have bands needed for its calculation. On the contrary, NDWI uses NIR and SWIR, which is less common on free remote sensing satellites. Even though overprediction of tree mortality using spectral indices is a common practice, there is significant promise in detecting trees and forests at high mortality risk (Bergmüller & Vanderwel, 2022). Nevertheless, various factors unrelated to tree mortality influence spectral metrics, such as species composition and forest structure. Consequently, these methods can only offer indirect information about tree mortality and do not explicitly determine whether tree crowns are dead (Glenn et al., 2008).

Various steps could be taken to achieve better SU and VIs performance accuracy. One is creating an ensemble of multiple metrics instead of using them independently. Following the findings of De Marzo et al. (2021), Grogan et al. (2015), Hislop et al. (2019) and Qiu et al. (2023), the combination of a few spectral indices and other metrics may improve the accuracy of forest disturbance detection. Recently, there has been a transition in the application of automatic change detection algorithms from utilizing time series of single spectral metrics, such as band 5, NDVI, and NBR, towards adopting ensemble approaches. These ensembles, which combine various change detection techniques, have demonstrated significant potential in capturing disturbances, mostly outperforming individual methods. Two is using higher spatial resolution data such as aerial imagery. This point is supported by the findings of Cheng et al. (2024), which indicate the importance of mapping individual dead trees in a Mediterranean forest (a California case study) to estimate tree mortality accurately. This is due to a large number of isolated dead trees or standing in small groups that were observed using sub-meter spatial resolution imagery, and at Landsat with a resolution of 30 m would not have been visible. In our case, we deal with tree mortality that is not recent. Thus, trees could be down, moved or disappeared. Presumably, the detection of more recent tree mortality would benefit from this approach of mapping individual dead trees.

There are various reasons for poor agreement between the magnitude of the change and the percentage of tree mortality. One of them is the availability of validation data. The validation dataset in this study consists of field observations and UAS data collected in 2023. One of the assumptions made was that due to the low regeneration of the vegetation in the area of interest, changes detected in the time frame chosen may be validated using a dataset collected in 2023. However, it was observed during the fieldwork that local people living nearby collect dry trees as firewood, so if these dead trees are found in the forest,

they might not be where they grew and died. Also, it negatively affects visual estimation of dead trees using UAS (here, dead tree trunks are one under another and very close to each other; field observations or LiDAR data may help in this case to differentiate stems from each other). If so, it affects both the accuracies of VIs and SU and the regression between the magnitude of the drop and the percentage of tree mortality. Thus, it is impossible to understand whether an error in the tool or the absence of accurate data for validation for those specific years affects the results. Spruce et al. (2019) mentioned that disagreements between validation data and satellite products seem to arise in areas of high heterogeneity of the landscape where patches of dead trees neighbour with non-forest and healthy forests, due to much coarser spatial resolution of testing dataset comparing to validation dataset. Another reason could be that these VIs such as NDVI or NDWI do not quantify the amount of vegetation or water. They are normalized values where a value of 1 means high biomass or a high amount of water but not how much of it is there. Another possible reason is that the coverage of dead trees in the plot is not calculated, but the ratio between dead trees and all trees is used as a value for the percentage of tree mortality. This is due to the difficulty of calculating the coverage. Problem concerns, for example, laying trees. Usually, it is canopy cover, which is counted towards tree coverage, but the problem of how to estimate canopy coverage of laying trees arises. With laying trees, it is only possible to calculate the surface coverage, but then how can the surface coverage of standing trees be estimated? Also, it is tricky to estimate the surface of dead trees because some of them have only stems, some of them have branches too, and some of them remain exactly the same as when they were alive. To improve the accuracy of predicting tree mortality percentage, consider coverage and find a way to include laying trees. It might be done by counting the surface or measuring the diameter at breast height (it can give an idea of how big a tree is). Also, vegetation health might play a role. Analyzing vegetation conditions and health in forests and crops often involves employing VIs derived from remote sensing data. This method, as highlighted by Aljahdali et al. (2021) and Beygi Heidarlou et al. (2024), is a common approach utilized to assess the state of vegetation cover. However, a brief duration of forest disturbances such as droughts allows an ecosystem to regain its original state without tree mortality (Gazol et al., 2018). Thus, drops in the VIs time series are noticed but not supported by the presence of tree mortality but by different stages in vegetation health.

Mapping tree mortality using remote sensing tools discussed in this study provides forest managers with valuable assistance in various aspects of forest management. Firstly, it enables early detection of tree mortality, allowing fast intervention and mitigation strategies to minimize further loss. Secondly, resources can be allocated more efficiently by identifying areas with high mortality rates. Additionally, remote sensing facilitates continuous monitoring of tree mortality over large area and extended periods, enabling forest managers to track trends and assess the effectiveness of used management practices. It also helps understand the drivers of mortality, such as drought, pests, diseases, or human activities, allowing for targeted management plans. Moreover, the discussed tools support informed decision-making for forest management, such as prioritizing areas for restoration; it helps assess overall forest health and resilience and identify vulnerable areas. The findings of this study might be extrapolated and used in further research with other data sources. For example, there is not a long enough time series available using Sentinel-2 data. Still, it might be helpful in the future to make time series with higher spatial resolution than Landsat, as well as to use hyperspectral data with higher spectral resolution. Current and future hyperspectral satellite missions (e.g. PRISMA (Italy), EnMAP (Germany), Surface Biology and Geology (USA) may contribute to monitoring tree mortality more accurately at a global scale.

6. RECOMMENDATIONS AND CONCLUSION

6.1. Recommendations

In order to prevent tree mortality, it is essential to have tools for early detection of decline in forest health and to take action before it is too late, which is the case of tree mortality. Analyzing the inter-annual changes in spectral metrics shows more promise for early detection than classifying based on a single date (Bárta et al., 2021). Future studies should also consider changes in the phenological cycles of forests. Instead of working with annual data, we can consider the whole yearly cycle and look for changes. This will probably help to detect different health statuses and take action before trees die.

Water and greenness-related indices respond to drought differently in drought-resistant species versus non-resistant species. Drought-resistant species first lose their greenness/biomass. If there are drops in NDVI values but not in NDWI values, it may mean that some level of disturbance is there and it is affecting forest health, but due to the good resilience of the forest, it is not (yet) influencing vegetation water content. Thus, NDVI can be used for early detection for drought-resistant species. In the areas where NDWI show changes earlier than NDVI, it may mean that stress is influencing forest health and that this forest is not resilient. NDWI could be more appropriate for detecting disturbance in drought-resistant species. In cases of drastic drought stress and continuing limited regeneration, the decline in greenness may eventually lead to substantial decreases in canopy water content, indicating an increasing probability of mortality.

Studies that have been detecting changes using the LandTrendr algorithm note it has been late in detection for one year (Bright et al., 2019; Qiu et al., 2023; Zhu et al., 2019). Due to the unavailability of a validation dataset for years of severe tree mortality, we could not support or reject this statement for the area of interest of this study. However, it is essential to take it into account.

LandTrendr has proven itself as a reliable tool for change detection. However, some time needs to be given before the change is detected. The tool tends to mistakenly mark pixels as vegetation loss the following year after the starting year.

SU is a reliable tool for detecting tree mortality. Its accuracy is higher than VIs, and both VIs and SU can detect different stages of forest health and not only tree mortality, as the reduction of vegetation percentage could be due to a reduction in biomass and not necessarily because of tree mortality. However, SU tends to overestimate vegetation percentage, especially within not dense canopies, which may lead to confusion.

6.2. Conclusion

Integrating UAS imagery and remote sensing tools offers valuable insights into tree mortality detection and forest management. UAS imagery has proven effective in complementing field observations and increasing their frequency without extending field campaigns. Overall, remote sensing plays a crucial role in enhancing forest management strategies and resilience in the face of environmental challenges. Remote sensing tools enable early detection of tree mortality, efficient resource allocation, and continuous forest health monitoring. The results of this research showed the usefulness of VIs from the Landsat time series in detecting tree mortality in a very open Mediterranean forest. In addition, we used the percentage of live vegetation derived from SU for the first time to detect tree mortality. A novel approach was made to calculate the percentage of vegetation per pixel using SU and then employ the LandTrendr technique to detect changes in it. Challenges remain in accurately quantifying tree mortality due to spatial resolution limitations of satellite missions and the complexities of distinguishing between standing and laying deadwood. Additionally, the verification of SU as an approach has shown

promise but leaves room for discussions on possible reasons for discrepancies. At this point, we could not determine if our estimation is in line with other studies due to very little research on this topic. The same issue arises when looking for quantifying the magnitude of the drop and tree mortality, as well as higher accuracy of estimation of tree mortality percentage with VIs compared to the number of dead trees. There is a considerable number of tasks remaining to be addressed in this context. Future research should address these challenges by exploring innovative approaches, such as combining various spectral metrics, estimating biomass to consider tree size and leveraging advancements in deep learning techniques.

7. ETHICAL CONSIDERATION

This study focuses on drought-induced tree mortality assessment in Lefka Ori. It did not collect any personal information from individuals in the study area, ensuring that the research does not violate the people's privacy rights.

Additionally, all the previous studies this research built upon were properly referenced in the body of the text and the reference list.

LIST OF REFERENCES

Aljahdali, M. O., Munawar, S., & Khan, W. R. (2021). Monitoring Mangrove Forest Degradation and Regeneration: Landsat Time Series Analysis of Moisture and Vegetation Indices at Rabigh Lagoon, Red Sea. *Forests 2021, Vol. 12, Page 52*, *12*(1), 52. https://doi.org/10.3390/F12010052

Almalki, R., Khaki, M., Saco, P. M., & Rodriguez, J. F. (2022). Monitoring and Mapping Vegetation Cover Changes in Arid and Semi-Arid Areas Using Remote Sensing Technology: A Review. *Remote Sensing 2022, Vol. 14, Page 5143*, *14*(20), 5143. https://doi.org/10.3390/RS14205143

Alvarez-Vanhard, E., Corpetti, T., & Houet, T. (2021). UAV & satellite synergies for optical remote sensing applications: A literature review. *Science of Remote Sensing*, *3*, 100019. https://doi.org/10.1016/J.SRS.2021.100019

Anderegg, W. R. L., Kane, J. M., & Anderegg, L. D. L. (2012). Consequences of widespread tree mortality triggered by drought and temperature stress. *Nature Climate Change 2012 3:1*, *3*(1), 30–36. https://doi.org/10.1038/nclimate1635

Anderson, L. O., Malhi, Y., Aragão, L. E. O. C., Ladle, R., Arai, E., Barbier, N., & Phillips, O. (2010). Remote sensing detection of droughts in Amazonian forest canopies. *New Phytologist*, *187*(3), 733–750. https://doi.org/10.1111/J.1469-8137.2010.03355.X

Barbeta, A., Mejía-Chang, M., Ogaya, R., Voltas, J., Dawson, T. E., & Peñuelas, J. (2015). The combined effects of a long-term experimental drought and an extreme drought on the use of plant-water sources in a Mediterranean forest. *Global Change Biology*, *21*(3), 1213–1225. https://doi.org/10.1111/GCB.12785

Bárta, V., Lukeš, P., & Homolová, L. (2021). Early detection of bark beetle infestation in Norway spruce forests of Central Europe using Sentinel-2. *International Journal of Applied Earth Observation and Geoinformation*, *100*, 102335. https://doi.org/10.1016/J.JAG.2021.102335

Bergmüller, K. O., & Vanderwel, M. C. (2022). Predicting Tree Mortality Using Spectral Indices Derived from Multispectral UAV Imagery. *Remote Sensing 2022, Vol. 14, Page 2195*, *14*(9), 2195. https://doi.org/10.3390/RS14092195

Beygi Heidarlou, H., Oprea-Sorescu, O., Marcu, M. V., & Borz, S. A. (2024). Mapping Small-Scale Willow Crops and Their Health Status Using Sentinel-2 Images in Complex Agricultural Areas. *Remote Sensing*, *16*(3). https://doi.org/10.3390/RS16030595

Brando, P. M., Paolucci, L., Ummenhofer, C. C., Ordway, E. M., Hartmann, H., Cattau, M. E., Rattis, L., Medjibe, V., Coe, M. T., & Balch, J. (2019). Droughts, Wildfires, and Forest Carbon Cycling: A Pantropical Synthesis. *Https://Doi.Org/10.1146/Annurev-Earth-082517-010235*, *47*, 555–581. https://doi.org/10.1146/ANNUREV-EARTH-082517-010235

Brewer, W. L., Lippitt, C. L., Lippitt, C. D., & Litvak, M. E. (2017). Assessing drought-induced change in a piñon-juniper woodland with landsat: A multiple endmember spectral mixture analysis approach. *International Journal of Remote Sensing*, *38*(14), 4156–4176. https://doi.org/10.1080/01431161.2017.1317940

Bright, B. C., Hudak, A. T., Kennedy, R. E., Braaten, J. D., & Henareh Khalyani, A. (2019). Examining post-fire vegetation recovery with Landsat time series analysis in three

western North American forest types. *Fire Ecology*, *15*(1), 1–14. https://doi.org/10.1186/S42408-018-0021-9/TABLES/7

Celik, B. (2023). QLSU (QGIS Linear Spectral Unmixing) Plugin: An open source linear spectral unmixing tool for hyperspectral & multispectral remote sensing imagery. *Environmental Modelling & Software*, *168*, 105782. https://doi.org/10.1016/J.ENVSOFT.2023.105782

Chaulagain, S., Stone, M. C., Morrison, R. R., Yang, L., Coonrod, J., & Villa, N. E. (2023). Determining the response of riparian vegetation and river morphology to drought using Google Earth Engine and machine learning. *Journal of Arid Environments*, *219*, 105068. https://doi.org/10.1016/j.jaridenv.2023.105068

Chen, J., Chen, Z., Huang, R., You, H., Han, X., Yue, T., & Zhou, G. (2023). The Effects of Spatial Resolution and Resampling on the Classification Accuracy of Wetland Vegetation Species and Ground Objects: A Study Based on High Spatial Resolution UAV Images. *Drones 2023, Vol. 7, Page 61*, *7*(1), 61. https://doi.org/10.3390/DRONES7010061

Chou, C. Ben, Weng, M. C., Huang, H. P., Chang, Y. C., Chang, H. C., & Yeh, T. Y. (2022). Monitoring the Spring 2021 Drought Event in Taiwan Using Multiple Satellite-Based Vegetation and Water Indices. *Atmosphere*, *13*(9), 1374. https://doi.org/10.3390/atmos13091374

Christopoulou, A., Sazeides, C. I., & Fyllas, N. M. (2022). Size-mediated effects of climate on tree growth and mortality in Mediterranean Brutia pine forests. *Science of the Total Environment*, *812*. https://doi.org/10.1016/J.SCITOTENV.2021.151463

Cohen, W. B., Healey, S. P., Yang, Z., Stehman, S. V., Brewer, C. K., Brooks, E. B., Gorelick, N., Huang, C., Hughes, M. J., Kennedy, R. E., Loveland, T. R., Moisen, G. G., Schroeder, T. A., Vogelmann, J. E., Woodcock, C. E., Yang, L., & Zhu, Z. (2017). How Similar Are Forest Disturbance Maps Derived from Different Landsat Time Series Algorithms? *Forests 2017, Vol. 8, Page 98*, *8*(4), 98. https://doi.org/10.3390/F8040098

Cohen, W. B., Yang, Z., Healey, S. P., Kennedy, R. E., & Gorelick, N. (2018). A LandTrendr multispectral ensemble for forest disturbance detection. *Remote Sensing of Environment*, *205*, 131–140. https://doi.org/10.1016/J.RSE.2017.11.015

Cowling, R. M., Rundel, P. W., Lamont, B. B., Arroyo, M. K., & Arianoutsou, M. (1996). Plant diversity in mediterranean-climate regions. *Trends in Ecology and Evolution*, *11*(9), 362–366. https://doi.org/10.1016/0169-5347(96)10044-6

Elmore, A. J., Mustard, J. F., Manning, S. J., & Lobell, D. B. (2000). Quantifying Vegetation Change in Semiarid Environments: Precision and Accuracy of Spectral Mixture Analysis and the Normalized Difference Vegetation Index. *Remote Sensing of Environment*, *73*(1), 87–102. https://doi.org/10.1016/S0034-4257(00)00100-0

Ewane, E. B., Mohan, M., Bajaj, S., Galgamuwa, G. A. P., Watt, M. S., Arachchige, P. P., Hudak, A. T., Richardson, G., Ajithkumar, N., Srinivasan, S., Corte, A. P. D., Johnson, D. J., Broadbent, E. N., de-Miguel, S., Bruscolini, M., Young, D. J. N., Shafai, S., Abdullah, M. M., Jaafar, W. S. W. M., … Cardil, A. (2023). Climate-Change-Driven Droughts and Tree Mortality: Assessing the Potential of UAV-Derived Early Warning Metrics. *Remote Sensing*, *15*(10). https://doi.org/10.3390/RS15102627

Filgueiras, R., Mantovani, E. C., Althoff, D., Fernandes Filho, E. I., & da Cunha, F. F. (2019). Crop NDVI monitoring based on sentinel 1. *Remote Sensing*, *11*(12). https://doi.org/10.3390/rs11121441

Food and Agriculture Organization of the United Nations. (2014). *Manual for Visual Assessment of Forest Crown Condition*. www.fao.org/publications

Frolking, S., Palace, M. W., Clark, D. B., Chambers, J. Q., Shugart, H. H., & Hurtt, G. C. (2009). Forest disturbance and recovery: A general review in the context of spaceborne remote sensing of impacts on aboveground biomass and canopy structure. *J. Geophys. Res*, *114*, 0–02. https://doi.org/10.1029/2008JG000911

Gao, B.-C. (1996). NDWI - A Normalized Difference Water Index for Remote Sensing of Vegetation Liquid Water From Space. In *REMOTE SENS. ENVIRON* (Vol. 7212). ©Elsevier Science Inc.

Garrity, S. R., Allen, C. D., Brumby, S. P., Gangodagamage, C., McDowell, N. G., & Cai, D. M. (2013). Quantifying tree mortality in a mixed species woodland using multitemporal high spatial resolution satellite imagery. *Remote Sensing of Environment*, *129*, 54–65. https://doi.org/10.1016/J.RSE.2012.10.029

Gaylord, M. L., Kolb, T. E., McDowell, N. G., & Meinzer, F. (2015). Mechanisms of piñon pine mortality after severe drought: a retrospective study of mature trees. *Tree Physiology*, *35*(8), 806–816. https://doi.org/10.1093/TREEPHYS/TPV038

Gazol, A., Camarero, J. J., Sangüesa-Barreda, G., & Vicente-Serrano, S. M. (2018). Post-drought resilience after forest die-off: Shifts in regeneration, composition, growth and productivity. *Frontiers in Plant Science*, *871*. https://doi.org/10.3389/FPLS.2018.01546/FULL

Glenn, E. P., Huete, A. R., Nagler, P. L., & Nelson, S. G. (2008). Relationship Between Remotely-sensed Vegetation Indices, Canopy Attributes and Plant Physiological Processes: What Vegetation Indices Can and Cannot Tell Us About the Landscape. *Sensors 2008, Vol. 8, Pages 2136-2160*, *8*(4), 2136–2160. https://doi.org/10.3390/S8042136

Grove, A. T., & Rackham, O. (1993). Threatened landscapes in the Mediterranean: examples from Crete. *Landscape and Urban Planning 24*, 279–292.

Haied, N., Foufou, A., Khadri, S., Boussaid, A., Azlaoui, M., & Bougherira, N. (2023). Spatial and Temporal Assessment of Drought Hazard, Vulnerability and Risk in Three Different Climatic Zones in Algeria Using Two Commonly Used Meteorological Indices. *Sustainability (Switzerland)*, *15*(10). https://doi.org/10.3390/SU15107803

Hartmann, H., Bastos, A., Das, A. J., Esquivel-Muelbert, A., Hammond, W. M., Martínez-Vilalta, J., Mcdowell, N. G., Powers, J. S., Pugh, T. A. M., Ruthrof, K. X., & Allen, C. D. (2022). *Annual Review of Plant Biology Climate Change Risks to Global Forest Health: Emergence of Unexpected Events of Elevated Tree Mortality Worldwide*. https://doi.org/10.1146/annurev-arplant-102820

He, Y., Chen, G., Potter, C., & Meentemeyer, R. K. (2019). Integrating multi-sensor remote sensing and species distribution modeling to map the spread of emerging forest disease and tree mortality. *Remote Sensing of Environment*, *231*, 111238. https://doi.org/10.1016/J.RSE.2019.111238

He, Y., Yang, J., & Guo, X. (2020). Green Vegetation Cover Dynamics in a Heterogeneous Grassland: Spectral Unmixing of Landsat Time Series from 1999 to 2014. *Remote Sensing 2020, Vol. 12, Page 3826*, *12*(22), 3826. https://doi.org/10.3390/RS12223826

Huete, A., & Didan, K. (2004). MODIS seasonal and inter-annual responses of semiarid ecosystems to drought in the Southwest U.S.A. *International Geoscience and Remote Sensing Symposium (IGARSS)*, *3*, 1538–1541. https://doi.org/10.1109/igarss.2004.1370605

Kattenborn, T., Lopatin, J., Förster, M., Braun, A. C., & Fassnacht, F. E. (2019). UAV data as alternative to field sampling to map woody invasive species based on combined Sentinel-1 and Sentinel-2 data. *Remote Sensing of Environment*, *227*, 61–73. https://doi.org/10.1016/J.RSE.2019.03.025

Kennedy, R. E., Yang, Z., & Cohen, W. B. (2010). Detecting trends in forest disturbance and recovery using yearly Landsat time series: 1. LandTrendr — Temporal segmentation algorithms. *Remote Sensing of Environment*, *114*(12), 2897–2910. https://doi.org/10.1016/J.RSE.2010.07.008

Kennedy, R. E., Yang, Z., Gorelick, N., Braaten, J., Cavalcante, L., Cohen, W. B., & Healey, S. (2018). Implementation of the LandTrendr Algorithm on Google Earth Engine. *Remote Sensing 2018, Vol. 10, Page 691*, *10*(5), 691. https://doi.org/10.3390/RS10050691

Li, K., Kirkland, S., Yeo, B. L., Tubbesing, C., Bandaru, V., Song, L., Holstege, L., Hartsough, B., Kendall, A., & Jenkins, B. (2023). Integrated economic and environmental modeling of forest biomass for renewable energy in California: Part I - Model development. *Biomass and Bioenergy*, *173*, 106774. https://doi.org/10.1016/j.biombioe.2023.106774

Li, P., Jiang, L., & Feng, Z. (2013). Cross-Comparison of Vegetation Indices Derived from Landsat-7 Enhanced Thematic Mapper Plus (ETM+) and Landsat-8 Operational Land Imager (OLI) Sensors. *Remote Sensing 2014, Vol. 6, Pages 310-329*, *6*(1), 310–329. https://doi.org/10.3390/RS6010310

Liu, F., Liu, H., Xu, C., Zhu, X., He, W., & Qi, Y. (2021). Remotely sensed birch forest resilience against climate change in the northern China forest-steppe ecotone. *Ecological Indicators*, *125*, 107526. https://doi.org/10.1016/J.ECOLIND.2021.107526

Liu, Q., Peng, C., Schneider, R., Cyr, D., McDowell, N. G., & Kneeshaw, D. (2023). Drought-induced increase in tree mortality and corresponding decrease in the carbon sink capacity of Canada's boreal forests from 1970 to 2020. *Global Change Biology*. https://doi.org/10.1111/gcb.16599

Marusig, D., Petruzzellis, F., Tomasella, M., Napolitano, R., Altobelli, A., & Nardini, A. (2020). Correlation of field-measured and remotely sensed plant water status as a tool to monitor the risk of drought-induced forest decline. *Forests*, *11*(1). https://doi.org/10.3390/f11010077

Mo, C., Tang, P., Huang, K., Lei, X., Lai, S., Deng, J., Bao, M., Sun, G., & Xing, Z. (2023). Evolution of Drought Trends under Climate Change Scenarios in Karst Basin. *Water (Switzerland)*, *15*(10). https://doi.org/10.3390/W15101934

Pause, M., Schweitzer, C., Rosenthal, M., Keuck, V., Bumberger, J., Dietrich, P., Heurich, M., Jung, A., & Lausch, A. (2016). In Situ/Remote Sensing Integration to Assess Forest Health—A Review. *Remote Sensing 2016, Vol. 8, Page 471*, *8*(6), 471. https://doi.org/10.3390/RS8060471

Proutsos, N. D., Solomou, A. D., Bourletsikas, A., Chatzipavlis, N., Petropoulou, M., Bourazani, K., Nikolopoulos, J. N., Georgiadis, C., & Kontogianni, A. B. (2022).

Assessing Drought for the Period 1955-2021 in Heraklion-Crete (S. Greece) Urban Environment.

Qiu, D., Liang, Y., Shang, R., & Chen, J. M. (2023). Improving LandTrendr Forest Disturbance Mapping in China Using Multi-Season Observations and Multispectral Indices. *Remote Sensing 2023, Vol. 15, Page 2381*, *15*(9), 2381. https://doi.org/10.3390/RS15092381

Riihimäki, H., Luoto, M., & Heiskanen, J. (2019). Estimating fractional cover of tundra vegetation at multiple scales using unmanned aerial systems and optical satellite data. *Remote Sensing of Environment*, *224*, 119–132. https://doi.org/10.1016/J.RSE.2019.01.030

Rouse, J. W., Haas, R. H., Schell, J. A., & Deering, D. W. (1974). Monitoring Vegetation Systems in the Great Plains with ERTS. *Third ERTS-1 Symposium NASA, NASA SP-351, Washington DC*, 309–317.

Roy, D. P., Kovalskyy, V., Zhang, H. K., Vermote, E. F., Yan, L., Kumar, S. S., & Egorov, A. (2016). Characterization of Landsat-7 to Landsat-8 reflective wavelength and normalized difference vegetation index continuity. *Remote Sensing of Environment*, *185*, 57–70. https://doi.org/10.1016/J.RSE.2015.12.024

Schiefer, F., Schmidtlein, S., Frick, A., Frey, J., Klinke, R., Zielewska-Büttner, K., Junttila, S., Uhl, A., & Kattenborn, T. (2023). UAV-based reference data for the prediction of fractional cover of standing deadwood from Sentinel time series. *ISPRS Open Journal of Photogrammetry and Remote Sensing*, *8*, 100034. https://doi.org/10.1016/j.ophoto.2023.100034

Schröter, D., Cramer, W., Leemans, R., Prentice, I. C., Araújo, M. B., Arnell, N. W., Bondeau, A., Bugmann, H., Carter, T. R., Gracia, C. A., De La Vega-Leinert, A. C., Erhard, M., Ewert, F., Glendining, M., House, J. I., Kankaanpää, S., Klein, R. J. T., Lavorel, S., Lindner, M., … Zierl, B. (2005). Ecology: Ecosystem service supply and vulnerability to global change in Europe. *Science*, *310*(5752), 1333–1337. https://doi.org/10.1126/SCIENCE.1115233

Schuldt, B., Buras, A., Arend, M., Vitasse, Y., Beierkuhnlein, C., Damm, A., Gharun, M., Grams, T. E. E., Hauck, M., Hajek, P., Hartmann, H., Hiltbrunner, E., Hoch, G., Holloway-Phillips, M., Körner, C., Larysch, E., Lübbe, T., Nelson, D. B., Rammig, A., … Kahmen, A. (2020). A first assessment of the impact of the extreme 2018 summer drought on Central European forests. *Basic and Applied Ecology*, *45*, 86–103. https://doi.org/10.1016/J.BAAE.2020.04.003

Silva, E. C. da, Albuquerque, M. B. de, Neto, A. D. de A., Junior, C. D. da S., Silva, E. C. da, Albuquerque, M. B. de, Neto, A. D. de A., & Junior, C. D. da S. (2013). Drought and Its Consequences to Plants – From Individual to Ecosystem. *Responses of Organisms to Water Stress*. https://doi.org/10.5772/53833

Somers, B., Verbesselt, J., Ampe, E. M., Sims, N., Verstraeten, W. W., & Coppin, P. (2010). Spectral mixture analysis to monitor defoliation in mixed-aged Eucalyptus globulus Labill plantations in southern Australia using Landsat 5-TM and EO-1 Hyperion data. *International Journal of Applied Earth Observation and Geoinformation*, *12*(4), 270–277. https://doi.org/10.1016/J.JAG.2010.03.005

Soriano-González, J., Angelats, E., Martínez-Eixarch, M., & Alcaraz, C. (2022). Monitoring rice crop and yield estimation with Sentinel-2 data. *Field Crops Research*, *281*. https://doi.org/10.1016/j.fcr.2022.108507

Spruce, J. P., Hicke, J. A., Hargrove, W. W., Grulke, N. E., & Meddens, A. J. H. (2019). Use of MODIS NDVI Products to Map Tree Mortality Levels in Forests Affected by Mountain Pine Beetle Outbreaks. *Forests 2019, Vol. 10, Page 811*, *10*(9), 811. https://doi.org/10.3390/F10090811

Strid, A. (1995). *The Greek mountain flora, with speciail reference to the CentraI European element*.

Sturm, J., Santos, M. J., Schmid, B., & Damm, A. (2022). Satellite data reveal differential responses of Swiss forests to unprecedented 2018 drought. *Global Change Biology*, *28*(9), 2956–2978. https://doi.org/10.1111/GCB.16136

Taherizadeh, M., Khushemehr, J. H., Niknam, A., Nguyen-Huy, T., & Mezősi, G. (2023). Revealing the effect of an industrial flash flood on vegetation area: A case study of Khusheh Mehr in Maragheh-Bonab Plain, Iran. *Remote Sensing Applications: Society and Environment*, *32*, 101016. https://doi.org/10.1016/j.rsase.2023.101016

Tao, C., Guo, T., Shen, M., & Tang, Y. (2023). Spatio-Temporal Dynamic of Disturbances in Planted and Natural Forests for the Saihanba Region of China. *Remote Sensing*, *15*(19), 4776. https://doi.org/10.3390/rs15194776

Turland, N. J., Chilton, J., & Press, J. R. (1993). Flora of the Cretan area. *Natural History Museum, London*.

Varlas, G., Stefanidis, K., Papaioannou, G., Panagopoulos, Y., Pytharoulis, I., Katsafados, P., Papadopoulos, A., & Dimitriou, E. (2022). Unravelling Precipitation Trends in Greece since 1950s Using ERA5 Climate Reanalysis Data. *Climate 2022, Vol. 10, Page 12*, *10*(2), 12. https://doi.org/10.3390/CLI10020012

Varouchakis, E. A., Corzo, G. A., Karatzas, G. P., & Kotsopoulou, A. (2018). Spatio-temporal analysis of annual rainfall in Crete, Greece. *Acta Geophysica*, *66*(3), 319–328. https://doi.org/10.1007/s11600-018-0128-z

Verbesselt, J., Robinson, A., Stone, C., & Culvenor, D. (2009). Forecasting tree mortality using change metrics derived from MODIS satellite data. *Forest Ecology and Management*, *258*(7), 1166–1173. https://doi.org/10.1016/j.foreco.2009.06.011

Vogiatzakis, I. N., Griffiths, G. H., & Mannion, A. M. (2003). Environmental factors and vegetation composition, Lefka Ori massif, Crete, S. Aegean. *Global Ecology and Biogeography*, *12*(2), 131–146. https://doi.org/10.1046/j.1466-822X.2003.00021.x

Woodall, C. W., Kamoske, A. G., Hayward, G. D., Schuler, T. M., Hiemstra, C. A., Palmer, M., & Gray, A. N. (2023). Classifying mature federal forests in the United States: The forest inventory growth stage system. *Forest Ecology and Management*, *546*, 121361. https://doi.org/10.1016/J.FORECO.2023.121361

Worqlul, A. W., Haddad, M., Alemayehu, S., & Govind, A. (2023). Developing a satellite-based combined land degradation index for monitoring environmental change: A case study in Tana-Beles watershed, Upper Blue Nile, Ethiopia. *Remote Sensing Applications: Society and Environment*, *32*, 101050. https://doi.org/10.1016/j.rsase.2023.101050

Xulu, S., Peerbhay, K., Gebreslasie, M., & Ismail, R. (2019). *Unsupervised Clustering of Forest Response to Drought Stress in Zululand Region, South Africa*. https://doi.org/10.3390/f10070531

Zhang, J., Xu, S., Zhao, Y., Sun, J., Xu, S., & Zhang, X. (2023). Aerial orthoimage generation for UAV remote sensing: Review. *Information Fusion*, *89*, 91–120. https://doi.org/10.1016/J.INFFUS.2022.08.007

Zhang, X., Wang, G., Xue, B., & A, Y. (2022). Changes in vegetation cover and its influencing factors in the inner Mongolia reach of the yellow river basin from 2001 to 2018. *Environmental Research*, *215*, 114253. https://doi.org/10.1016/j.envres.2022.114253

Zhou, Q., Hill, M. J., Sun, Q., & Schaaf, C. B. (2016). *International Journal of Remote Sensing Retrieving understorey dynamics in the Australian tropical savannah from time series decomposition and linear unmixing of MODIS data Retrieving understorey dynamics in the Australian tropical savannah from time series decomposition and linear unmixing of MODIS data*. https://doi.org/10.1080/01431161.2016.1154224

Zhu, L., Liu, X., Wu, L., Tang, Y., & Meng, Y. (2019). Long-Term Monitoring of Cropland Change near Dongting Lake, China, Using the LandTrendr Algorithm with Landsat Imagery. *Remote Sensing 2019, Vol. 11, Page 1234*, *11*(10), 1234. https://doi.org/10.3390/RS11101234

Zhu, Z. (2017). Change detection using landsat time series: A review of frequencies, preprocessing, algorithms, and applications. *ISPRS Journal of Photogrammetry and Remote Sensing*, *130*, 370–384. https://doi.org/10.1016/J.ISPRSJPRS.2017.06.013

Zhu, Z., Wang, S., & Woodcock, C. E. (2015). Improvement and expansion of the Fmask algorithm: cloud, cloud shadow, and snow detection for Landsats 4–7, 8, and Sentinel 2 images. *Remote Sensing of Environment*, *159*, 269–277. https://doi.org/10.1016/J.RSE.2014.12.014

APPENDIX

The figures below illustrate LandTrendr's outputs for sites 1 and 2. For the exclusion of non-significant changes and bare soil, pixels whose magnitude of change is more than 100 and pre-change spectral value is more than 300 (for NDVI, because values starting with 0.3 illustrate presence of vegetation) or 0 (for NDWI, because areas having values higher than 0 illustrate (some) presence of water in them and together with absence of water bodies in the area of interest highlight all the possible patches of vegetation) are only included in the Figures 36, 37, 40, 41.

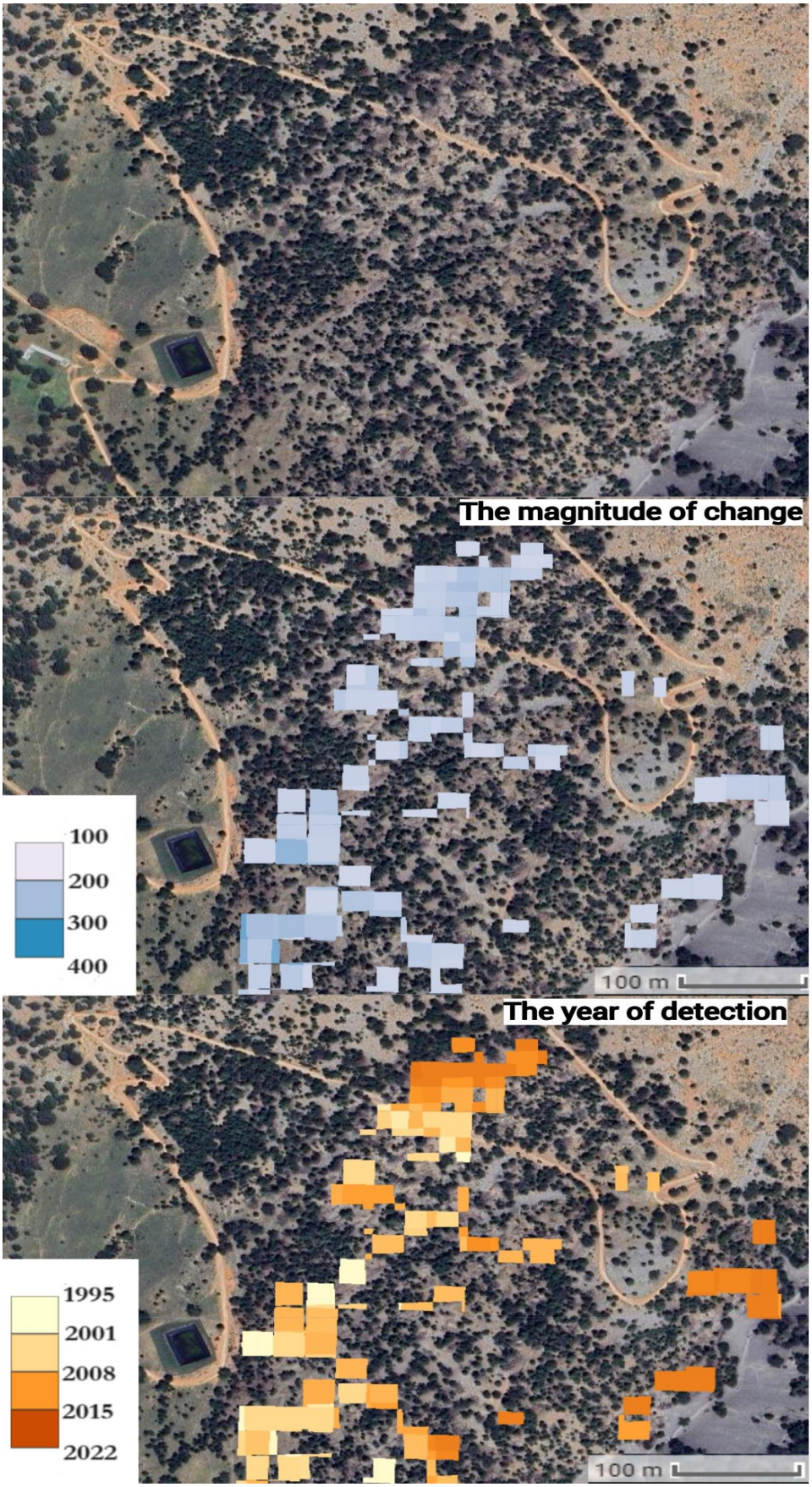

Figure 36. NDVI×1000 the magnitude of change and the year of detection for site 1 using Landtrendr

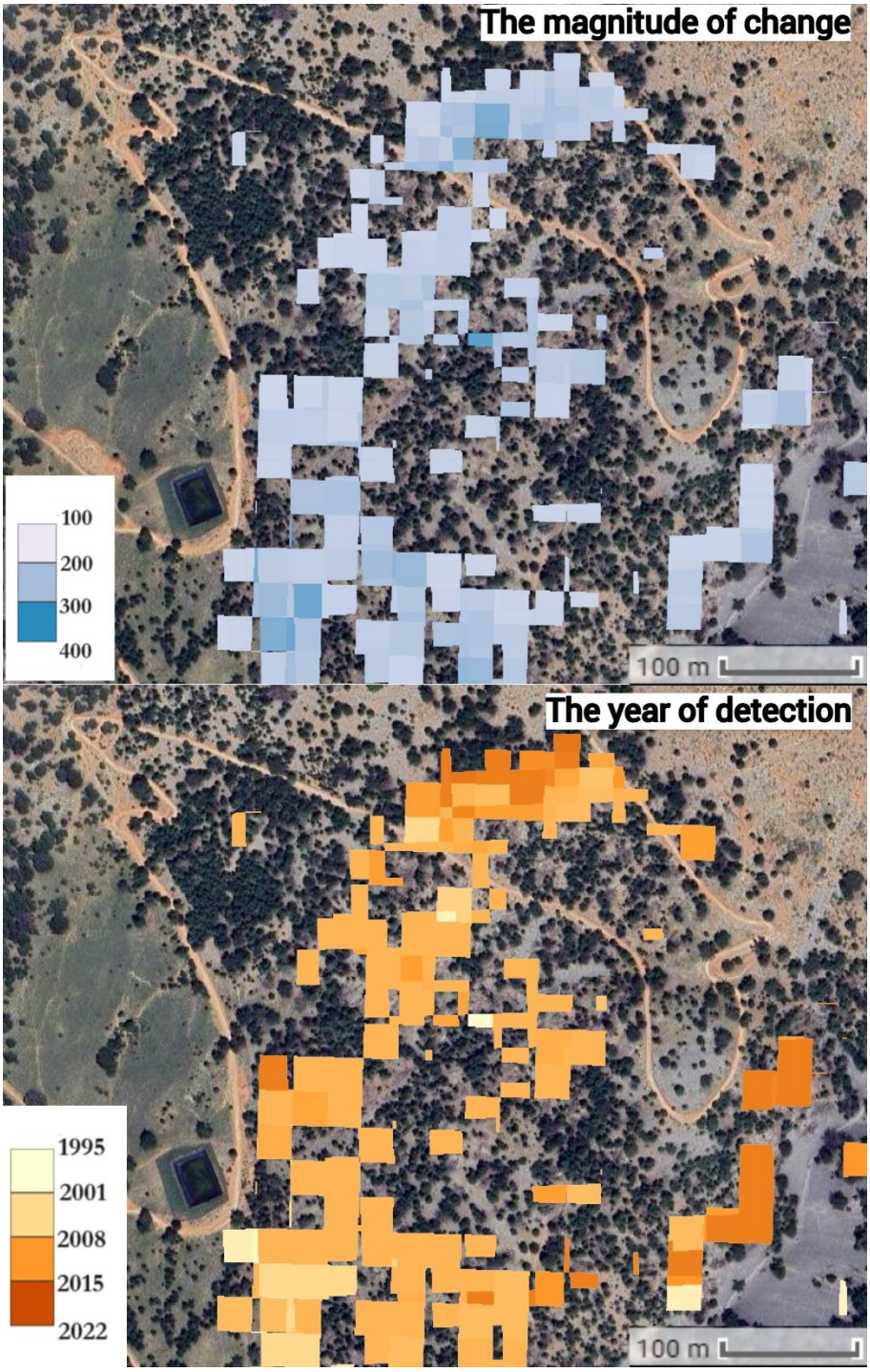

Figure 37. NDWI×1000 the magnitude of change and the year of detection for site 1 using Landtrendr

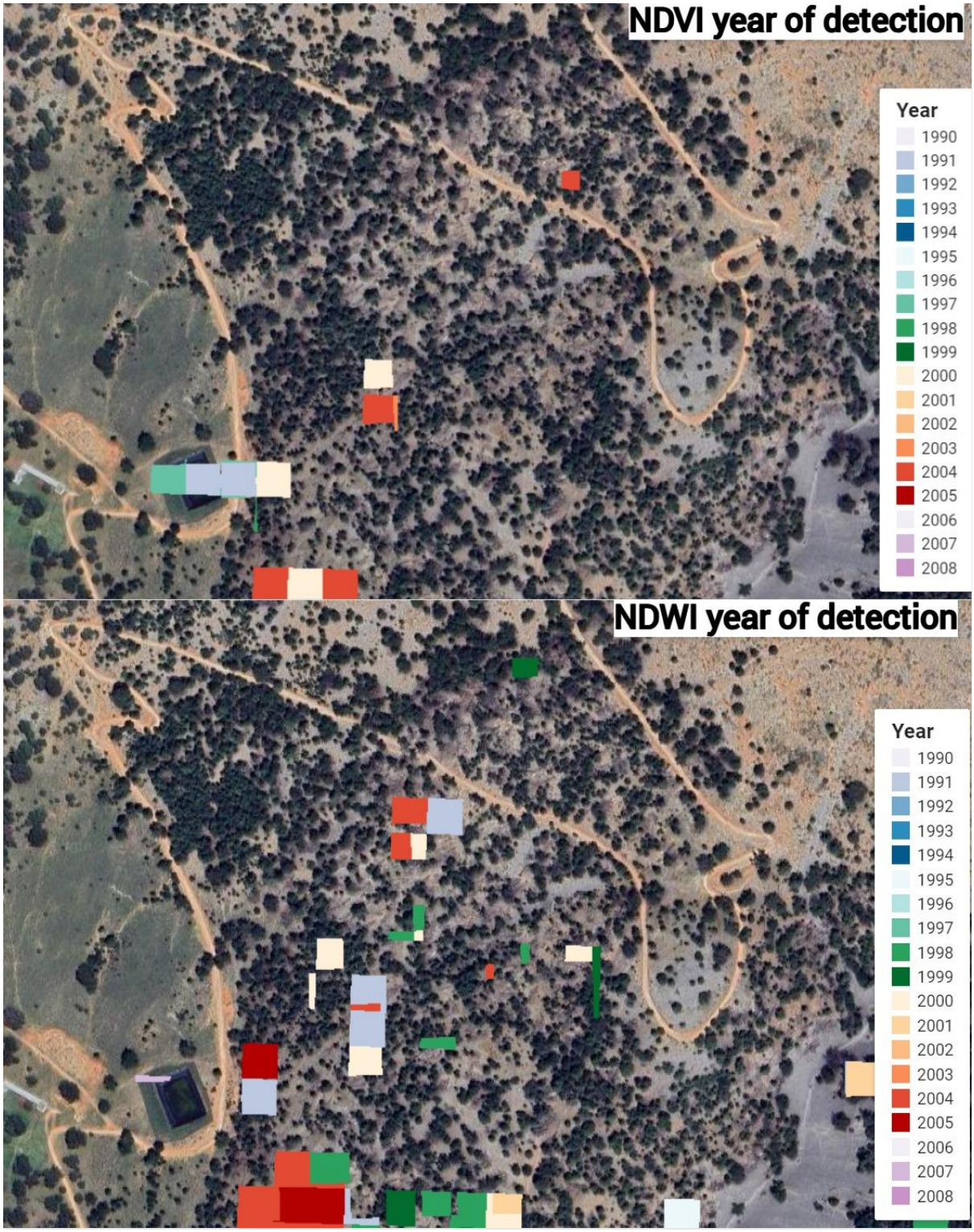

Figure 38. Changes happened in 1990-2008 for stie 1 using Landtrendr, without defined pre-change spectral value and with magnitude of change more than 100

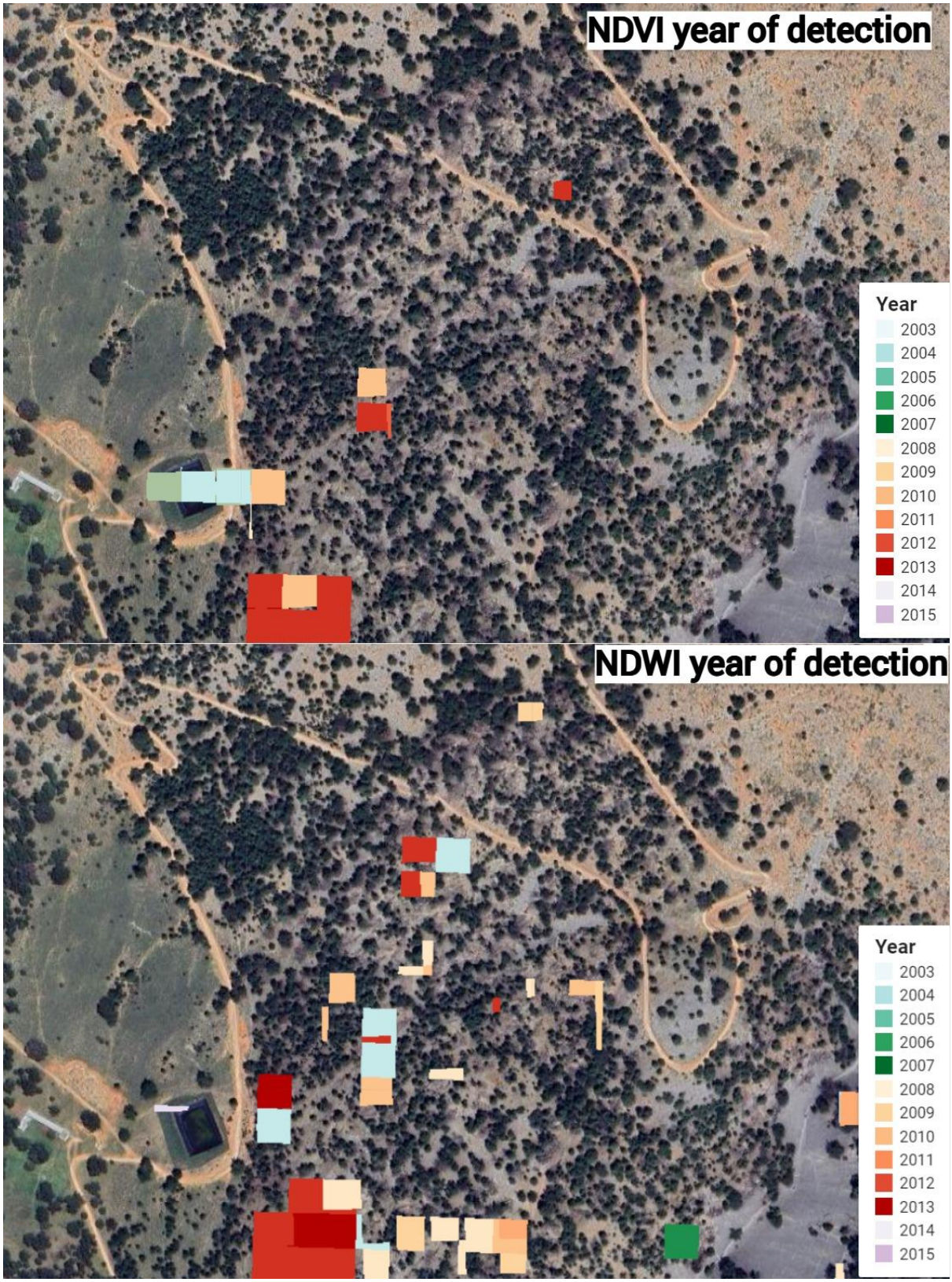

Figure 39. Changes happened in 2003-2015 for stie 1 using Landtrendr without defined pre-change spectral value and with magnitude of change more than 100

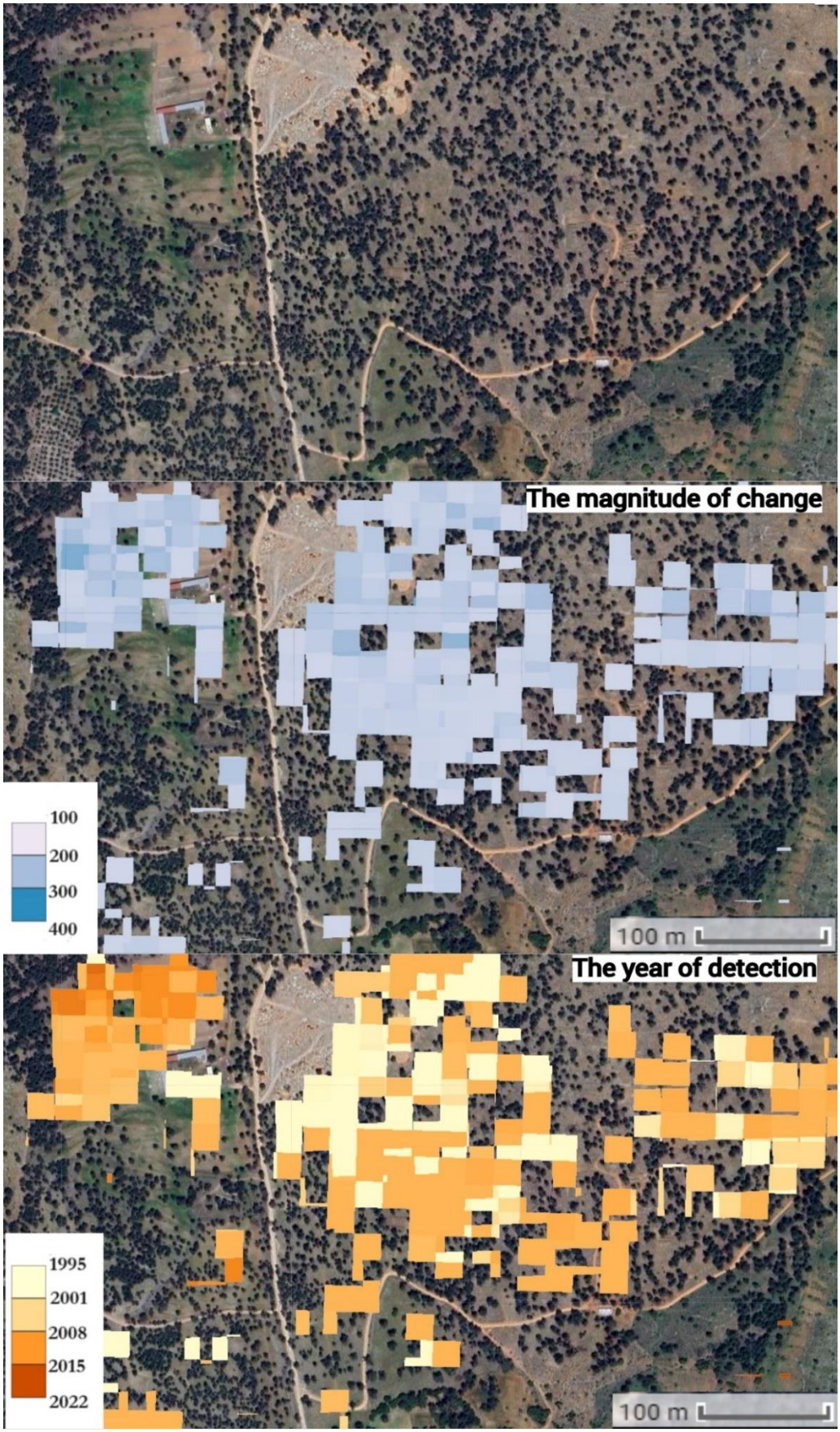

Figure 40. NDVI×1000 the magnitude of change and the year of detection for site 2 using Landtrendr

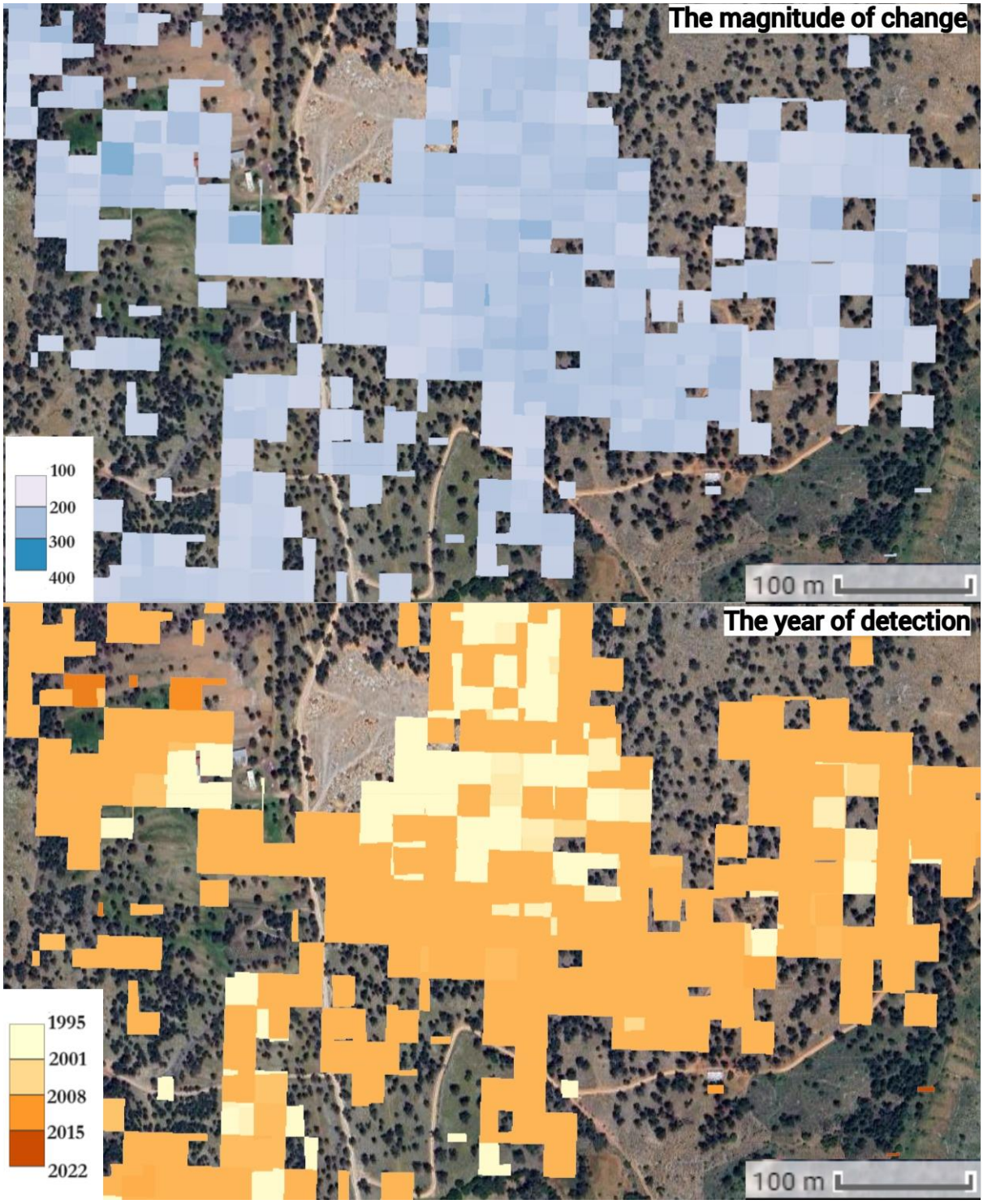

Figure 41. NDWI×1000 the magnitude of change and the year of detection for site 2 using Landtrendr

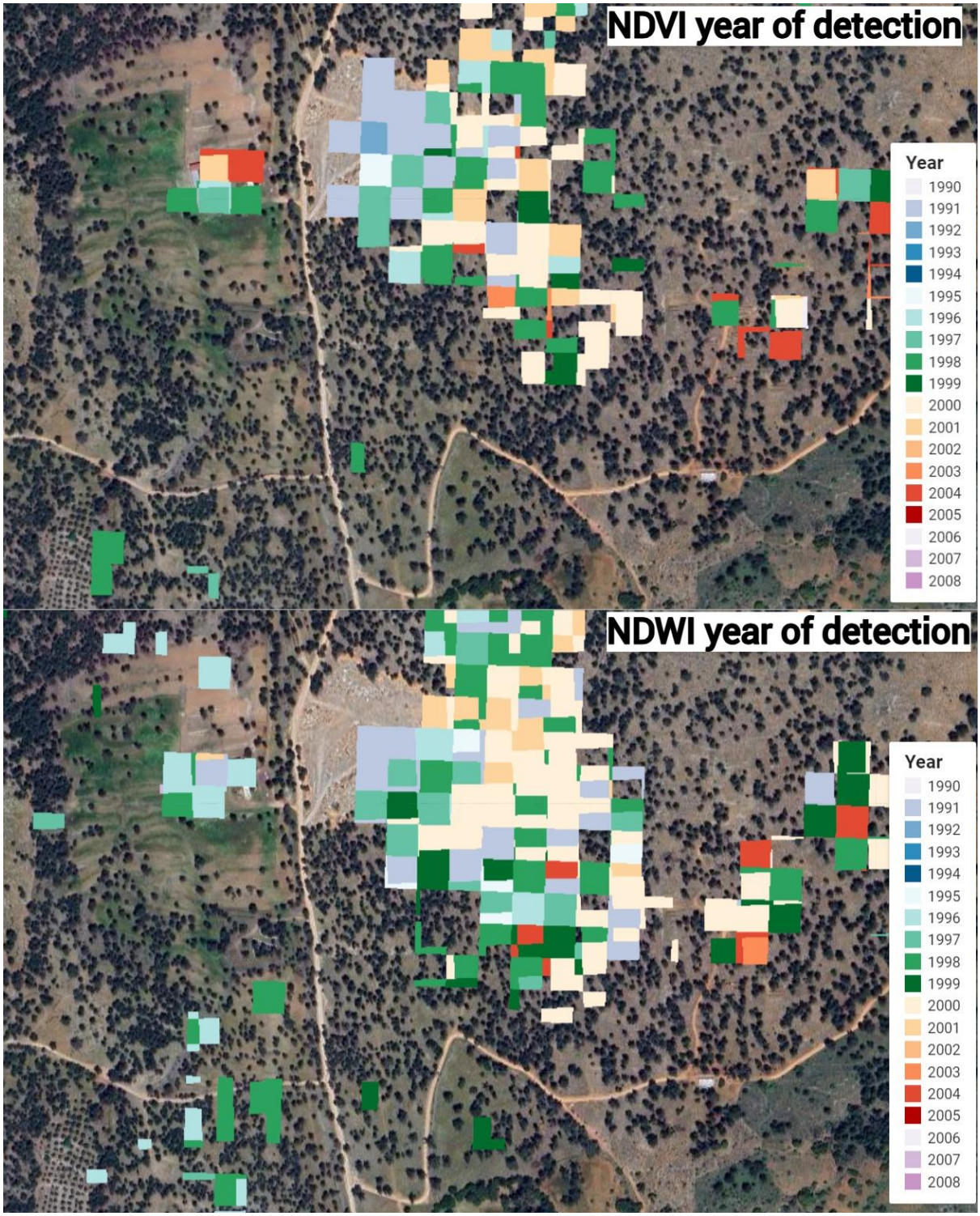

Figure 42. Changes happened in 1990-2008 for stie 2 using Landtrendr without defined pre-change spectral value and with magnitude of change more than 100

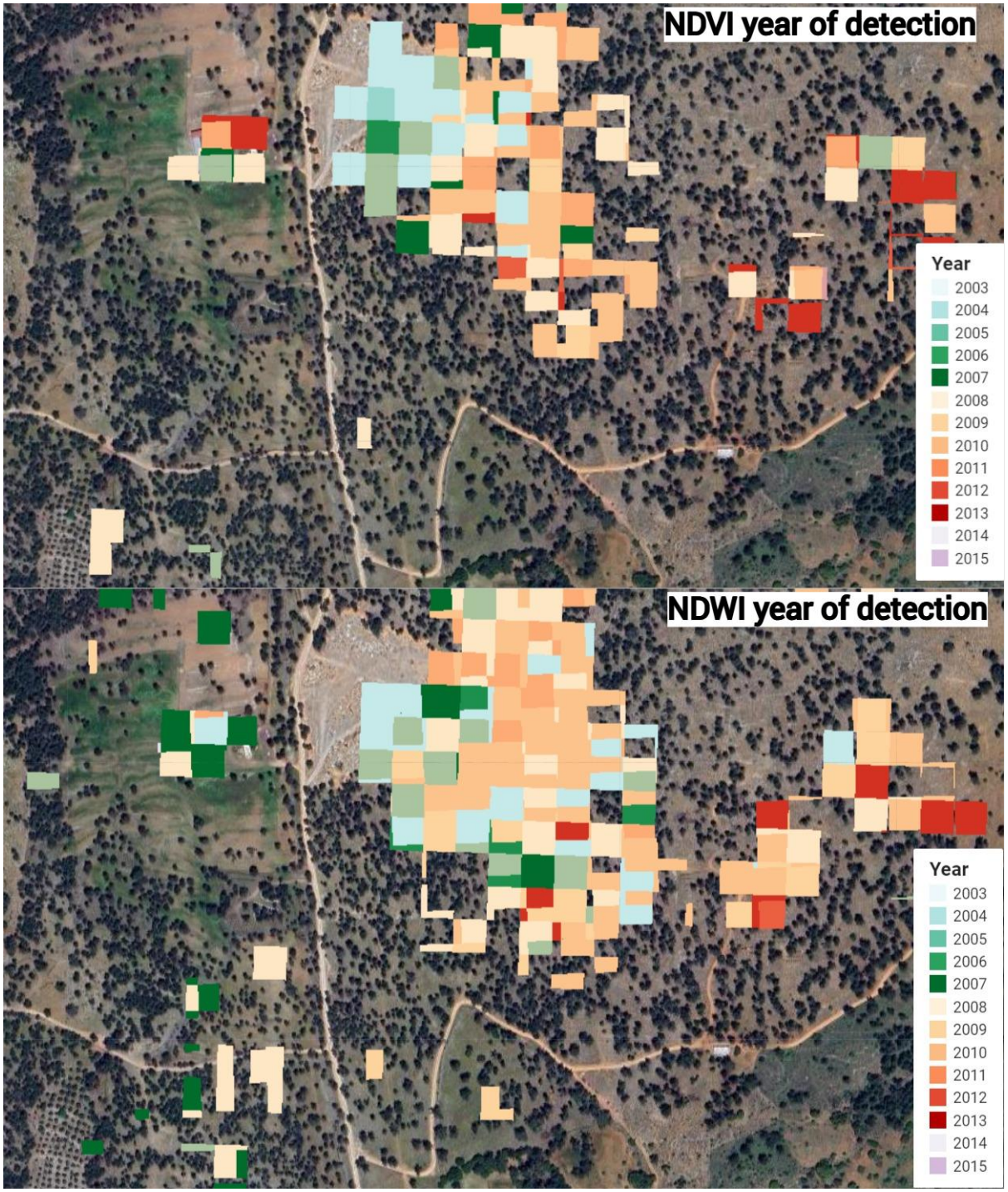

Figure 43. Changes happened in 2003-2015 for stie 2 using Landtrendr without defined pre-change spectral value and with magnitude of change more than 100